



Saltillo, Coahuila a 28 de febrero de 2022

Coordinación de Posgrado

Presente

Por este conducto nos permitimos informar a esta coordinación que, el documento de Tesis preparado por VÍCTOR DANIEL LECHUGA ISLAS titulado **Development of Multifunctional Polymeric Catalyst and their Application In Polyester Recycling (Desarrollo de Catalizadores Poliméricos Multifuncionales y su Aplicación en la Depolimerización de Poliésteres)**, el cual fue presentado el día 23 de febrero de 2022, ha sido modificado de acuerdo a las observaciones, comentarios y sugerencias, realizadas por el Comité Evaluador asignado. Por tal motivo, avalamos que el documento adjunto corresponde a la versión final del documento de Tesis.

Atentamente,


SINODALES




Dr. Ricardo Acosta Ortiz
Presidente



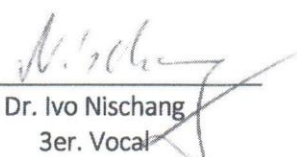
Dr. Dámaso Navarro Rodríguez
Secretario



Dr. Ramón Enrique Díaz de León Gómez
1er. Vocal




Dr. Johannes Christopher Brendel
2do. Vocal




Dr. Ivo Nischang
3er. Vocal

Vo. Bo. ASESORES



Dr. Ramiro Guerrero Santos



Dr. Carlos A. Guerrero Sánchez

TESIS CON CARACTER ABIERTO

PROGRAMA: DOCTORADO EN TECNOLOGÍA DE POLÍMEROS

AUTOR: VÍCTOR DANIEL LECHUGA ISLAS FIRMA 

TITULO: Development of Multifunctional Polymeric Catalyst and their Application In Polyester Recycling (Desarrollo de Catalizadores Poliméricos Multifuncionales y su Aplicación en la Depolimerización de Poliésteres)

ASESORES: Dr. Ramiro Guerrero Santos

FIRMA 

Dr. Carlos A. Guerrero Sánchez

FIRMA 

El Centro de Investigación en Química Aplicada clasifica el presente documento de tesis como ABIERTO.

Un documento clasificado como Abierto se expone en los estantes del Centro de Información para su consulta. Dicho documento no puede ser copiado en ninguna modalidad sin autorización por escrito del Titular del Centro de Información o del Director General del CIQA.

Saltillo, Coahuila, a 23 de Febrero de 2022

Sello de la Institución





Dr. Oliverio Santiago Rodríguez Fernández
Director General del CIQA



CENTRO DE INVESTIGACIÓN EN QUÍMICA APLICADA
Programa de Doctorado en Tecnología de Polímeros

TESIS

Development of Multifunctional Polymeric Catalyst and their Application In Polyester Recycling (Desarrollo de Catalizadores Poliméricos Multifuncionales y su Aplicación en la Depolimerización de Poliésteres)

Presentada por:

VÍCTOR DANIEL LECHUGA ISLAS

Para obtener el grado de:

Doctor en Tecnología de Polímeros

Asesorado por:

Dr. Ramiro Guerrero Santos
Dr. Carlos A. Guerrero Sánchez

Febrero, 2022

CENTRO DE INVESTIGACIÓN EN QUÍMICA APLICADA
Programa de Doctorado en Tecnología de Polímeros

TESIS

Development of Multifunctional Polymeric Catalyst and their Application In
Polyester Recycling (Desarrollo de Catalizadores Poliméricos Multifuncionales
y su Aplicación en la Depolimerización de Poliésteres)

Presentada por:

VÍCTOR DANIEL LECHUGA ISLAS


Para obtener el grado de:

Doctor en Tecnología de Polímeros


Asesorado por:

Dr. Ramiro Guerrero Santos
Dr. Carlos A. Guerrero Sánchez


SINODALES




Dr. Ricardo Acosta Ortiz
Presidente



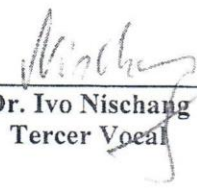
Dr. Dámaso Navarro Rodríguez
Secretario



Dr. Ramón Enrique Díaz de León Gómez
Primer Vocal



Dr. Johannes Christopher Brendel
Segundo Vocal



Dr. Ivo Nischang
Tercer Vocal

Saltillo, Coahuila, México.

Febrero, 2022

DECLARACIÓN

Declaro que la información contenida en la Parte Experimental así como en la Parte de Resultados y Discusiones de este documento y que forman parte de las actividades de investigación y desarrollo realizadas durante el período que se me asignó para llevar a cabo mi trabajo de tesis, será propiedad del Centro de Investigación en Química Aplicada.

Saltillo, Coahuila a 23 de Febrero de 2022



VÍCTOR DANIEL LECHUGA ISLAS

Nombre y Firma



Development of Multifunctional Polymeric Catalyst and their Application In Polyester Recycling

Tesis para obtener el grado de Doctor en Tecnología de Polímeros

Presentada por

Víctor Daniel Lechuga Islas

Supervisada por

Dr. Ramiro Guerrero Santos

Centro de Investigación en Química Aplicada (CIQA), Department of Macromolecular
Chemistry and Nanotechnology, Saltillo, México.

Dr. Carlos A. Guerrero Sánchez

Friedrich Schiller Universität Jena (FSUJ), Laboratory of Organic and Macromolecular
Chemistry (IOMC) / Jena Center for Soft Matter (JCSM), Jena, Germany.

February 2022

This study was supported by the *Consejo Nacional de Ciencia y Tecnología* (CONACYT, Mexico), scholarship number **705399**, and the *Deutscher Akademischer Austauschdienst* (DAAD, Germany), scholarship number **57440919** – Bi-National Supervised Doctorates, 2019/20.

Acknowledgements

This thesis was conducted at the *Centro de Investigación en Química Aplicada* (CIQA, Mexico), and the Laboratory of Organic and Macromolecular Chemistry (IOMC), Friedrich Schiller University Jena (FSUJ, Germany), both institutions are gratefully acknowledged.

This project would not have been possible without the support of many people. I am foremost grateful to my supervisors: Dr. Carlos Guerrero Sánchez for his outstanding ideas, guides, help, and prolific supervision during this project, and Dr. Ramiro Guerrero Santos for his constructive comments and vision to strive toward excellent research. I had a great time during this project. Thank you for all the confidence you entrusted me with.

I also would like to acknowledge the Department of Macromolecular Chemistry and Nanomaterials at CIQA, a special thanks to M.S. Hortensia Maldonado T., and B.S. Judith Cabello R., for their helpful assistance during the beginning of this project. Thanks also to the people who helped me with all the administration work at the *Coordinación de Posgrado* at CIQA, including Dr. Leticia Larios, M.S. Aída E. García, and Nancy Espinosa.

I thank Prof. Dr. Ulrich S. Schubert and his group for giving me the opportunity to do part of my PhD thesis at the Friedrich Schiller University Jena (FSUJ), Germany. It was a special pleasure for me to work and collaborate in the group.

I am also grateful to my committee: Dr. Dámaso Navarro, Dr. Ramón Díaz, and Dr. Ricardo Acosta for fruitful discussions, valuable suggestions, and expert advice to enrich this work. I hope I have learned and applied several of your teachings here and in future projects.

I am deeply grateful to the part-time students who helped me a lot with the experimental parts of this project: Robin Curth and, especially, I would like to thank Dulce Sánchez C. for her valuable experimental assistance and willingness to learn and collaborate in this project.

Moreover, I am also grateful to the always supportive staff at CIQA and FSUJ. Special thanks to Dr. Jesus Lara and Steffi Stumpf for their assistance with SEM analysis, Carolin Kellner for cytotoxicity studies, Renzo Paulus for his assistance with thermal

Acknowledgements

studies, Sandra Köhn for EA measurements, Katja Gattung and Ulrike Kaiser for all the paperwork in Jena, Dr. Grit Festag for SEC measurements, Dr. Johannes C. Brendel, Dr. Ivo Nischang for AUC measurements and great collaboration, and Dr. Jürgen Vitz for his kind support during my stay in Jena.

For the good times and collaboration, I also wish to thank my colleagues and friends at CIQA and FSUJ. A special thanks to Alicia de San Luis, Carolina Ventura, César Muñoz, Claude St. Thomas, Ilya Anufriev, Jens Ulbrich, Julien Alex, Luana Vieira, Marco De Jesus, Miguel Carrillo, Roberto Yañez, Paulina Lugo, Paul Klemm and to all who directly or indirectly have lent their hand in this venture. Thank you, muchas gracias, danke schön!

I am especially grateful to my family for providing me with unfailing support and continuous help throughout my years of study. This accomplishment would not have been possible without them. I wish to express my deepest gratitude to Melisa Trejo, her love, dedication, and encouragement have sustained and uplifted me to continue with this and our wonderful life project. Thank you!

And of course, I wish to express my gratitude for financial support to the *Consejo Nacional de Ciencia y Tecnología* (CONACYT) and the *Deutscher Akademischer Austauschdienst* (DAAD) through the research grant: Bi-nationally supervised Doctoral Degrees / Cotutelle.

Summary

Nowadays, multiple methodologies have been developed to recycle polyesters, including physical methods (based on exhaustively designed processes)^{1,2} and chemical methods (*e.g.*, methanolysis, glycolysis, and acid or basic hydrolysis). These latter represent promising research areas with the main goal of breaking polyesters chain all the way down to their monomeric units (depolymerization). Then, the monomer can be used as a feedstock to obtain new recycled PET (r-PET) or new materials thereof (upcycling) in fully sustainable approaches.³ However, the main drawbacks of chemical recycling methods are the use of toxic catalysts and the intrinsic impurities found in post-consumer polyesters, which both are difficult to remove from the final product; the scenario is completed with the relatively extreme conditions (*e.g.*, temperature, pressure, ultrasonics, time of reaction, among others) required in depolymerization procedures. These factors significantly constrain the applicability and economic viability of chemical methods at an industrial scale. The progress of novel and more efficient and reusable catalysts, *v. gr.*, ionic liquids (ILs), represent a promising approach to generate circular consumption-recycling systems (closed-loop) systems to increase the efficiency of polyester recycling processes.⁴ Nevertheless, there are still multiple barriers to overcome to achieve more efficient chemical recycling procedures with practical recovery for catalysts and impurity separation. For example, current state-of-the-art technologies mainly focus in specific types of post-consumer polyesters, such as polyethylene terephthalate (PET), and make it impossible to obtain food-grade recycled materials from any type of waste (*e.g.*, different coloration, multilayered or opaque materials);⁵ either because the developments do not allow the separation of contaminants (additives, adhesives, colorants or dyes) or because of the complicated removal and potential toxicity of the catalysts used.

Hence, this research aimed to develop an efficient method for the chemical recycling of PET by introducing novel polymeric catalysts with functionalities that could tackle the current limitations of these procedures; *i.e.*, to yield high conversion of depolymerization and high selectivity of monomer, and the effective separation of catalysts and impurities from the products of depolymerization to yield high purity monomer. To

reach this goal, this thesis describes the development of series of multifunctional polymeric catalysts (MPCs) with stimuli-responsive capabilities to address the mentioned limiting factors and to generate suitable chemical recycling strategies for implementation on a commercial scale.

The functionalities of the MPCs were carefully designed to accomplish the following functions: 1. Catalyze the glycolysis of post-consumer polyesters, 2. Remove intrinsic impurities from the process, and 3. Recover the MPC from glycolysis mixtures. Such capabilities were possible by adjusting the physicochemical properties of the MPCs to provide them with thermo-responsive behavior in aqueous and glycol solutions. These features were essential to choose the optimal MPCs using high throughput experimental approaches.

The developed glycolysis procedure using novel MPCs allowed a PET conversion of up to 99% with a selectivity for the recycled monomer over 90%. We demonstrated that the catalytic activity of the MPCs was scarcely affected by the different colorations of post-consumer PET. Moreover, using tailored MPCs and the developed approach, the colorants could be removed from the products of glycolysis. In sum, balancing the functionalities of the MPCs allowed the on-demand modification of the catalytic system for the recycling of specific types of post-consumer PET. After the purification of the products, the thermo-responsive MPCs could be spontaneously separated from the final solution by decreasing the temperature for its isolation or reuse for following cycles of chemical recycling. Thus, towards the progress of catalysts with superior performance reusability and removal capabilities in the chemical recycling of polyesters, we report a quasi-homogeneous catalytic process employing thermo-responsive polymeric catalysts that combine the advantages of heterogeneous and homogeneous catalyst for the depolymerization of PET.

Scope of the thesis

This document is structured in the following chapters:

Chapter 1 provides a literature background of methods for the recycling of PET and highlights relevant chemical recycling methods. Moreover, stimuli-responsive polymers based on poly(ionic liquids) (PILs) are introduced, focusing on their novel features and potential applications described in the literature.

Chapter 2 covers the experimental methods of synthesizing MPCs via Reversible Addition-Fragmentation chain Transfer (RAFT) polymerization and the experimental methods for the glycolysis of post-consumer PET using the new MPCs. Firstly, ionic monomers were synthesized and polymerized to yield PILs with Cl⁻ anions. After an anion exchange reaction with appropriate metal chlorides, halometallate PILs were obtained, setting the chemical pathway to MPCs. A similar procedure was followed to prepare copolymers with variable structure and compositions (*i.e.*, block, *quasi*-block, and statistical copolymers). Thus, copolymers possessing stimuli-responsive, impurity affinity, and containing ionic sites were designed to accomplish the following functions during the glycolysis of PET: 1. Catalyze the depolymerization of polyester (PIL segment), 2. Remove intrinsic impurities of the process (impurity-affinity segment), and 3. Recover the MPCs from depolymerization mixtures (stimuli-responsive segment).

Chapter 3 describes the examination of the physicochemical properties of the obtained library of (co)polymers. Particularly, the unique thermo-responsive behavior of the obtained copolymers in aqueous and glycol solutions, and the effects of variables such as polymer structure, composition, and molar mass, concentration, and solvents, are described.

Chapter 4 provides a comprehensive examination of the glycolysis of PET using the synthesized copolymers as catalysts. As schematically depicted in Figure 1, the main raw material is post-consumer PET, used without intensive cleaning or sorting pre-treatments, which can contain different colorations or grades. First, a series of halometallate PILs were evaluated to select the MPC with suitable anions and composition for the best catalytic performance (conversion and selectivity). After that, the selected MPC was subjected to

an optimization process using an automated parallel procedure to examine the kinetics of the glycolysis reaction and determine the optimized conditions. Moreover, tests regarding the catalyst recovery, via its thermo-responsive behavior and subsequent methods of reuse are presented. Finally, the removal capacity of specific dyes is described, whereby MPCs with different structures were used to validate that the water-soluble dyes can be removed from the recycled monomer. In that way, a reaction mechanism is suggested, where the MPCs provide the advantages of homogeneous catalysts, for an excellent catalytic performance, and heterogeneous catalysts, for isolating impurities and the catalyst from the depolymerization products.

Chapter 5 presents the conclusion and outlook of this research, emphasizing on the advantages of using MPCs for the chemical recycling of polyesters. In sum, the gap between state-of-the-art and upcycling technology to reach industrial-scale exploitation for the case of PET has been narrowed with the methodologies presented in this work.

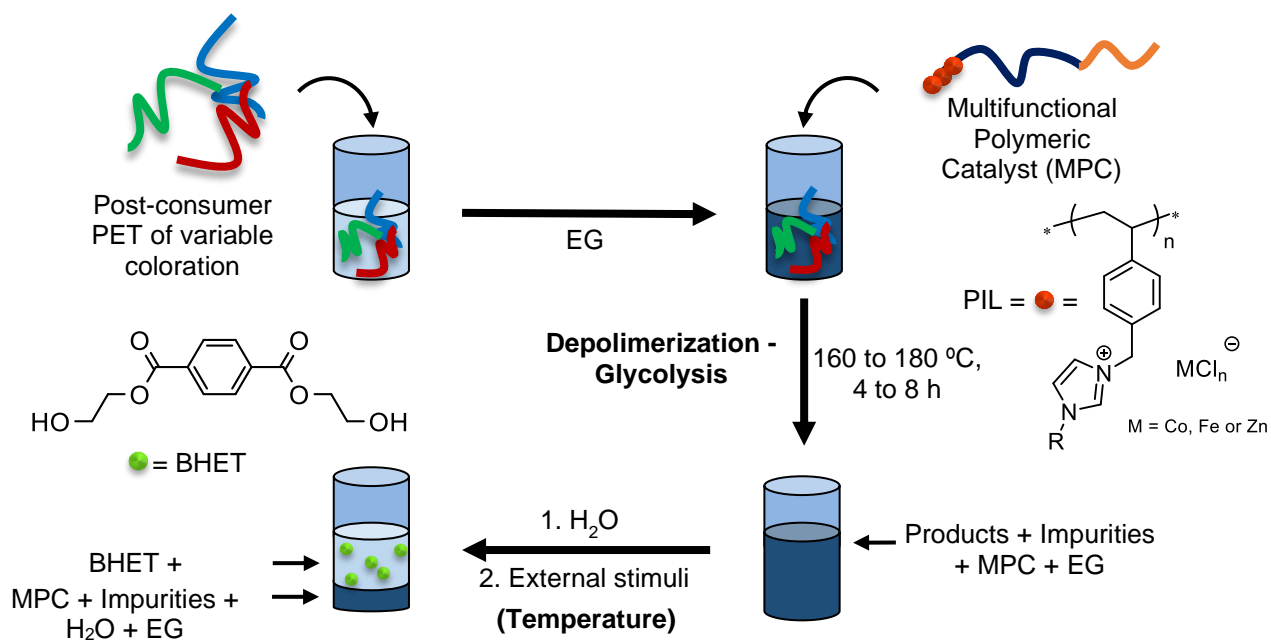


Figure 1 Scheme of the proposed system for the glycolysis of post-consumer PET in ethylene glycol (EG), catalyzed by a thermo-responsive MPC, to obtain monomer (bis(2-hydroxy ethyl) terephthalate (BHET)).

Parts of this work are based on the following publications:

Lechuga-Islas, V. D. Guerrero-Santos R., Schubert U.S., and Guerrero-Sanchez C. (Poly)ester and (poly)amide compositions, method for modifying (poly)esters or (poly)amides and catalyst therefor, *PCT Patent Application*, European Patent Office, **2022**, application number PCT/EP2022/000018.

Lechuga-Islas, V. D., Sánchez-Cerrillo, D. M., Stumpf, S., Guerrero-Santos R., Schubert, U.S., and Guerrero-Sanchez C., Thermo-responsive polymer catalyst: switching from homogenous catalysis to heterogeneous separations, **2022** –*Submission in Progress*.

Trejo-Maldonado, M., **Lechuga-Islas, V. D.**, Anufriev, I., Nischang, I., Guerrero-Santos R., Elizalde-Herrera, L. E., Schubert, U.S., and Guerrero-Sanchez C., All-aqueous, surfactant-free, and pH-driven nanoprecipitation methods to formulate dual-responsive polymer nanoparticles as potential drug nanocarriers, **2022** – *Submission in Progress*.

Lechuga-Islas, V. D., Guerrero-Sanchez C., Guerrero-Santos R., Vitz, J., and Schubert, U.S. High-Throughput / High-Output Experimentation in Polymer Research, , *Macromolecular Engineering: From Precise Synthesis to Macroscopic Materials and Applications*, (eds. N. Hadjichristidis, Y. Gnanou, K. Matyjaszewski and M. Muthukumar), ed. Wiley & Sons, **2022** – *book chapter*.

Lechuga-Islas, V. D., Trejo-Maldonado, M., Stumpf, S., Guerrero-Santos R., Elizalde-Herrera, L., Schubert, U.S., and Guerrero-Sanchez C. Separation of Volatile Compounds from Polymers by Physisorption, *Eur. Polym. J.*, **2021** (159), 110748.

Lechuga-Islas, V.D. Trejo-Maldonado M., Schubert U.S., and Guerrero-Sanchez C. Separation of Volatile Compounds from Polymers by Physisorption for High Throughput Applications, *Patent Application*, German Patent and Trademark Office, **2021**, application number 102021004383.9.

Lechuga-Islas, V. D., Festag, G., Rosales-Guzman, M., Vega-Becerra, O., Guerrero-Santos R., Schubert, U.S., and Guerrero-Sanchez C. Quasi-block copolymer design of quaternized derivatives of poly (2-(dimethylamino) ethyl methacrylate): Investigations on thermo-induced self-assembly, *Eur. Polym. J.*, **2020** (124), 109457.

Resumen

Uno de los mayores esfuerzos para reducir la contaminación generada por plásticos derivados de poliésteres se basa en su reciclado por una variedad de métodos físicos y químicos (depolimerización). Hasta la fecha, los procesos químicos destacan por el uso de catalizadores novedosos, como líquidos iónicos (LIs), los cuales prometen generar sistemas de consumo-reciclado tipo circular (*closed-loop*). No obstante, aún existen varias dificultades en las estrategias de reciclado químico para aumentar la viabilidad económica del proceso. Por ejemplo, los tratamientos de reciclado reportados imposibilitan la obtención de material reciclado grado alimenticio; ya sea porque los procesos no permiten la separación de contaminantes secundarios (aditivos y colorantes) o por la complicada remoción y potencial toxicidad de los catalizadores empleados.

Tomando en cuenta ambas dificultades, es decir, la generación de procesos sustentables y la facilidad de separación de impurezas y catalizadores de los productos del reciclado químico, este trabajo de investigación tiene como objetivo desarrollar estrategias que permitan el reciclado químico de tereftalato de polietileno (PET) y generar un proceso que se adhiera a los principios de la química verde. Para este fin, se plantea el uso de catalizadores poliméricos multifuncionales (CPMs), conformados por segmentos: hidrófilo (sensible a estímulos externos), hidrófobo e ILs. De este modo, los CPMs introducen propiedades y estructuras moleculares específicas que permitan incrementar la viabilidad de los procesos de reciclado químico. Este trabajo de tesis reporta los resultados obtenidos en el uso de CPMs en el reciclado químico de PET de posconsumo de diferente coloración.

Las funcionalidades de los CPMs fueron diseñadas para lograr las siguientes funciones: 1. Catalizar la glicólisis de PET de posconsumo, 2. Eliminar las impurezas intrínsecas de PET de posconsumo y 3. Recuperar el catalizador polimérico de la mezcla final de depolimerización. Adicionalmente, el estudio de las propiedades fisicoquímicas de los CPMs demostró el comportamiento termosensible de estos materiales en soluciones tipo glicol. Dichos estudios fueron esenciales para elegir los CPMs óptimos para la glicólisis de PET mediante un procedimiento automatizado en paralelo.

Empleando los CPMs seleccionados, el proceso de glicólisis alcanzó una conversión de PET de hasta el 99% con una selectividad por el monómero superior al 90%. Más aún, la actividad catalítica de los CPMs no es afectada por las diferentes coloraciones de PET de posconsumo. Además, utilizando CPMs específicos y la metodología descrita, fue posible eliminar colorantes de los productos de glicólisis para obtener monómero reciclado sin coloración y con alta pureza. Por lo tanto, equilibrar las funcionalidades de los CPMs permitió la modificación “*ad hoc*” del sistema catalítico para el reciclaje químico de tipos específicos de PET posconsumo. Después de la purificación de los productos, los CPMs pudieron separarse espontáneamente de la solución final disminuyendo la temperatura para su aislamiento o reutilización para los siguientes ciclos de reciclaje químico. De este modo, en la búsqueda del desarrollo de catalizadores con actividad catalítica superior y con capacidades de eliminación de impurezas y del propio catalizador en el reciclaje químico de poliésteres, este trabajo reporta un proceso catalítico cuasi homogéneo catalizado por catalizadores poliméricos termosensibles que combinan las ventajas de los catalizadores heterogéneos y homogéneos para la depolimerización de PET.

Table of contents

Summary.....	[i]
Scope of the thesis.....	[iii]
Resumen	[vi]
Table of contents	[viii]
List of Tables	[xi]
List of Figures.....	[xii]
List of Abbreviations.....	[xvii]
Chapter 1 Theoretical background	1
1.1. Introduction.....	2
1.2. Synthesis and manufacture of PET	3
1.3. Methodologies for the recycling of PET	5
1.3.1. Primary recycling	6
1.3.2. Secondary recycling.....	6
1.3.3. Tertiary recycling	8
1.3.3.1. Hydrolysis and methanolysis	11
1.3.3.2. Glycolysis.....	11
1.3.3.3. Ionic liquids applied in the catalyzed glycolysis of PET	16
1.3.3.4. Separation and reuse of IL catalysts	19
1.3.4. Polymers derived from Ionic Liquids	22
1.3.4.1. PILs as materials with response to external stimuli.....	24
1.3.4.1.1. Potential applications of thermo-responsive PILs	27
1.4. Summary.....	29

1.5. Hypothesis and research objectives	31
1.5.1. Hypothesis	31
1.5.2. Objective	31
1.5.2.1. Specific objectives	32
Chapter 2 Experimental section	33
2.1. Materials	34
2.2. Synthesis of IL monomers	34
2.3. Synthesis of polymer libraries	35
2.4. Synthesis of (co)polymer PIL precursors	36
2.4.1. Synthesis of <i>quasi</i> -block and block copolymer precursors	37
2.5. Anion exchange reactions	40
2.6. General procedure for the glycolysis of post-consumer PET	41
2.7. Kinetic studies of PET depolymerization	43
2.8. Characterization methods	45
Chapter 3 Synthesis and characterization of MPCs	49
3.1. Synthesis of IL monomers	50
3.2. Synthesis and characterization of homopolymer precursors derived from [BVMIM]Cl and [BVBIM]Cl	52
3.3. Synthesis and characterization of (co)polymer libraries derived from copolymers of [BVBIM]Cl and DMAEMA	55
3.3.1. Synthesis and characterization of <i>quasi</i> -block and block copolymer precursors	60
3.3.2. Synthesis and characterization of halometallate [PIL]MCl _n	66
3.3.2.1. Solution properties of [PIL]MCl _n	72

3.3.2.2. Solution properties of halometallate [PIL]MCl _n copolymers	83
Chapter 4 Glycolysis of post-consumer PET using MPCs.....	87
4.1. Preliminary experiments - Selection of catalyst	88
4.2. The parallel platform for the glycolysis of post-consumer PET	91
4.3. Screening of MPCs as catalysts	93
4.4. Optimization of PET glycolysis using MPCs.....	98
4.4.1. Kinetic investigations on PET glycolysis using MPCs	99
4.4.2. Influence of the type of post-consumer PET	103
4.4.2.1. Removal of hydrophobic impurities	109
4.5. Reusability of the MPCs	111
Chapter 5 Conclusions and outlook.....	117
5.1. Conclusions	118
5.2. Outlook	120
5.3. References.....	121
5.4. Appendix	128

List of Tables

Table 1 General factors rated in the selection of PET for recycling processes. ¹⁶	6
Table 2 Minimum requirements for the physical recycling of PET.	7
Table 3 Examples of catalysts used in the glycolysis of PET. ¹⁸	15
Table 4 Experimental details for the synthesis of homopolymer [PIL]Cl precursors. .	37
Table 5 Experimental details for the synthesis of statistical copolymer precursors (P([BVBIM]Cl-co-DMAEMA).	37
Table 6 Experimental details for the synthesis of MacroCTA agents I-V	38
Table 7 Experimental details and characterization of <i>quasi</i> -block precursors (PDMAEMA- <i>qb</i> -P(DMAEMA-co-[BVBIM]Cl)).	39
Table 8 Experimental details for the synthesis of block copolymers precursors PMMA- <i>b</i> -P([BVMIM]Cl-co-DMAEMA) (D5) and PMMA- <i>b</i> -P([BVMIM]Cl-co-DMAEMA) (D6). ..	40
Table 9 Characterization of homopolymer [PIL]Cl precursors prepared by RAFT polymerization.	54
Table 10 Properties of synthesized statistical copolymers P([BVBIM]Cl-co-DMAEMA)	55
Table 11 Properties of MacroCTA agents I to V	62
Table 12 Properties of <i>quasi</i> -block (D1-D4) and block copolymers (D5-D6).	62
Table 13 Solubility properties of representative [PIL]Cl and their halometallate derivatives (M series) in EG, H ₂ O, and mixtures thereof (10 mg mL ⁻¹ at 25°C). ^{a)}	72
Table 14 Overview of the properties of P([BVMIM]ZnCl _n) (M2) in EG solutions, as a function of concentration, measured by DLS.	75
Table 15 Overview of the properties of P([BVMIM]ZnCl _n) (M2 to M5) in EG solutions, as a function of the molar ratio of ZnCl ₂ , measured by DLS.....	78
Table 16 Solubility properties of selected copolymers with variable structure and compositions in solutions of EG, H ₂ O, and mixtures thereof. ^{a)}	83

Table 17 Properties and catalytic performance of the MPCs used in this study.....	97
Table 18 Elemental Analyses of post-consumer PET feedstocks and BHET obtained from glycolysis reactions using MPCs.	109

List of Figures

Figure 1 Scheme of the proposed system for the glycolysis of post-consumer PET in ethylene glycol (EG), catalyzed by a thermo-responsive MPC, to obtain monomer (bis(2-hydroxy ethyl) terephthalate (BHET)).....	iv
Figure 2 Routes of reaction for the synthesis of commercial PET.....	4
Figure 3 Scheme of the mechanism of depolymerization of polyester in acidic and neutral conditions.....	9
Figure 4 Different methods of PET chemolysis and the value-added products derived therefrom (TPA = terephthalic acid; DMT = dimethyl terephthalate; BHET = bis(2-hydroxy ethyl) terephthalate). ²⁴	10
Figure 5 Proposed reaction scheme for the glycolysis of PET (I) and the catalyzed glycolysis of PET with metallic salts (II).....	13
Figure 6 Common cations and anions in ILs.....	16
Figure 7 The effect of Bmim]MCl _n catalysts on the glycolysis of PET. Reaction conditions: PET 2 g, catalyst 1 wt.%, reaction time 5 h, and temperature 180 °C. Reproduced from Yue <i>et al.</i> ⁴⁸	18
Figure 8 Mechanism of the glycolysis of PET in the presence of metal-containing ionic liquids.....	19
Figure 9 Examples of imidazolium-type IL monomers with extended use in the synthesis of PILs: (I) vinyl imidazolium, (II) styrenics, and (III) acrylamide derivatives.	22

Figure 10 Photographs of 2 wt.% solution of P(NIPAM- <i>b</i> -PIL) (a) in water at room temperature, (b) in 1.1 M aqueous KBr at room temperature, and (c) in 1.1 M aqueous KBr at 60 °C.....	25
Figure 11 Chemical structures and the synthetic route to spherical polymer brushes with a PIL core and a PNIPAM shell. Reproduced from Ref. 82	26
Figure 12 Transmittance measurements of (A) [PIL]Cl derived from butyl imidazole and (B) [PIL]Cl derived from methylpyridine in chloroform; straight line: heating, broken line: cooling. Reproduced from Ref. 85.	27
Figure 13 Pictures of the automated parallel synthesizers used in this work: A) ASW2000 and B) FORMAX.....	36
Figure 14 Front picture of the formulation block in the FORMAX platform. The inset shows a picture of the disassembled reactor, showing the mechanical stirrer used in this work.	42
Figure 15 A) SEC traces of standard BHET solutions at different concentrations. B) Calibration curve, obtained by the intensity signal of BHET solutions in SEC.....	44
Figure 16 ¹ H NMR spectrum (DMSO- <i>d</i> ₆) of monomers [BVMIM]Cl (A) and [BVBIM]Cl (B).	51
Figure 17 General synthetic scheme to produce [PIL]Cl precursors by RAFT polymerization (i) and anion exchange reaction to yield [PIL]MCl _n (ii).	52
Figure 18 Representative ¹ H NMR spectra (DMSO- <i>d</i> ₆) of P([BVMIM]Cl) (A2).	53
Figure 19 ¹ H NMR spectrum of a representative example of P([BVBIM]Cl-co-DMAEMA).	56
Figure 20 SEC traces of the series of P([BVBIM]Cl-co-DMAEMA) (C7 to C11) in aqueous eluent.	57
Figure 21 Monomer conversion and ln([M] ₀ /[M] _t) as a function of time for different compositions of a series of P([BVBIM]Cl-co-DMAEMA) (C1-C4).....	59

Figure 22 Methods for the synthesis of block-like copolymers: A) Synthesis of block copolymers in a conventional multi-step procedure. B) Synthesis of <i>quasi</i> -block copolymers in a one-pot procedure.....	61
Figure 23 Representative SEC traces of MacroCTA I (left) and II (right) and their respective <i>quasi</i> -block derivatives.	63
Figure 24 DOSY NMR spectra in DMSO- d_6 solution of A) PMMA (Sample V) and B) PMMA- <i>b</i> -(P([BVMIM]Cl) (Sample D6).	65
Figure 25 ^1H NMR spectra of P([BVBIM]Cl) (B1) and its anion exchanged chlorozincate derivatives.....	67
Figure 26 Raman spectra of P([BVBIM]Cl) (B1) and its anion exchanged chlorozincate derivatives at $R = 0.25, 0.5, 0.75,$ and 0.8	68
Figure 27 TGA curves of A) P([BVMIM]Cl) (A1) and B) P([BVBIM]Cl) (B1) and its anion exchanged chlorozincate derivatives.....	70
Figure 28 DSC thermograms of P([BVBIM]Cl) (A1) and its anion exchanged chlorozincate derivatives.....	71
Figure 29 Representative pictures of the thermo-responsive behavior of a solution of P([BVMIM]ZnCl $_n$) (M2) in EG (20 mg mL $^{-1}$). B) Temperature and transmittance curves of a solution of P([BVMIM]ZnCl $_n$) (M2) in EG (20 mg mL $^{-1}$) as a function of time. C) Transmittance measurements of P([BVMIM]ZnCl $_n$) (M2) in EG solutions (10 and 20 mg mL $^{-1}$); solid line: heating; dotted line: cooling.....	74
Figure 30 Plots of the A) d_H (nm) and B) derived count rate and PDI as a function of temperature, recorded by DLS, for a solution of M2 in EG (10 mg mL $^{-1}$).	76
Figure 31 T_{CP} dependance on DP of solutions of [PVMIM]ZnCl $_n$ derivatives in EG ($R = 0.75,$ 10 mg mL $^{-1}$).....	77
Figure 32 Transmittance measurements of halometallate PILs M1 and M8 (Table 13) in EG solutions (10 mg mL $^{-1}$); solid line: heating; dotted line: cooling.....	79

Figure 33 SEM images and particle size distributions of polymeric nanoparticles casted at room temperature from solutions of P([BVMIM]ZnCl _n) (M2 , 10 mg mL ⁻¹) in different solvents: A) EG, B) glycerol, and C) 1,3-propanediol.....	81
Figure 34 A) Transmittance measurements solutions of [PIL]ZnCl _n (P([BVBIM]ZnCl _n), M8) and copolymers P([BVBIM]ZnCl _n -co-DMAEMA) with variable molar composition [BVBIM]Cl:DMAEMA = 54:46 and 37:63 in EG (10 mg mL ⁻¹); solid line: heating; dotted line: cooling. SEM images and particle size distributions of polymer nanoparticles casted at room temperature from solutions of [PIL]ZnCl _n B) PDMAEMA- <i>qb</i> -P([BVBIM]ZnCl _n -co-DMAEMA) (M10) and C) PDMAEMA- <i>qb</i> -P([BVBIM]ZnCl _n -co-DMAEMA) (M11) in EG (10 mg mL ⁻¹).	85
Figure 35 Effect of halometallate PIL catalysts (precursors and metal chloride indicated, <i>R</i> = 0.7) on the glycolysis of post-consumer PET and selectivity of BHET.	90
Figure 36 Effect of the amount of standard catalyst on the conversion of PET and selectivity of BHET using different procedures (oil bath and FORMAX platform).	92
Figure 37 Effect of the molar ratio (<i>R</i>) of the [PIL]ZnCl _n (M2 to M5 , Table 13) on the glycolysis of PET and selectivity of BHET (isolated).....	94
Figure 38 Effect of the molar ratio of MPCs (P([BVBIM]ZnCl _n -co-DMAEMA), series C) on the conversion of PET and selectivity of BHET (FORMAX platform, 1 atm, 180 °C, and 4h).	95
Figure 39 Comparison of BHET yield during the glycolysis of PET (170 °C, 8 wt.% catalyst) using SEC and 1H NMR techniques.	100
Figure 40 Effect of A) temperature (8 wt.% catalyst), and B) MPC:PET weight ratio (180 °C), as a function of time, on BHET yield during the depolymerization of waste PET using MPCs.	101
Figure 41 Scheme of the proposed mechanism for glycolysis reaction catalyzed by MPCs.	102

Figure 42 Effect of the coloration of post-consumer PET on catalyzed glycolysis using MPC M9 as catalyst (T = 180 °C, t = 4h, 500 rpm).....	104
Figure 43 A) FTIR and B) ¹ H NMR spectra (DMSO-d ₆) of the main product of glycolysis (BHET) after purification by crystallization.	106
Figure 44 TGA curves of BHET obtained from the glycolysis of A) blue PET, B) black PET, C) green PET, and D) Mixture of blue, black, green, and transparent PET.	107
Figure 45 DSC curves of BHET obtained from A) blue PET, B) black PET, C) green PET and D) Mixture of blue, black, green, and transparent PET.	108
Figure 46 Image of the blue-colored post-consumer PET flakes used in this work (right) and products of glycolysis reaction using a MPC. BHET was obtained as a white crystalline solid (left). The aqueous solution of MPC/EG (yellow solution) was washed with fractions of hexane/diethyl ether (X3) to isolate an organic mixture with remnant dyes (impurities).	111
Figure 47 Effect of the reusability of MPCs on the glycolysis of PET and selectivity of BHET (isolated): A) Catalyst P([BVMIM]ZnCl _n) (M2) and B) Catalyst P([BVBIM]ZnCl _n -co-DMAEMA) (M9); R = 0.75 / T = 180 °C / t = 4h / 500 rpm.	113
Figure 48 SEM images of residual PET after glycolysis catalyzed by MPC C2 : A) shows the overall image of the degraded PET and B) shows the porous surface of PET after the diffusion of the solvent and catalyst. C) EDX spectrum of residual PET after glycolysis (using MPC) and isolation.....	115
Figure 49 Schematic representation of the proposed system for the glycolysis of post-consumer PET, catalyzed by a thermo-responsive MPC, to obtain highly pure monomer BHET.....	116

List of Abbreviations

Abbreviation	Long name
[Bmim]	1-Butyl-3-methylimidazolium
[BVBIM]Cl	1-butyl-3-(4'-vinylbenzyl)-1H-imidazol-3-ium chloride
[BVMIM]Cl	1-methyl-3-(4'-vinylbenzyl)-1H-imidazol-3-ium chloride
[PIL]Cl	Cl-type poly(ionic liquids)
[PIL]MCl _n	Halometallate PIL
[PIL]ZnCl _n	Chlorozincate PIL
ACVA	4,4'-Azobis(4-cyanovaleric acid)
ATRP	Atom transfer radical polymerization
BF ₄	Tetrafluoroborate anion
BHET	Bis(2-hydroxy ethyl) terephthalate
<i>ca.</i>	Latin: <i>circa</i> ; of approximately
CDTPA	4-Cyano-4-[(dodecylsulfanylthiocarbonyl)sulfanyl]pentanoic acid
CHCl ₃	Chloroform
Cl	Chloride anion
Conv.	Conversion
CTA	Chain transfer agent
D	Diffusion coefficient
\bar{M}	Molar mass distribution
d_H	Hydrodynamic diameter
DLS	Dynamic Light Scattering
DMAc	Dimethylacetamide
DMAEMA	2-(dimethylamino)ethyl methacrylate
DMSO	Dimethyl sulfoxide
DMT	Dimethyl terephthalate
DOSY	Diffusion Ordered Spectroscopy
DP	Degree of polymerization
DS	Dimethyl Sulfone
DSC	Differential scanning calorimetry
<i>e.g.</i>	Latin: <i>exempli gratia</i> ; for example
EA	Elemental Analysis
EDX	Energy-dispersive X-ray spectrometer
EG	Ethylene glycol
EtOH	Ethanol

EVA	Ethylene vinyl acetate
FTIR	Fourier transform infrared
H bond	Hydrogen bond
HTE	High Throughput Experimentation
<i>i.e.</i>	Latin: <i>id est</i> ; that is
ILs	Ionic liquids
LCST	Lower critical solution temperature
M	Molar concentration
M/CTA	Ratio of monomer to CTA
M/macroCTA	Ratio of monomer to macroCTA
M ⁺	Positively charged metal ion
macroCTA	Macro chain transfer agent
MCl _n	Halometallate anion
MeOH	Methanol
MMA	Methyl methacrylate
M _n	Number average molecular weight
MPC	Multifunctional polymeric catalyst
MWCO	Molecular weight cutoff
NH	Needle head
NMR	Nuclear Magnetic Resonance
NTf ₂	Bis(trifluoromethanesulfonyl)imid
OAc	Acetic acetate anion
P([BVBIM]Cl)	Poly(1-butyl-3-(4'-vinylbenzyl)-1H-imidazol-3-ium chloride)
P([BVBIM]Cl-co-DMAEMA)	Poly(1-butyl-3-(4'-vinylbenzyl)-1H-imidazol-3-ium chloride-co-2-(dimethylamino)ethyl methacrylate)
P([BVBIM]MCl _n)	Poly(1-butyl-3-(4'-vinylbenzyl)-1H-imidazol-3-ium metal chloride)
P([BVBIM]ZnCl _n)	Poly(1-butyl-3-(4'-vinylbenzyl)-1H-imidazol-3-ium zinc chloride)
P([BVMIM]Cl)	Poly(1-methyl-3-(4'-vinylbenzyl)-1H-imidazol-3-ium chloride)
P([BVMIM]MCl _n)	Poly(1-methyl-3-(4'-vinylbenzyl)-1H-imidazol-3-ium metal chloride)
P([BVMIM]ZnCl _n)	Poly(1-methyl-3-(4'-vinylbenzyl)-1H-imidazol-3-ium zinc chloride)
<i>p.a.</i>	Latin: per annum; per year
P2VP	2-polyvinyl pyridine
PBT	Polybutylene terephthalate
PC	Polycarbonate
PCL	Polycaprolactone

PDI	Polydispersity index
PDMAEMA	Poly(2-(dimethylamino)ethyl methacrylate)
PDMAEMA-qb-P(DMAEMA-co-[BVBIM]Cl)	Poly(2-(dimethylamino)ethyl methacrylate- <i>quasi-block</i> -(1-butyl-3-(4'-vinylbenzyl)-1H-imidazol-3-ium chloride))
PET	Polyethylene terephthalate
PF ₆	Hexafluorophosphate anion
PILs	Poly(ionic liquids)
PLA	Poly(lactic acid)
PMMA	Poly(methyl methacrylate)
PNIPAM	Poly(<i>N</i> -isopropylacrylamide)
PVA	Polyvinyl acetate
PVC	Polyvinyl chloride
R or X_{MCl_n}	Molar fraction of metal chloride anion
RAFT	Reversible Addition-Fragmentation chain Transfer polymerization
RAFT/MADIX	RAFT/macromolecular design via the interchange of xanthates
RI	Refractive Index
RID	Refractive Index Detection
<i>r</i> -PET	Recycled PET
r.t.	Room temperature
SD	Standard Deviation
SEC	Size Exclusion Chromatography
SEM	Scanning Electron Microscopy
T_{CP}	Cloud point temperature
TFA	Terephthalic acid
TFAA	Trifluoroacetic acid
T_g	Glass transition temperature
TGA	Thermogravimetric analysis
THF	Tetrahydrofuran
TPA	Terephthalic acid
UCST	Upper critical solution temperature
UV	Ultraviolet
V_T	Total volume

Chapter 1

Theoretical background

1.1. Introduction

The reduction in the use of natural resources and handling of waste materials are factors of significant impact on environmental conservation practices. Hence, materials recycling and the creation of sustainable chemical practices, currently represent essential research and development efforts. Among these endeavors, research in polyester recycling has received significant attention, focusing on designing of efficient chemical processes to increase performance and productivity.

Polyesters are derivatives from fossil-based resources and have a remarkable number of applications. Nowadays, polyester production has reached more than 70 million tons, *p.a.*⁶ Polyesters with considerable production include polyethylene terephthalate (PET), polybutylene terephthalate (PBT), and polycarbonate (PC).^{7,8} The main applications of polyesters include textile fibers, food storage (bottle containers), household products, electronic products, and coatings. Because of the enormous increase in polyester consumption in recent years and the lack of environmental conservation practices, a significant amount of these materials become waste and accumulate in the environment. Thus, the alerts concerning the climatic change have pointed out plastics as one of the most important pollutants.

Additionally, recent studies have shown the outrageous extent of plastics in the world's oceans, including several studies that have confirmed the presence of microplastics in bottled and tap water.^{9,10} Consequently, polyester recycling and reducing the amount of polyester waste have become important research fields to maintain a sustainable consumption of these materials.¹¹ The following section provides a literature background of methods for the treatment and recycling of post-consumer PET and highlights the most relevant chemical recycling methods including the features provided by novel types of catalysts.

1.2. Synthesis and manufacture of PET

The recycling of polyesters via physical methods is a well-established process at industrial level. Polyesters with a significant recycling rate include mainly post-consumer PET materials, a versatile thermoplastic with a variety of application as fibers, packing films, food containers, and beverage bottles, which have demonstrated a stable increase in consumption since 2008. These products comprise one of the most common materials in landfills.

The wide application of PET is due to its versatile mechanical and thermal properties; furthermore, it is semicrystalline, with high hardness, light weight, transparency, thermal resistance, chemical resistance against oxygen and water, and presents ease of processing. The combination of such properties makes PET a very versatile material and one of the main components in the global consumption of plastics. For instance, more than 50% synthetic fibers and most of the food and beverage containers produced worldwide are based on PET with a global consumption exceeding \$17 trillion dollars *p.a.* The leading producers of this polyester are Du Pont, Eastman Chemical Company, Imperial Chemical Industries and DSM Engineering Plastics, and are commercialized under different names such as Arnitel, Mylar, Rynite, Melinex, among others.¹²

The chemical synthesis of commercial PET is carried out via polycondensation through two different reaction routes. As observed in Figure 2, ethylene glycol (EG) is reacted in the presence of **(1)** terephthalic acid (TFA) or **(2)** dimethyl terephthalate (DMT) to produce the monomer bis(2-hydroxy ethyl) terephthalate (BHET). The reaction **1** is performed at 240 to 260 °C under 3 to 5 kPa of pressure, while reaction **2** is performed at 140 to 220 °C under 100 kPa. After the initial reaction, the transesterification between molecules of BHET occurs to displace EG at 250 to 280 °C and 2 to 3 kPa. The resulting oligomers are then polycondensated at 270 to 280 °C and 100 to 500 kPa. At this stage, the polymer is suitable for applications not requiring high molar masses; however, if higher molar masses are required, the polymer is further subjected to a third solid-state

polymerization, at 200 to 240 °C and 100 kPa. After synthesis, the raw polymer can be processed via extrusion, injection molding, etc.^{1,12}

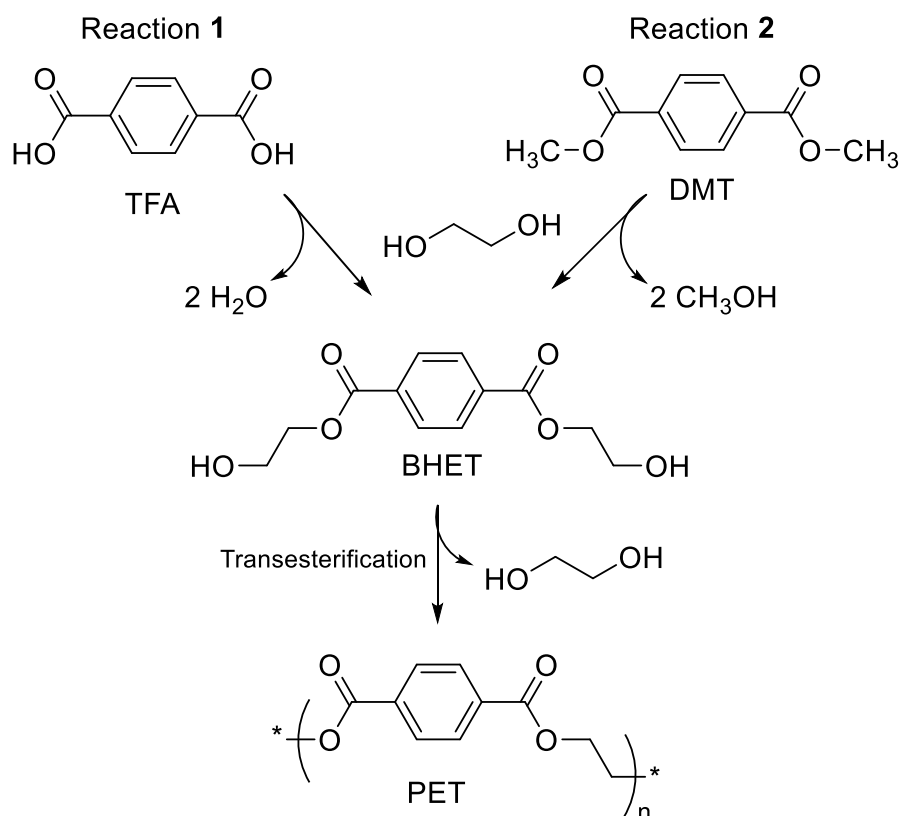


Figure 2 Routes of reaction for the synthesis of commercial PET.

The synthesis of PET usually requires metal catalysts (e.g., Sb, Co, Mn or Ti), such metals can be found in trace quantities (100 to 200 ppm) in the final materials. In addition, according to the final application, the properties of PET materials can be modified by additives added during their processing. Some of the additives with substantial presence in final products of PET are polyvinyl acetate (PVA), polyvinyl chloride (PVC), adhesives, dyes or colorants, ethylene vinyl acetate (EVA), cellulose, UV protectors, and plasticizers.¹³

The processed PET is used in a wide variety of applications due to its excellent properties coupled with a low-cost raw material. This generalized application has resulted in the inevitable creation of large amounts of waste derived from post-consumer PET; which has generated difficulties to manage plastic debris derived from these kinds of materials. There are three main strategies for managing plastic debris: disposing in a landfill, incineration, and recycling. As mentioned below, each method presents limitations:

- **Landfill.** The most significant disadvantage with disposing of plastic waste in landfills is the inevitability of using large spaces. Such areas could be used in more productive activities. Moreover, the slow degradation of most plastics means that the occupied spaces will not be available for long periods. Likewise, plastic debris also acts as secondary contaminants in the environment; by releasing organic compounds of low molar mass such as additives (e.g., acetaldehyde, benzene, xylenes, ethyl benzenes, among others).^{14,15}

- **Incineration.** Incineration overcomes some of the limitations of the elimination of plastic debris in landfills. Incineration of plastic waste might even be used to produce energy. However, incineration releases harmful compounds to the environment, for example, heavy metals, carbon- and oxygen-based free radicals, etc., not to mention the significant amounts of greenhouse gases, especially carbon dioxide.¹⁴ The enormous limitations of post-consumer plastic management via landfills and incineration have increased efforts in the search for recycling methodologies.

- **Recycling.** There are two main strategies for the recycling of PET: mechanical and chemical recycling. Mechanical recycling is a procedure widely applied in industry as a profitable development.¹ On the other hand, chemical recycling is still an emergent technology that allows obtaining recycled monomer through the depolymerization of post-consumer PET. The recycled monomer can be reacted to produce new recycled plastic (*r*-PET). Some of the chemical recycling strategies implemented so far are reviewed next.

1.3. Methodologies for the recycling of PET

PET is considered one of the most recycled materials, and after aluminum, it is the material with the greater commercial value in terms of post-consumer materials. For this reason, the recycling of PET is one of the procedures with more significant implementation in the industry of polymer recycling.² Recycling methods of PET can be categorized into four groups denominated primary, secondary, tertiary and quaternary recycling. Each of those has applicability as a function of the source of raw material and desired products. Table 1 presents some of the factors to consider in the selection of the recycling approach.

The following sections describe the recycling procedures implemented in the depolymerization of PET as a function of its source and cleanness.

Table 1 General factors rated in the selection of PET for recycling processes.¹⁶

Purity	Example of feedstock	Recovery process	General economics of the process	Process convenience
High	Food and beverage packaging of PET	Secondary recycling- Re-melting	Satisfactory	Simple
Medium	Uncoated heavy gauge film fibrous waste, colored PET, coated PET	Tertiary recycling - Glycolysis, methanolysis, etc.	Increasing costs	Increasing complexity
Low	Laminates coated thin gauge film	Pirolysis	Well-established costs	Relatively convenient

1.3.1. Primary recycling

Also known as re-extrusion. It is related to the recycling of post-consumer materials with similar characteristics. Although simple and low cost, this procedure requires decontaminated materials, and can only be used with a single type of feedstock, which makes it an unpopular method in industry.¹²

1.3.2. Secondary recycling

The secondary recycling refers to the mechanical or physical recycling methods, which have been marketed since the 1970's. These methods involve the decontamination of PET and re-processing of pellets by mechanical means. The secondary recycling consists of a series of steps of selecting and sorting, removing contaminants, reducing size by grinding, extrusion by heating, and reformation.¹² The minimum requirements for PET recycling under physical processes are listed in Table 2.

Table 2 Minimum requirements for the physical recycling of PET.

Property	Requirement
Flake size	0-4-8 mm
Melting temperature	>240 °C
Viscosity (η)	> 0.7 dL g ⁻¹
Water content	<0.02 % p/p
Dye content	<10 ppm
PVC content	<50 ppm
Polyolefin content	<10 ppm
Metal content	<3 ppm

Some of the main drawbacks of secondary recycling are related to the heterogeneity of the feedstock materials and the thermal degradation (molar mass and intrinsic viscosity reduction) of the recycled product after each recycling cycle.¹⁷ Another problem is the number of contaminants that can significantly inhibit the recycling process, which can result in severe deterioration of the recycled plastic. For instance, recycled plastic might acquire an undesirable grayish color due to the combination of materials with different coloration.¹⁸ In addition, the presence of additives in postconsumer PET contributes significantly to the decrement of the chemical and physical properties of *r*-PET. For example, PVA and PVC are common additives that can produce hydrochloric and acetic acid during the mechanical recycling process. These acids can act as catalysts for chain cleavage reactions; therefore, producing hydrolytic thermal degradation.¹²

To date, mechanical recycling developments do not resolve the separation of additives or contaminants by well-established procedures. Therefore, the addition of intensive steps for classifying, separating, cleaning, and drying post-consumer materials is strictly necessary. In summary, mechanical recycling methods address the environmental shortcoming of both landfill and incineration methods, but the addition of several exhaustive procedures of sorting and decontamination, make these approaches expensive and inefficient.

1.3.3. Tertiary recycling

The tertiary recycling, commonly known as chemical recycling or chemolysis, comprises the complete or partial depolymerization of polymeric chains of PET down to their monomeric units. Therefore, the monomer can be purified and used as raw material to obtain new materials in fully sustainable upcycling processes.^{3,19}

Among the different methods of recycling, chemical recycling is the only approach accepted as sustainable development –defined as a process that meets the need of the present without compromising the ability of future generations to meet their own needs.³ The chemical recycling of PET does not need the consumption of large amounts of resources (energy, chemicals, and time). In this way, the environment has the least possible impact; however, these developments require large turnovers to be cost-effective.^{16,20}

The dominant mechanism of depolymerization in an acidic and neutral environment consists of three reversible reactions . As shown in Figure 3, in Step I, the carbonyl groups in the polymeric chain undergo protonation to obtain a hydroxyl group in acidic conditions. In Step II, a hydroxyl group, coming from the solvent, slowly attacks the protonated carbon in the ester group. In Step III, the proton in the carbonyl group is quickly removed to form water or alcohol (depending on the solvent) and produce the chain cleavage. It is important to emphasize that the pH of the system influences the depolymerization mechanism; however, the breakdown of the ester groups occurs in any acidic conditions yielding similar products.²¹

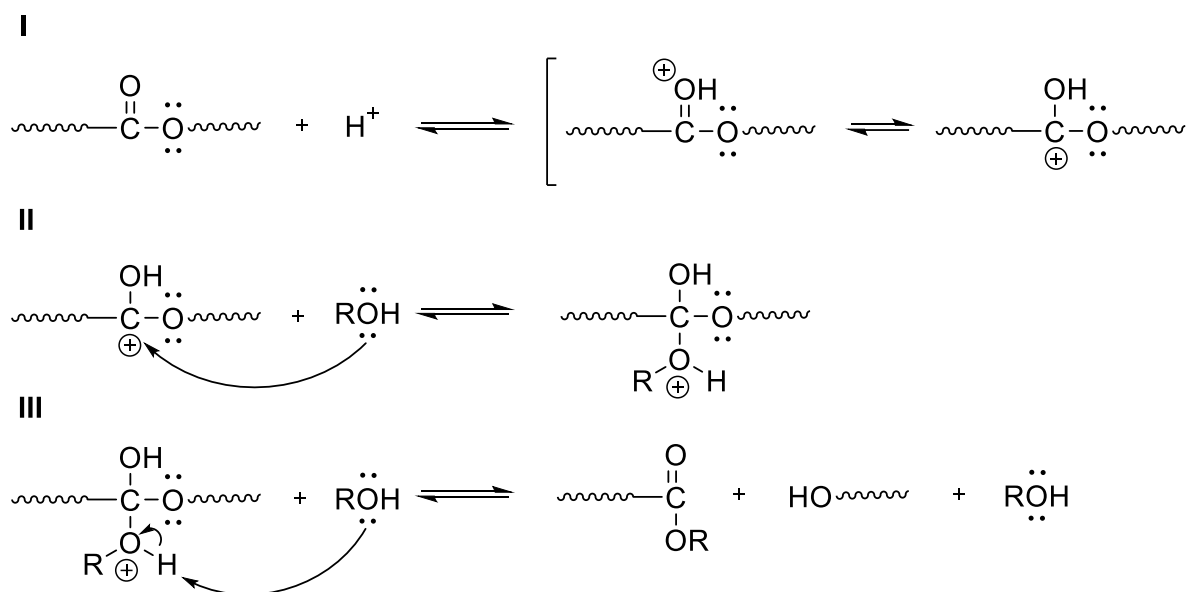


Figure 3 Scheme of the mechanism of depolymerization of polyester in acidic and neutral conditions.

Figure 4 illustrates the main pathways in the chemical recycling of PET. The molecule carrying the hydroxyl group draw the distinction between methods: glycol for glycolysis, methanol for methanolysis, and water for hydrolysis. Other methods include pyrolysis, aminolysis, and ammonolysis.

Since the first patent was published in the 1950's,²² abundant investigations have been carried out to understand the reaction mechanism and improve product performance and process sustainability. Figure 4 summarizes the different routes for PET depolymerization, as well as some examples of derived products. Other condensation polymers such as polyesters, polyamides, polyacetals, and polycarbonates can also undergo the same depolymerization reactions.²³

The depolymerization rate depends on parameters such as temperature, pressure, PET:solvent ratio, and the type and amount of catalyst. Another crucial characteristic of depolymerization reactions is that the transformation from PET to oligomers, dimers, and monomers comprises reversible reactions. Therefore, prolonging the reaction time might lead to an increase in the yield of oligomers as byproducts.²⁴

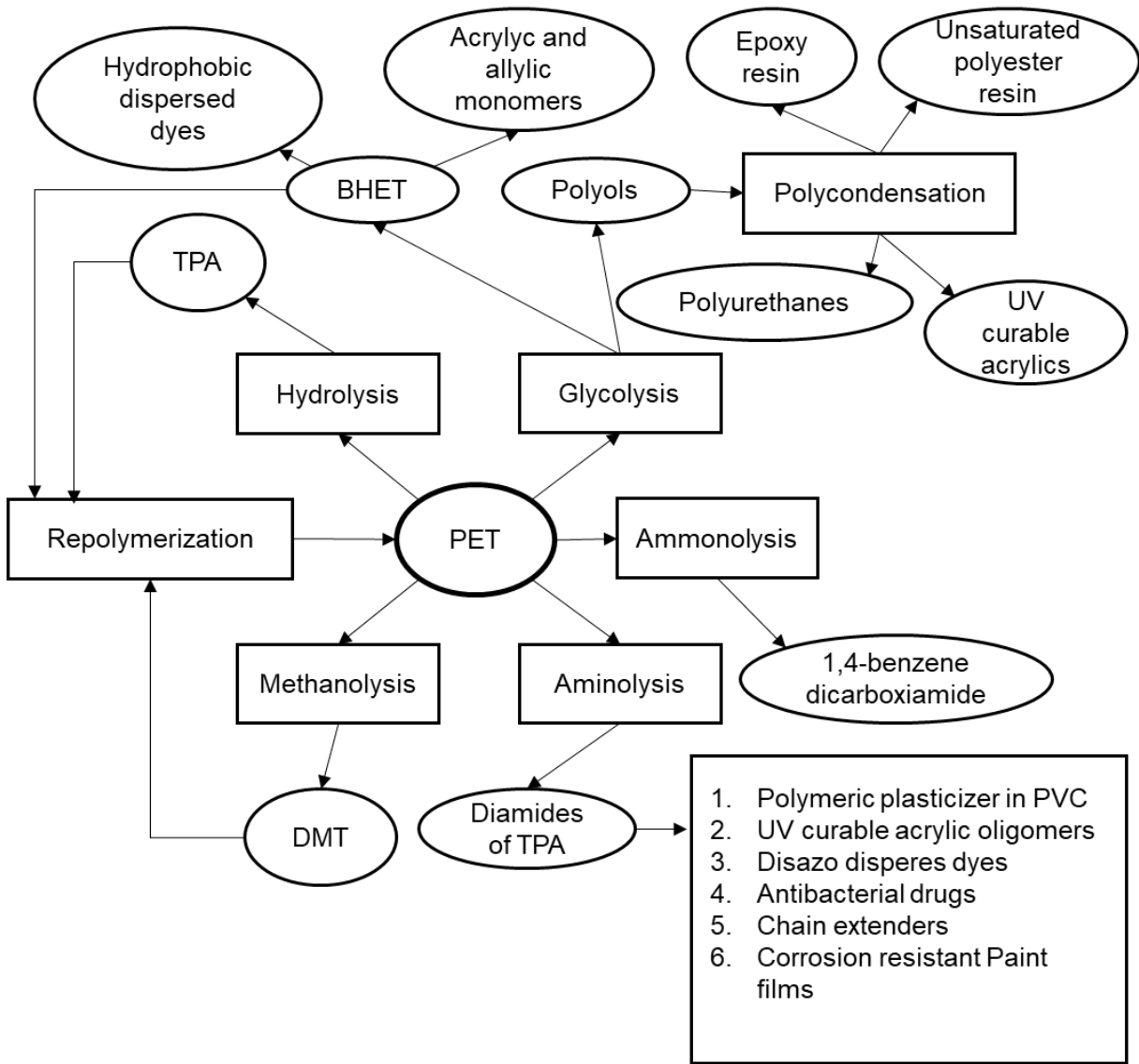


Figure 4 Different methods of PET chemolysis and the value-added products derived therefrom (TPA = terephthalic acid; DMT = dimethyl terephthalate; BHET = bis(2-hydroxy ethyl) terephthalate).²⁴

1.3.3.1. Hydrolysis and methanolysis

The hydrolysis approach involves the depolymerization of PET down to terephthalic acid (TPA) and EG by adding water in an acid, neutral or alkaline environment. According to this method, the most common materials include sulfuric acid for acidic hydrolysis, caustic soda for alkaline hydrolysis, and water or steam for neutral hydrolysis.²⁵ The method of hydrolysis usually requires the presence of metal acetates to catalyze the transesterification reaction. The most considerable disadvantages of this process are the corrosive conditions and the difficulties in recovering the produced TPA, which need several purification steps.^{26,27}

The methanolysis approach involves the depolymerization of PET down to DMT and EG under conditions of high temperature (180 to 280 °C) and pressure (0.2 to 0.4 kPa). The transesterification reaction is usually catalyzed by metal acetates or lead dioxide. After reaction completion, it is crucial to deactivate the catalyst. Otherwise, the product DMT may have losses in subsequent reactions. The products comprise a mixture of glycols, alcohols, terephthalic derivatives, and DMT. Thus, the separation of such a mixture makes methanolysis a costly approach. Albeit methanolysis can withstand contaminants, the presence of water can poison the catalyst and form azeotropes. Currently, methanolysis is a discontinued process in industry, due to the high costs related to the purification of DMT.²⁸

1.3.3.2. Glycolysis

The depolymerization of PET by glycolysis is conducted using EG (or other glycols) to produce bis(2-hydroxy ethyl) terephthalate) (BHET) and other derived oligomers. Subsequently, the obtained BHET and oligomers can be used as recycled monomer to manufacture resins, polyurethanes, copolyesters, acrylic coatings, and hydrophobic colorants. Likewise, the purified BHET can be added together with virgin BHET to produce *r*-PET in either of the main production lines, based on DMT or TPA (Figure 2). The most common solvents include glycols such as EG, triethylene glycol, and dipropylene glycol.²⁹ Glycolysis is the preferred option for producing high-quality *r*-PET; however, it is not a

suitable approach to remove low levels of contaminating impurities, *v.gr.*, copolymers, colorants or dyes, and additives.³⁰

The glycolysis approach involves the transesterification reaction of PET in the presence of an excess of glycol at temperatures in the range of 180 to 240 °C. Since glycolysis is a slow reaction, catalysts are generally required.³¹ Besides its versatility, glycolysis represents the least expensive chemical recycling procedure. Due to these reasons, several investigations have focused on developing sustainable and more efficient glycolysis protocols. The latter through the progress of highly specific and cost-effective catalysts and monomer purification methods. Correspondingly, research on the possible application of glycolysis products has attracted attention in recent years.^{32,33}

The kinetics of PET glycolysis have demonstrated the slow rate of reaction (Figure 5, Route I); in addition, the transformation of PET into BHET remains at low conversion.²⁷ For this reason, numerous efforts have been directed to increase the rate of depolymerization and the selectivity of BHET. The development of efficient catalyst has emphasized on reaching glycolysis procedures under moderate reaction conditions (*e.g.*, temperature, pressure, reaction time, PET/EG ratio, PET/catalyst ratio), and sustainable methods, with the possibility of reusing the catalyst.¹⁸

One of the most studied system to increase the efficiency of glycolysis is catalysis by the addition of metal salts.³⁴ In the catalyzed reaction (Figure 5, route II), the carbonyl groups of the polymer chain of PET become electrophilic by adding a positively charged metal (M^+) to the oxygen atom. Next, the pair of electrons of oxygen, coming from the solvent (EG), initiate the reaction by attacking the electrophilic carbon of the ester group. Finally, the hydroxyl group of the EG forms a covalent bond, which generates the breaking of the polyester chain to form short-chain oligomers and, subsequently, the monomer BHET.³⁵

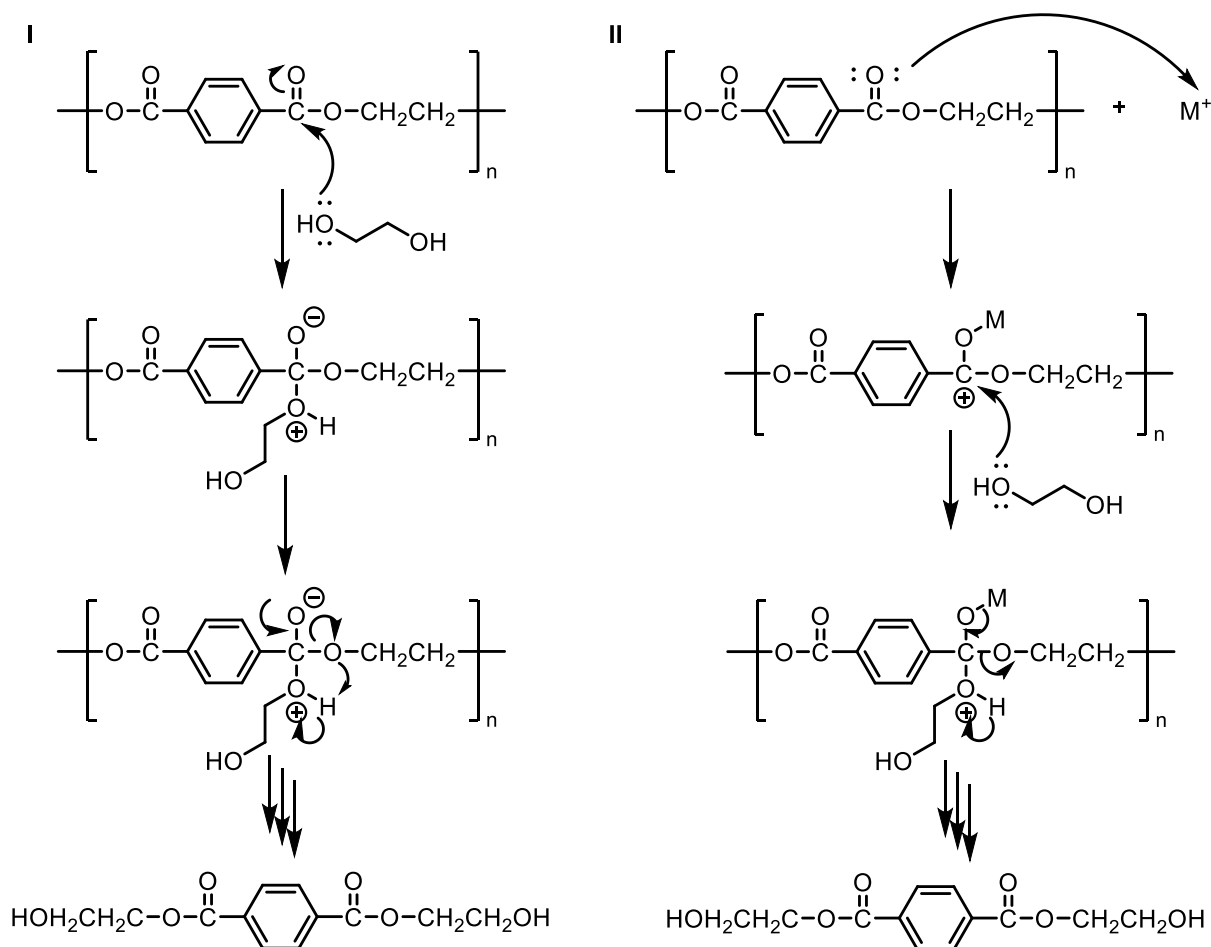


Figure 5 Proposed reaction scheme for the glycolysis of PET (I) and the catalyzed glycolysis of PET with metallic salts (II).

In 1988, Vaidya and Nadkarni reported for the first time the use of zinc acetate as a catalyst for the synthesis of polyols from post-consumer PET.^{36,37} Subsequent investigations have shown that the order of catalytic activity of metallic acetates and other derivatives follows the order $Zn^{2+} > Mn^{2+} > Co^{2+} > Pb^{2+}$; under conditions of 3 hours of heating at 196 °C and a catalyst/PET ratio of 0.01 wt.%.^{31,38}

Several catalyzed glycolysis systems have been based on heavy metals, which adversely affect the environment and act as contaminants in the final products. Some of the latest reports propose using metal chlorides, where zinc chloride ($ZnCl_2$) has exposed the highest yield of BHET (73%).³⁵ To achieve a good outcome and selectivity above 80%, catalytic systems using lower reaction temperatures have been proposed. Previous reports have shown a decrease in the selectivity of BHET due to the high temperatures.

Some of the suggested alternatives include metal oxides and catalysts deposited on silica nanoparticles. In this way, the surface area and the distribution of the catalyst on the support is more extensive, and it has enabled to achieve yields of BHET above 90%.^{39,40}

Likewise, many reports on glycolytic reactions promoted by specific catalysts and reaction conditions have appeared. Table 3 lists some examples of the catalytic systems reported to date. As shown, in recent years, ionic liquids (ILs) have attracted attention as catalysts due to their high catalytic performance and their ability to remain active after several glycolysis cycles; in addition. Remarkably, such results were obtained under mild reaction temperatures ($< 200\text{ }^{\circ}\text{C}$) and atmospheric pressure.¹⁸ The following sections examine some of the conditions reported in ILs-catalyzed glycolysis of PET.

Table 3 Examples of catalysts used in the glycolysis of PET.¹⁸

Catalyst	Yield of BHET [%]	Temp [°C]	Time [min]	EG/PET ratio	Cat/PET ratio [wt.%]	Ref.
Zinc acetate	85.6	196	180	5 wt.%	1.0	Xi <i>et al.</i> , 2005 ³¹
Zinc acetate	63	200	150	2.77 mol%	0.3	Troev <i>et al.</i> , 2003 ⁴¹
Titanium phosphate	98					
Zinc acetate	63	190	480	6 mol%	0.5	Shukla y Kukarni, 2002 ⁴²
Lead acetate	62					
Sodium carbonate	62					
Sodium bicarbonate	62					
Acetic acid	62					
Lithium hydroxide	64	190	480	6 mol%	0.5	Shukla y Harad, 2005 ⁴³
Sodium sulfate	66					
Potassium sulfate	64					
Potassium sulfate	64					
β -zeolite	66	196	480	6 mol%	1.0	Shukla <i>et al.</i> , 2008 ⁴⁴
γ -zeolite	65					
Zinc chloride	73	197	480	10 mol%	0.5	Pingale <i>et al.</i> , 2010 ³⁵
Lithium chloride	59					
Magnesium chloride	56					
Iron chloride	56					
Magnesium Oxide supported on Silica Nano Particles	>90					
Ultrasmall cobalt nanoparticles	77	180	180	27.8 wt.%	1.5	Rinaldi <i>et al.</i> , 2018 ⁴⁵
[Bmim]Cl	>65	190	120	10 wt.%	5.0	Wang <i>et al.</i> , 2009 ⁴⁶
[Bmim]OH	71	190	120	10 wt.%	5.0	Yue <i>et al.</i> , 2011 ⁴⁷
[Bmim]ZnCl ₃	83	180	300	Data not shown	1.0	Yue <i>et al.</i> , 2014 ⁴⁸
[Bmim]MnCl ₃	50					
[Bmim]FeCl ₃	15					
[Bmim]Cl immobilized in bentonite	44	190	180	6 wt.%	3.3	EIMetwally <i>et al.</i> , 2015 ⁴⁹
Metal Organic Frameworks	80	197	100	1 wt.%	1.0	Bai <i>et al.</i> , 2017 ⁵⁰
Graphite carbon nitride	80	196	30	11.1 wt.%	2.5	Su <i>et al.</i> , 2020 ⁵¹

[Bmim] = 1-Butyl-3-methylimidazolium

1.3.3.3. Ionic liquids applied in the catalyzed glycolysis of PET

As discussed, glycolysis is the most straightforward and most efficient approach for the depolymerization of PET. Therefore, it is appealing to make an in-depth review of the latest reports of ILs applied in the glycolysis of PET.

ILs are composed of cations and anions that are found in the molten state below 100 °C. Most ILs are monovalent, and their liquid character is derived from a selection of ionic structures, which tend to coordinate weakly with ions of opposite charge. In addition, ILs have low molecular interaction and asymmetric chemical structures.⁵² Common ILs include structures derived from imidazolium, pyridinium, alkylammonium, alkylphosphonium, etc. Generally, the structure directly influences their properties. The most used anions include a wide range of halides, acidic mineral anions, among others (Figure 6).⁵³ Interest in ILs research is grounded on their distinctive properties, such as low to null volatility, ease of handling, zero flammability, polarizability, high conductivity, solubilizing effects, and catalytic activity in organic reactions.⁵⁴

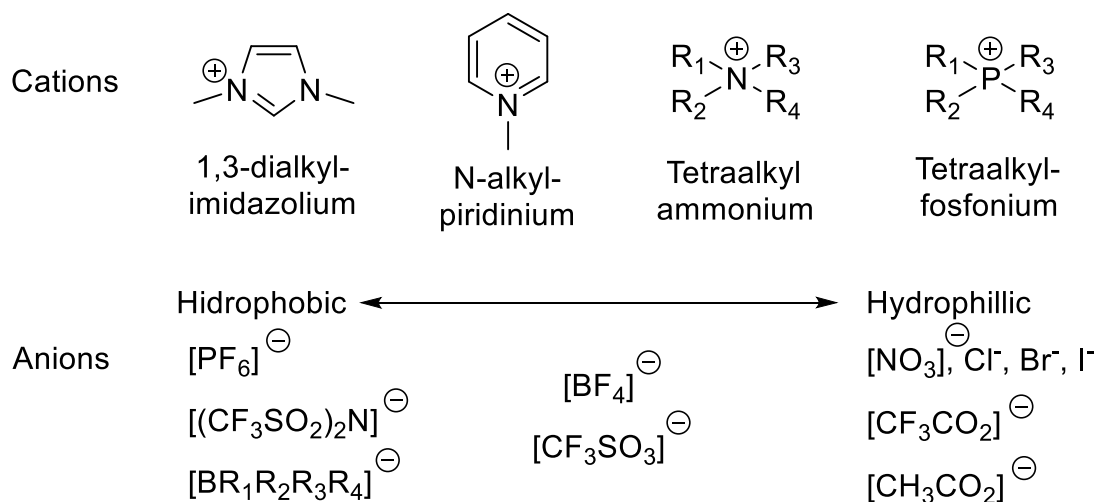


Figure 6 Common cations and anions in ILs.

The first reports on applying ILs as catalysts in PET glycolysis date back to 2009. The exploration of PET glycolysis catalyzed by ILs is driven by the handling simplicity, ease of purification steps for the products, and potential catalyst recovery. In this regard, catalyst separation has many more difficulties in conventional systems, such as catalysts

based on metallic salts, acids, or bases,⁴⁶ where the separation of catalyst from glycolysis products is complex and expensive.

Wang *et al.*,⁵⁵ investigated the potential catalytic activity of acidic, basic and neutral ILs based on imidazolium derivatives. The basic and neutral ILs accelerated the rate of glycolysis, but the synthesis of these type of catalyst is complex and expensive, while the acidic ILs presented chemical instability at temperatures above 180 °C. Therefore, neutral ILs with sound catalytic effects at an affordable price were preferred. It was found that 1-butyl-3-methylimidazolium bromide ([Bmim]Br) and 1-butyl-3-methylimidazolium chloride ([Bmim]Cl) showed the highest activity in the depolymerization of PET, under moderate reaction conditions (180 °C, 8h). The reported PET conversion was above 98%. However, the yield of BHET was not quantified. On the other hand, the possible reuse of [Bmim]Br was accomplished in more than one glycolysis cycle. A kinetic study indicated that the depolymerization of PET in the presence of [Bmim]Br is a first-order reaction with an activation energy of 232.8 kJ mol⁻¹.⁴⁶

Yue *et al.*,⁴⁷ focused on basic ILs as catalyst for the depolymerization of PET. In this case, 1-butyl-3-methylimidazolium hydroxyl ([Bmim]OH) was reported to exhibit higher catalytic activity than neutral ionic liquids [Bmim]Br and [Bmim]Cl. This study showed a PET conversion close to 100%, with a BHET yield of 71% (T =190 °C, 2 h). The catalyst:PET ratio in these reactions increased to 5.0 wt.%, concerning systems with metal salts (0.3 to 1.0 wt.%); however, this excess of catalyst is compensated with the ability to recover and reuse ILs, which maintains the feasibility of the system. Subsequent investigations have shown that ILs with halometallate anions are also effective catalysts in PET glycolysis. As shown in Figure 7, the conversion of PET, using ILs with halometallate anions ([Bmim]MCl_n) under similar conditions, follows the trend [Bmim]ZnCl₃ > [Bmim]MnCl₃ > [Bmim]FeCl₄ > [Bmim]CuCl₃. The maximum conversion of PET was 98%, with a yield of BHET of 83% in optimized systems of [Bmim]ZnCl₃. Furthermore, it was shown that the catalyst could be reused six additional times, without a significant decrease in the yield of BHET.⁴⁸

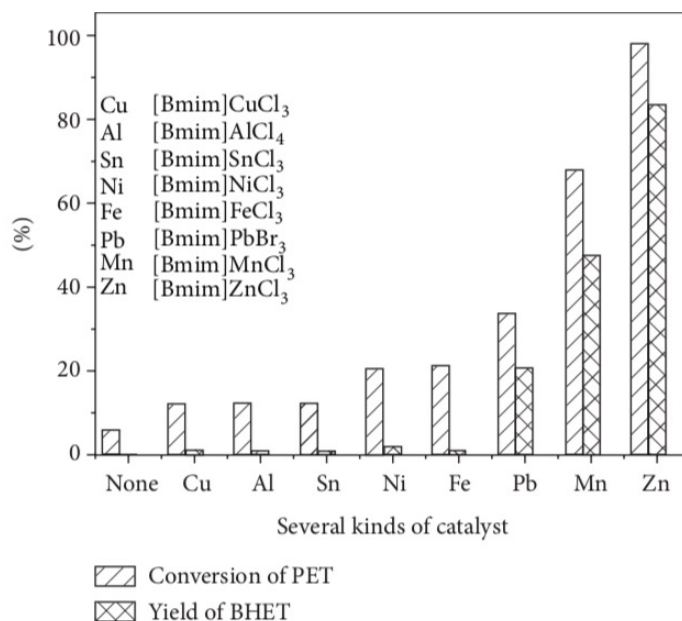


Figure 7 The effect of $[Bmim]MCl_n$ catalysts on the glycolysis of PET. Reaction conditions: PET 2 g, catalyst 1 wt.%, reaction time 5 h, and temperature 180 °C. Reproduced from Yue *et al.*⁴⁸

These results led to the proposal of a glycolysis reaction mechanism similar to the mechanism proposed for catalysis with metal salts. As shown in Figure 8, the initial step of reaction (I) of such catalyzed system involves the interaction of the cation in the catalyst ($[Bmim]^+$) with the carbonyl group of the ester in the polymer chain of PET.

Subsequently, an hydroxyl group, coming from the solvent (EG), attacks the partially positively charged carbon in the ester group, forming a tetrahedral intermediate. At the same step, the hydroxyl group in EG coordinates with the metal anion (MCl_n^-) (I). Next, the electrons in the oxygen coordinated to the $[Bmim]^+$ group are transferred to form the carbonyl group (C=O) again (II). Finally, the acyl-oxygen bond is broken, and the $-OCH_2CH_2-$ group is released, which then forms species of the type $HOCH_2CH_2-$, in combination with protons (H^+) present in the medium. The reaction is repeated n -times inducing the breakdown of acyl-oxygen bonds until the formation of the monomer BHET (III).

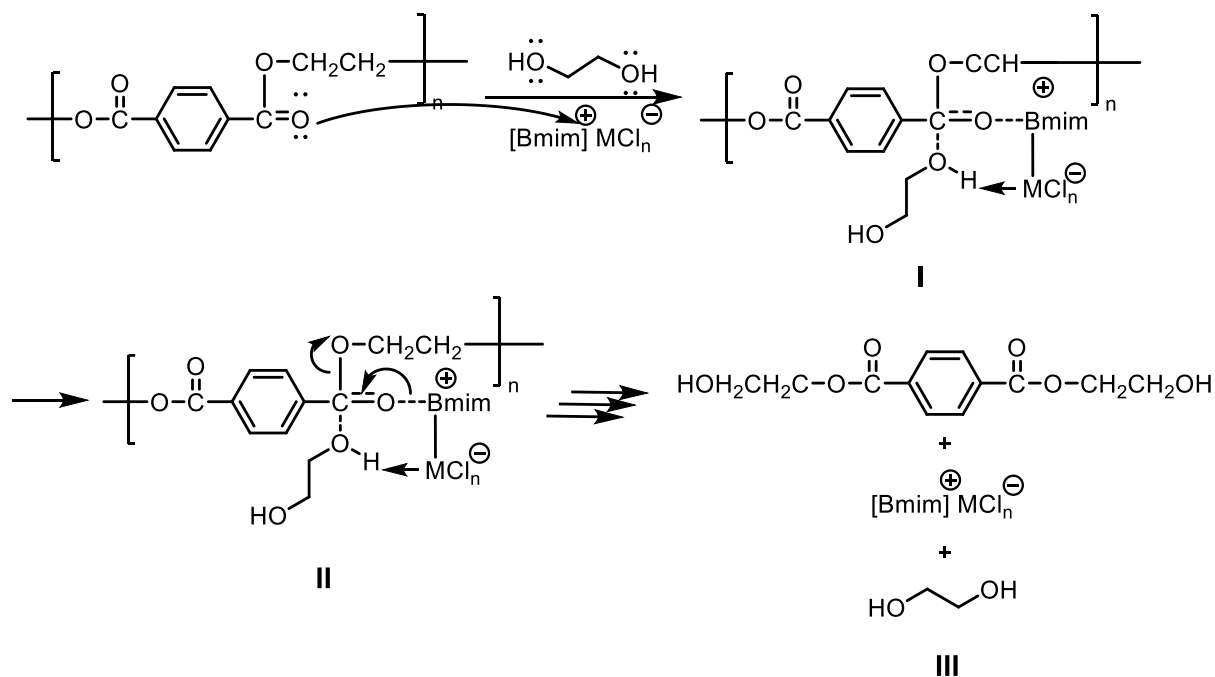


Figure 8 Mechanism of the glycolysis of PET in the presence of metal-containing ionic liquids.

Additional findings regarding the glycolysis procedure indicate the effect of the size of PET flakes. Yue *et al.*, showed that a smaller flake size of the feedstock to be depolymerized aided the conversion and yield of PET and BHET, respectively. This fact is mainly because PET is dissolved slowly in EG during the reaction; therefore, the decrease in size of the material is beneficial to expand the surface area available to carry out the glycolysis reaction.²⁰

1.3.3.4. Separation and reuse of IL catalysts

As described above, to date a wide variety of IL-based catalytic systems have been developed for PET glycolysis. However, two significant drawbacks remain unresolved: (i) high temperatures and pressures are usually needed, (ii) the separation of impurities and catalyst from glycolysis products is considerably challenging, involving several purification steps.⁴⁴ Such steps generally consist of crystallization, filtration, and distillation of the products and catalysts. This operation has been successfully applied in the reviewed reports of IL catalyzed glycolysis;⁴⁶⁻⁴⁸ however, removing impurities or additives (common in post-consumer polyesters), after depolymerization remains as a significant limitation.

We have put forward that the functionalization of ILs might represent a promising pathway to induce the phase separation of catalysts and enhance the separation step of products and catalyst after glycolysis.⁴⁶ One of the first trials to improve the separation methods was immobilizing an IL catalyst on a magnetic support. EIMetwally *et al.*, reported a complex IL catalyst composed of ferrous acetate ([Bmim-Fe][OAc]₃) supported on bentonite (clay composed of multiple minerals). The catalyst yielded a conversion of PET of 100% and a selectivity of BHET of 44%. Although the selectivity of BHET remained low, the upgrading of such a system is the capability to separate the heterogeneous catalyst by simple filtration. Finally, the catalyst was dried and applied in up to six more glycolysis cycles without losing catalytic activity.⁴⁹

The effective catalyst removal from the glycolysis products represents a key opportunity for optimizing the depolymerization of PET catalyzed by ILs. Furthermore, post-consumer PET is a material produced in different grades or qualities (fiber, film, molding, etc.); thus, it may contain multiple components or additives (such as, adhesives, colorants or dyes, polymeric additives, plasticizers, UV protectors or stabilizers for processing, among others).^{29,56,57} Such additives, although in low concentrations, interfere during and after the recycling procedures. These impurities generate recycled materials with inadequate mechanical properties and material degradation during reprocessing.^{1,58} Similarly, the low purity of recycled materials prevents its re-integration to food-grade applications, the main area of application of PET.⁵⁹

In the search for methods that allow the separation of additives, byproducts, and impurities from the glycolysis products, some of the latest developments suggest using supported ILs on nanoparticles as catalyst. The technology patented by Vilaplana-Artigas *et al.*,⁶⁰ comprises the use of a complex catalyst formed by [Bmim]Cl or [Bmim]FeCl₄ supported on metallic nanoparticles (Fe₂O₃). The catalyst also contains hydrophobic segments, which encapsulate the colorants and impurities from post-consumer PET. The catalyst also permits an effective glycolysis yield of up to 92% conversion of PET. Once the depolymerization is completed, the separation of the catalyst and purification of BHET was conducted by adding of water and applying magnetic fields. This methodology allowed the separation of two phases: aqueous phase, composed of BHET/EG/H₂O; and

the organic phase, sediment formed of catalyst and colorants. The catalyst can be redispersed in EG for further glycolysis cycles. In this approach, the magnetic catalyst is simply recovered by applying a magnetic field; and the pre-treatment procedures of selection and cleaning of PET are moderate. Furthermore, this technology could be applied in the recycling of different colorations or grades (fiber or film) of PET.^{59,60}

The described approach represents an important advance for optimizing catalysts with separation capabilities after the glycolysis reactions. However, the use of magnetic particles at an industrial scale represents a disadvantage in implementing magnetic fields for large-volume reactors. For that reason, Vilaplana-Artigas suggest the optimization of the system using other separation techniques such as temperature or centrifugation, however these approaches were not explored in detail (example 8).⁶⁰

As described above, for homogeneous catalysts, such as ILs and metallic salts, the main challenges depend on the probable residuals left in the final products of depolymerization which may have detrimental effects on the quality of the same. Additionally, the operations for isolating and recovering the catalysts from the products are complex and time-consuming. For solid heterogeneous catalyst, such as supported ILs, their poor dispersity and large size limited the contact between catalytic sites and ester groups of PET chains, which reduced the catalytic performance; considered as the main weakness of these type of catalysts. All things considered, it is necessary to develop new kinds of catalysts, with good catalytic performance, straightforward reusability, and capabilities to remove catalysts and common contaminants from the depolymerization products.

1.3.4. Polymers derived from Ionic Liquids

In recent years, the polymerization of monomeric ILs has emerged as a novel platform to combine the advantages of ILs with the general properties of polymers.^{61,62} Poly (ionic liquids) (PILs) have attracted interest in materials science, not only due to the combination of the unique properties of ILs, but also in the search for the creation of new properties and functions. The main advantages offered by PILs are properties such as low glass transition temperature (T_g), which offers new processing possibilities to manufacture ionic polymers as functional materials; in addition to mechanical stability and durability.⁶³

PILs can be synthesized via two basic strategies: (1) direct polymerization of IL monomers, and (2) chemical modification of existing polymers.⁵³ Currently, the chemical structure of IL monomers is dominated by the polymerization of imidazolium-type compounds, which can be sub-classified into three groups: vinyl imidazolium, styrenics, and acrylamides (Figure 9).

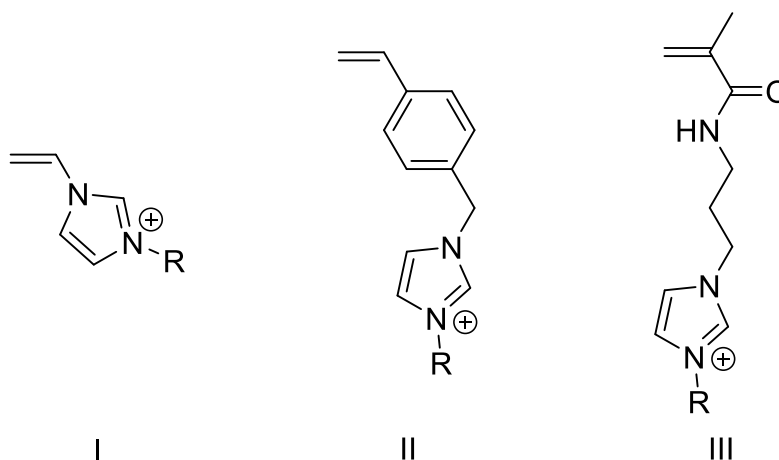


Figure 9 Examples of imidazolium-type IL monomers with extended use in the synthesis of PILs: (I) vinyl imidazolium, (II) styrenics, and (III) acrylamide derivatives.

In the last decade, the manufacture of PILs has become an important field in polymer science.^{61,62} The development of reversible-deactivation radical polymerization techniques such as reversible addition-fragmentation chain transfer polymerization (RAFT), and atom transfer radical polymerization (ATRP) has potentialized the production of PILs with well-defined properties.^{64–68}

The ATRP technique was the first approach for the synthesis of PILs. However, there are drawbacks to maintain control over molar mass and distribution of the final polymers; due to the possible complexation and/or ion exchange of the copper catalyst, used in ATRP, with the ionic sites of ILs and PILs formed.^{69,70} The key advance in the control of the molecular structure of PILs was developed via the polymerization of IL monomers by the RAFT technique. Since the RAFT technique does not involve using metallic salts, the problems mentioned for ATRP approaches are avoidable. Moreover, taking advantage of the living nature of the RAFT technique, several researchers have been able to access block copolymers with PIL segments.⁷¹

It is worth noting that the chemical structure of the IL monomers has a critical influence on the selection of RAFT agents (or chain transfer agents (CTA)). For instance, for acrylamide and styrenic IL monomers (Figure 9), the ionic site is separated from the vinylic group; in this approach, the RAFT polymerization proceeds without any alteration from the cationic imidazolium ring. On the other hand, the polymerization of N-vinylimidazolium type monomers is more challenging, since the radical species generated are highly reactive, due to their non-conjugated nature. Dithioester-type CTAs control well the polymerization of methacrylate and styrenic IL monomers, however, suitable conditions to control the polymerization of N-vinylimidazolium monomers are more problematic to find by conventional RAFT.⁷² RAFT/MADIX (macromolecular design via the interchange of xanthates) controlled polymerization is tolerant to radical polymerization of non-conjugated monomers, which has been employed in the synthesis of polymers derived from N-vinylimidazolium-type PILs.⁷³

As noted above, alternatively, the synthesis of PILs can be achieved by chemical modification of existing polymers, *i.e.*, using a polymeric template and attaching the IL fragments to it. The advantage of this approach is that the resulting PILs will adopt the same degree of polymerization, macromolecular architecture and molar mass distribution as their precursor polymer, avoiding the synthesis and polymerization of IL monomers. Such a strategy is fundamental when a direct polymerization route cannot yield the desired PIL structures or properties, for example, PILs with ultra-high molar mass.⁷²

In recent years, the introduction of PILs in block copolymer systems has been a topic of particular interest. This novel family of copolymers imparts the unique properties of PILs and is complemented by the features of structural stability, additional mechanical properties and/or stimuli-responsive behavior, conveyed by the polymeric segments. These characteristics provide the copolymer with unique capabilities such as self-assembly properties or response to external stimuli (ionic strength, temperature, pH, etc.), which can be exploited in novel applications.⁷⁴ This strategy has been explored in the search for copolymers with specific properties for their application as energy conversion devices,⁷⁵ gas separation,⁷⁶ precursor of nanostructured materials,⁶⁷ oil recovery,⁷⁷ polyelectrolytes,⁷⁸ among others.⁵³ The following section describes examples of recent reports on the synthesis of PILs with response to external stimuli, one of the most attractive fields in the research and development of PILs.

1.3.4.1. PILs as materials with response to external stimuli

To date, reports of PILs with response to external stimuli are scarce. Thermo-responsive PILs are some of the unusual examples in literature. Two methodologies are mainly employed for the production of PILs sensitive to external stimuli: (i) specific ILs and polymers are mixed by different routes to form non-covalent bonds, and (ii) IL monomers are grafted to or copolymerized with other monomers or polymers via covalent linkages.⁷⁹

Thermo-responsive polymers are a type of stimuli-responsive polymers that can undergo phase transitions in solution. Generally, they are classified into (i) lower critical solution temperature (LCST)-type polymers that undergo solution phase separation at an elevated temperature and (ii) upper critical solution temperature (UCST)-type polymers that undergo solution phase separation at a reduced temperature. Thermo-responsive polymers bearing IL functionalities (PILs) can show LCST-type as well as UCST-type phase behaviors in various solvents depending on the balance of hydrophilicity and hydrophobicity between cations and anions of the ionic moieties.⁸⁰ As a relatively new variety of stimuli-responsive polymers, thermo-responsive PILs encompass the unique combination of properties derived from ILs and thermo-responsive polymers which are expected to show highly specialized applications.

One of the first reports of these types of PILs was from Antonietti *et al.* who synthesized doubly hydrophilic copolymers by RAFT/MADIX polymerization. The copolymers composed of PNIPAM (poly(*N*-isopropylacrylamide)) and PILs derived from monomers based on 1-vinylimidazolium demonstrated temperature-sensitive behavior. The non-ionic segments of the copolymers are soluble in aqueous solutions, but the increase of temperature triggers an LCST transition of the PNIPAM block, which is manifested by the desolvation and subsequent precipitation of the polymers; *i.e.*, there is a change of hydrophilicity in the polymer system, which generates a change in morphology of the polymer as a function of temperature. Similarly, the response to ionic strength in the PIL segment was demonstrated by adding KBr salt to aqueous solutions of P(NIPAM-*b*-PIL). As illustrated in Figure 10, the addition of KBr induces the collapse of the PIL segment by electrostatic repulsion and increasing the temperature of the solution prompts the precipitation of the PNIPAM segment. These stimuli-responsive PILs were evaluated as a precursor of mesoporous graphitic materials.^{67,81}

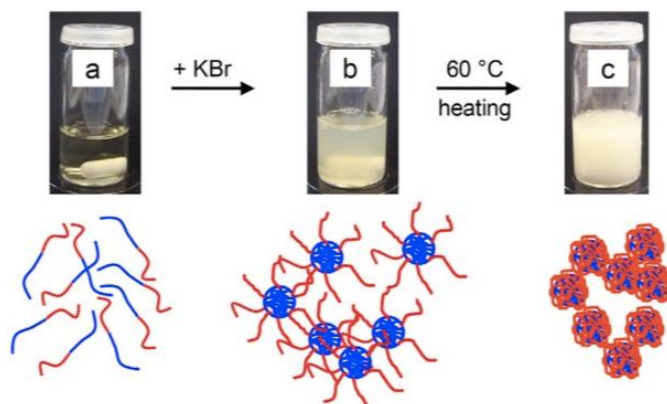


Figure 10 Photographs of 2 wt.% solution of P(NIPAM-*b*-PIL) (a) in water at room temperature, (b) in 1.1 M aqueous KBr at room temperature, and (c) in 1.1 M aqueous KBr at 60 °C.

Yuan *et al.*, extended the previous study using PILs based on vinyl imidazole with long-chain alkyl substituents.⁸² As shown in Figure 11, the synthesis of nanoparticles ($d_H = 25$ to 120 nm) was achieved by polymerizing vinyl imidazole monomer in aqueous dispersion. Afterward, a thermo-responsive segment of PNIPAM was grafted to the surface of the PIL nanoparticles through ATRP. In this way, the size of nanoparticles was tuned as a function of temperature and ionic strength.

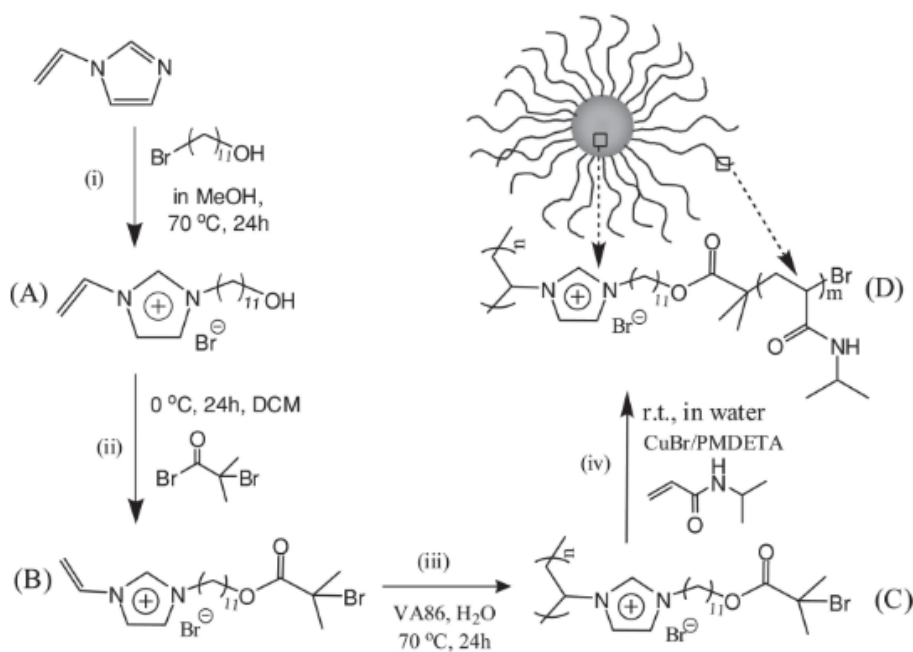


Figure 11 Chemical structures and the synthetic route to spherical polymer brushes with a PIL core and a PNIPAM shell. Reproduced from Ref. 82

In similar approaches the groups of Lu *et al.*,⁸³ and Mori *et al.*,⁸⁴ have reported the synthesis of nanoparticles stabilized by ionic interactions, which copolymerized with NIPAM are sensitive to pH and temperature in the same system. In this way, the nanoparticle size could be modified through external stimuli and the structure of the copolymer.⁸⁴

Another interesting feature of PILs is the ability to modify the ionic strength and hydrophilicity of the system by anion exchange reactions. For instance, imidazole-based PILs (see for instance Figure 12) can show different solution behavior in aqueous or organic solutions via anion exchange with hydrophobic counter anions, such as PF_6^- , BF_4^- , and NTf_2^- .⁸⁵ Thus, the acidity of the protons in the imidazolium cation is modified by the presence of anions, which governs the formation of hydrogen bonds with the solvent. In this manner, the hydrogen bonds in the polymeric solution are modified as a function of temperature. Interestingly, due to that feature, anion exchanged imidazolium PIL derivatives can also show LCST or UCST behavior in aqueous and organic solvents, such as chloroform, acetone, benzene, methanol, ethanol, among others.^{80,86,87}

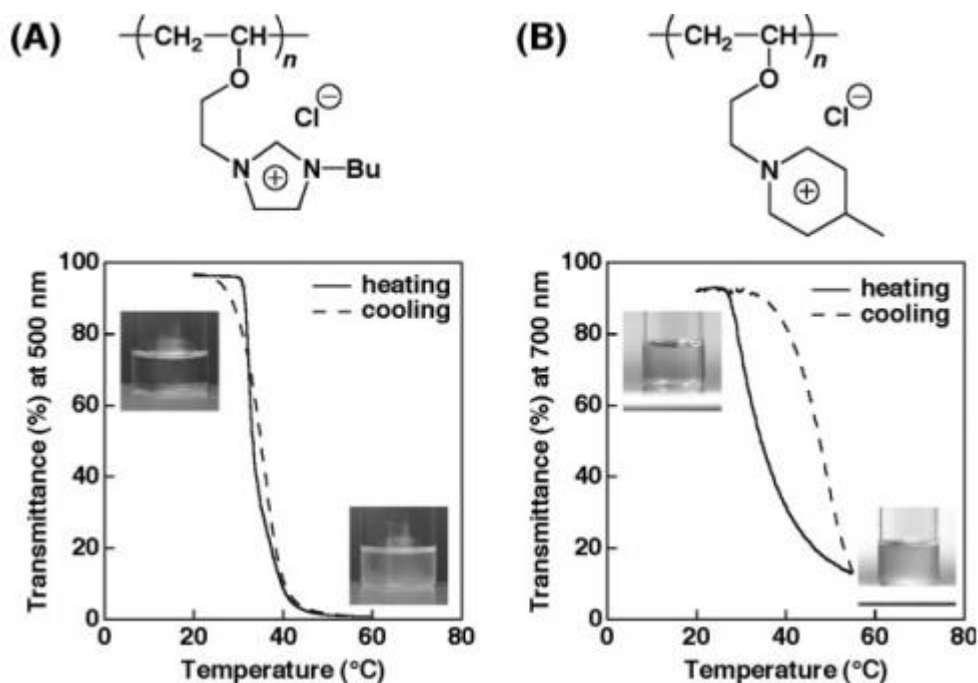


Figure 12 Transmittance measurements of (A) [PIL]Cl derived from butyl imidazole and (B) [PIL]Cl derived from methylpyridine in chloroform; straight line: heating, broken line: cooling. Reproduced from Ref. 85.

These studies exemplify the (co)polymerization of IL monomers as a potential and accurate method to control the phase behavior of polyelectrolytes in an aqueous or organic solution. Thus, towards the fine-tuning of PIL (co)polymers, anion exchange reactions represent a promising pathway to create polymeric materials with distinctive properties and applications.

1.3.4.1.1. Potential applications of thermo-responsive PILs

Initially, research on PILs began in the search for solid polyelectrolytes as candidates for conductive materials. Given the unique combination of physicochemical properties of PILs, various kinds of highly specific applications are expected by exploiting their thermo-responsive behavior. Currently, some research groups have extended the application of PILs including polymeric electrolytes, stabilizers, materials with active anions, carbon production, catalysis, CO₂ separation and transformation, energy harvesting, sensors, catalytic supports, among others.⁷²

Moreover, as shown in the examples referred above, the copolymerization of PILs with other stimuli-responsive monomers have boosted the potential applications of PIL derivatives. For instance, the research groups of Antonietti M. *et al.*⁶⁷ and Mecerreyes D. *et al.*^{71,78} have reported interesting PIL-based materials to accomplish specialized applications, for example carbon precursors,⁶⁷ oil recovery,⁷⁷ polyelectrolytes,⁷⁸ among others.⁵³

The distinctive mechanical stability of PILs, respect to their IL precursors, also makes them appropriate materials for catalyzed reactions. The application of PILs in catalysis can be classified into three types according to their function in the catalyzed reaction: (i) catalyst, (ii) pre-catalyst, or (iii) catalyst support. The ease of fine-tuning the properties of the PILs through anion exchange or macromolecular structure and modern processing techniques have boosted the development of catalysts with possibilities for recycling and reuse. Currently, there is a significant trend to exploit PILs as heterogeneous catalysts to tackle the deficiencies of ILs systems grafted onto solid particles.⁷² Similarly, different reports point out ILs as catalyst in important organic reactions, such as alkylation, ring opening, hydrolysis, Diels-Alder, oxidation, reduction, transesterification, to mention a few.⁸⁸⁻⁹¹ Therefore, PILs, with defined structure and properties, represents an area of potential application for the synthesis of polymeric catalysts, which can deliver excellent catalytic performance different reactions, and at the same time, fulfill complementary functions originated from the functionalities included in the polymer chain.

This research proposes to take advantage of the PILs catalytic activity and functionalization through copolymerization with stimuli-responsive polymers. Particularly, the design of copolymers able to fulfill the essential aspects involved in a sustainable development of chemical recycling methods.

1.4. Summary

Recent developments in the design of chemical recycling methods of post-consumer PET have been summarized in this theoretical background. The basis of PET depolymerization is a catalyzed transesterification reaction. These procedure has several challenges to overcome, such as achieving high catalytic performance with under mild reaction conditions and removing of impurities and catalysts from depolymerization products and solvents. As reviewed, another of the key barriers in the chemical recycling of PET is finding a method to operate with mixtures of raw materials irrespective of its coloration, cleanness, and grade.

Given the exceptional physicochemical properties of PILs, we anticipate that PIL-based catalysts have potential to show additional features depending on their structural diversity, composition, etc. Hence, the utilization of PIL systems as catalysts provides the opportunity to discover attractive features that may further upgrade the capabilities of chemical recycling developments.

This research investigation is focused on the design of multifunctional polymer catalysts (MPCs) based on functionalized PIL (co)polymers. As described in the referenced literature, IL and PIL derivatives with tailored structure and properties, represent novel materials with potential application as catalysts in relevant chemical reactions. Thus, MPCs encompassing ionic and thermo-responsive functional groups could catalyze the glycolysis of PET and remove the catalyst and impurities after the reaction.

The technology to remove the color, impurities, and catalyst from products of glycolysis is a current handicap to improve in chemical recycling methods. By implementing MPCs, it is envisioned to develop a feasible and cost-effective method to obtain high purity monomer via a quasi-homogeneous catalyzed glycolysis.

This critical aspect could be achieved by the removal of color and impurities along with catalyst recovery using the stimuli-responsive functionalities of the MPCs. Therefore, it is expected to increase the amount of recyclable post-consumer polyesters, become less dependent on fossil-based resources, and contribute to the circular economy. Furthermore, although the production of specialized polymeric materials has been explored by several authors to create complex catalysts,⁷² systematic research of polymeric catalysts remains as an unexplored and complex field of study. Therefore, in this investigation, we expect to produce early investigation in the development of MPCs that encompass the catalytic properties of ILs and the structural and functional properties of polymers. To this end, this research proposes the use of High Throughput Experimentation (HTE) procedures to synthesize and examine the catalytic performance of the MPCs in the glycolysis of PET.

1.5. Hypothesis and research objectives

1.5.1. Hypothesis

The use of multifunctional polymer catalysts (MPCs) could lead to efficient polyester depolymerization developments. If a polymeric catalyst is provided by specific functionalities: (i) to perform the glycolysis of PET in high yield (PIL segment); (ii) to perform the separation of impurities and additives (impurity-compatible segment); and (iii) to allow the recovery of catalyst through the application of an external stimuli (stimuli-responsive segment), then the efficiency of the catalyzed glycolysis of polyesters could be boosted to tackle the current disadvantages of chemical recycling developments.

1.5.2. Objective

This project is aimed to design and synthesize MPCs of well-defined structure and properties, for their screening as novel catalytic systems in post-consumer PET depolymerization via catalyzed glycolysis. Such MPCs must be able to catalyze the depolymerization of post-consumer PET, capture additives and impurities, and allow the separation and recovery of the catalytic systems from the products. Altogether, it is envisioned to develop of a highly efficient approach to obtain highly pure recycled monomer, which could be used as feedstock to produce of new food grade materials in fully sustainable recycling approaches.

1.5.2.1. Specific objectives

1. To design and synthesize stimuli-responsive PILs based on imidazolium functionalities and well-defined properties via RAFT polymerization.
2. To characterize the physicochemical properties of a library of MPCs composed of homopolymer, statistical copolymers, *quasi*-block, and block copolymers.
3. To study the solution properties of the libraries of MPCs in aqueous and glycol solutions.
4. To develop first studies in the application of MPCs derived from halometallate PILs.
5. To develop a HTE procedure for the screening of MPCs in PET glycolysis.
6. To perform an optimization examination for the glycolysis of PET by selecting suitable MPCs and conditions of reaction through HTE.
7. To develop an efficient purification procedure to obtain highly pure BHET monomer from the glycolysis of post-consumer PET feedstocks of variable coloration.
8. To develop a isolation method for the MPC and impurities after the reaction of glycolysis.

Chapter 2

Experimental section

2.1. Materials

Synthesis of MPCs: 1-Methyl imidazole (99%), 1-butyl imidazole (98%), and the monomers 2-(dimethylamino)ethyl methacrylate (DMAEMA, 98.5%), methyl methacrylate (MMA) and 4-vinylbenzyl chloride (90%) were acquired from TCI Chemicals. Monomers were treated with inhibitor removers (Aldrich) prior to use. The thermal initiator 4,4'-Azobis(4-cyanovaleric acid) (ACVA, 75%) and the internal reference 1,3,5-trioxane (>99%) were acquired from Aldrich and used without further purification. The RAFT agent 4-Cyano-4-[(dodecylsulfanylthiocarbonyl)sulfanyl]pentanoic acid (CDTPA) was acquired from STREM Chemicals and used as received. The salts used for anion exchange (ZnCl_2 (98%), $\text{CuCl}_2 \cdot 2\text{H}_2\text{O}$, (99%), FeCl_3 (99%), CoCl_2 (98%), and NaBF_4 (98%) were acquired from Aldrich and used as received.

Polyethylene terephthalate (PET) degradation: PET flakes ($A \sim 2 \text{ mm}^2$) were obtained from post-consumer food containers and soft drink bottles of different colorations. Before the glycolysis procedure, the PET flakes were washed with H_2O and methanol (three times each). The final flakes were filtrated, dried in a vacuum oven at $90 \text{ }^\circ\text{C}$ for 12 h, and stored before use. Dimethyl Sulfone (DS, 99%), ethylene glycol (EG, 99%), glycerol (99%), and 1,3-propanediol (98%) were acquired from Aldrich and used as received.

2.2. Synthesis of IL monomers

A slightly modified procedure from the literature was used for the synthesis of the ionic monomers.⁹² Briefly, 1-butylimidazole (8.03 g, 8.5 mL, 64.6 mmol) and 4-vinylbenzyl chloride (9.75 g, 9.0 mL, 63.9 mmol) were dissolved in CHCl_3 (80 mL) in a 250-mL round-bottom flask. N_2 was sparged in the solution for 20 minutes to remove O_2 , after that, the solution was heated at reflux ($45 \text{ }^\circ\text{C}$) for 24 h. The reaction was then stopped and allowed to cool to room temperature. Then, the mixture was extracted with water (3 x 20 mL), and the aqueous phase was freeze dried to remove the solvents. Finally, 12.6 g (71% yield) of 1-butyl-3-(4'-vinylbenzyl)-1H-imidazol-3-ium chloride ([BVBIM]Cl) were obtained as a colorless viscous liquid. The same procedure was followed for the synthesis of 1-methyl-

3-(4'-vinylbenzyl)-1H-imidazol-3-ium chloride ([BVMIM]Cl) (72% yield), using 1-methylimidazole as reactant.

- ^1H NMR of 1-methyl-3-(4'-vinylbenzyl)-1H-imidazol-3-ium chloride ([BVMIM]Cl).

^1H NMR (DMSO- d_6 , 300 MHz) δ = 9.51 (s, 1H, N-CH), 7.99 – 7.67 (m, 2H, CH=CH), 7.65 – 7.28 (m, 4H, ArH), 6.74 (dd, J = 17.7, 10.9 Hz, 1H, Ar-CH), 5.87 (dd, J = 17.6, 1.0 Hz, 1H, CH=CH), 5.47 (s, 2H, N-CH₂), 5.29 (dd, J = 10.9, 1.0 Hz, 1H, CH=CH), 3.87 (s, 3H, N-CH₃).

- ^1H NMR of 1-butyl-3-(4'-vinylbenzyl)-1H-imidazol-3-ium chloride ([BVBIM]Cl).

^1H NMR (DMSO- d_6 , 300 MHz) δ = 9.93 (s, 1H, N-CH), 8.00 (dd, J = 16.2, 1.7 Hz, 2H, CH=CH), 7.62 – 7.31 (m, 4H, ArH), 6.69 (dd, J = 17.7, 10.9 Hz, 1H, Ar-CH), 5.82 (d, J = 17.7 Hz, 1H, CH=CH), 5.56 (s, 2H, N-CH₂), 5.23 (d, J = 10.9 Hz, 1H, CH=CH), 4.22 (t, J = 7.2 Hz, 2H, N-CH₂), 1.73 (p, J = 7.3 Hz, CH₂-CH₂), 1.18 (h, J = 7.4 Hz, 2H, CH₂-CH₂), 0.81 (t, J = 7.3 Hz, 3H, CH₂-CH₃).

2.3. Synthesis of polymer libraries

Polymerizations were performed in an automated parallel synthesizer (ASW2000, Figure 13A) from Chemspeed Technologies AG (Switzerland). The synthesizer was equipped with a reactor blocks consisting of 4 or 16 glass reaction vessels (100 and 13 mL, respectively) provided with thermal jackets connected in series through the reaction block to a heating/cooling system (Hüber, -20 to 140 °C) and a vortex agitation (up to 1400 rpm). Besides, each reaction vessel was equipped with a cold-finger reflux condenser (~5 °C). A liquid handling system composed of a needle head (NH) was used for liquid transfers. The NH was connected to a solvent reservoir bottle (ethanol (EtOH)) for needle rinsing after each liquid transfer. Before each experiment, the reaction vessels were heated to 130 °C followed by applying 10 cycles of vacuum and filling with nitrogen (2 minutes each) to deplete moisture and oxygen. After this pre-treatment, RAFT polymerization experiments were performed according to the procedures described in the following sections.

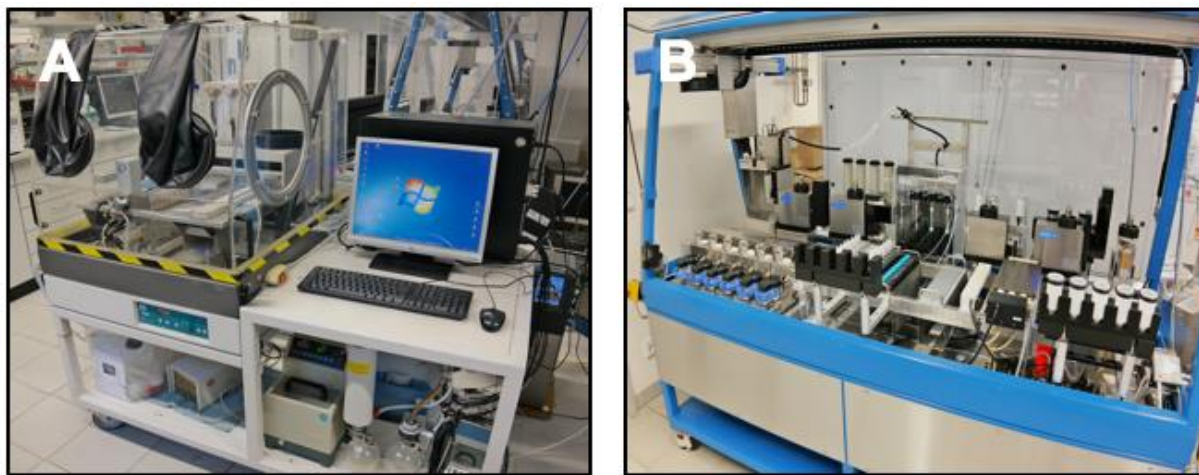


Figure 13 Pictures of the automated parallel synthesizers used in this work: A) ASW2000 and B) FORMAX.

2.4. Synthesis of (co)polymer PIL precursors

Figure 17 describes the followed synthetic route to produce [PIL]Cl precursors (Cl-type PILs). A series of PILs with variable degrees of polymerization, composition and structure were obtained according to the RAFT agent fraction, monomer, and methodologies. A representative synthesis procedure is as follows: a septum sealed flask was charged with the stated quantities of [BVBIM]Cl, comonomer, ACVA, CDTPA and 1,3,5-trioxane (Table 4). The mixture was stirred in DMSO until complete homogenization. Then, the reaction mixture was charged into the reactors of the automated parallel synthesizer and degassed by sparging N_2 for 20 minutes. Subsequently, the reactor block was sealed under a N_2 atmosphere and heated to 80 °C for 12 to 24 h. The onset of the polymerization was considered once the reaction temperature was reached. The monomer conversion was followed by withdrawing samples from the reactor at different times and analyzing the samples by 1H NMR. After the reaction time elapsed, the polymeric solution was concentrated by rotatory evaporation and purified by dialysis in deionized water (48 h, r.t., 1.0 kg mol⁻¹ MWCO). The final product was freeze-dried for 24 h to obtain a yellow-colored solid.

Table 4 Experimental details for the synthesis of homopolymer [PIL]Cl precursors.

Entry	Structure	[M/CTA]	Solvent [mL]	Monomer [mmol]	CDTPA [mmol]	ACVA [mmol]	Trioxane [mmol]
A1	P([BVMIM]Cl)	23.02	8.0	5.0	0.217	0.043	0.710
A2	P([BVMIM]Cl)	44.32	8.0	5.0	0.056	0.011	0.710
A3	P([BVMIM]Cl)	123.3	25.6	16.5	0.134	0.020	2.27
A4	P([BVMIM]Cl)	214.7	25.6	16.5	0.077	0.012	2.27
B1	P([BVBIM]Cl)	18.0	5.4	7.2	0.40	0.080	0.60
B2	P([BVBIM]Cl)	36.1	5.4	7.2	0.20	0.040	0.60
B3	P([BVBIM]Cl)	72.3	5.4	7.2	0.10	0.020	0.60

Series of copolymers with variable monomer composition were obtained using the automated synthesizer and polymerization method described above. Table 5 summarizes the experimental details for the synthesis of statistical hydrophilic copolymers.

Table 5 Experimental details for the synthesis of statistical copolymer precursors (P([BVBIM]Cl-co-DMAEMA).

Entry	[M / CTA]	V _r [mL]	[BVBIM]Cl [mmol]	DMAEMA [mmol]	CDTPA [mmol]	ACVA [mmol]	Trioxane [mmol]
C1	43.3	7.5	3.0	0.75	0.051	0.008	0.667
C2	49.0	7.5	2.3	1.5	0.052	0.008	0.667
C3	54.7	7.5	1.5	2.3	0.054	0.008	0.667
C4	51.9	7.5	1.9	1.9	0.054	0.008	0.667
C5	60.5	7.5	0.75	3.0	0.055	0.008	0.667
C6	63.9	8.0	1.35	1.5	0.234	0.035	0.710
C7	105.7	7.0	1.05	4.2	0.049	0.012	0.622
C8	119.7	8.0	2.4	3.6	0.050	0.012	0.710
C9	133.7	10.0	4.5	3.0	0.056	0.014	0.880
C10	147.6	10.0	6.0	1.5	0.051	0.012	0.880
C11	154.6	10.0	6.8	0.8	0.048	0.012	0.880

2.4.1. Synthesis of *quasi*-block and block copolymer precursors

Synthesis of PDMAEMA and PMMA macroCTA agents. Macro chain transfer agents (macroCTA) were prepared according to the following procedure: pre-determined quantities of CPADB, ACVA initiator, and 1,3,5-trioxane were dissolved in the corresponding solvent (Table 6). Next, the mixture was transferred into the reactors of the synthesizer. Later, a pre-determined amount of DMAEMA or MMA monomer was added

into the reactors to yield a total reaction volume of 60 mL with initial monomer concentration from 1 to 4 M. By varying CDTPA concentration, different degrees of polymerization (DP) were targeted (assuming complete monomer conversion). The reaction mixtures were degassed by sparging N₂ for 20 minutes. Subsequently, the reactor block was sealed under a N₂ atmosphere and heated for 5 to 15 h; the reflux condenser temperature was set at 5 °C. The onset of the polymerizations was considered once the reaction temperature was reached. The monomer conversion was followed by ¹H NMR by withdrawing samples from the reactors at different times. After the pre-desired monomer conversion was achieved, the polymeric solution was concentrated by vacuum evaporation. Finally, the MacroCTAs **I** to **III** were purified for characterization by three dissolution (in THF)/precipitation (cold hexane) cycles. The final product was dried in a vacuum oven at 40 °C to obtain a yellowish brittle solid. The MacroCTA **IV** and **V** were purified by three dissolution (in acetone)/precipitation (MeOH) cycles; the final product was dried in a vacuum oven as described before.

Table 6 Experimental details for the synthesis of MacroCTA agents **I-V**.

MacroCTA	Polymer	Time [h]	Conversion [%] ^{c)}	[M/CTA]	Solvent [mL]	Monomer [mmol]	CDTPA [mmol]	ACVA [mmol]	Trioxane [mmol]
I	PDMAEMA	6	68	66	60	60	0.91	0.01	5.33
II	PDMAEMA	6	58	130	60	60	0.46	0.07	5.33
III	PDMAEMA	5	64.8	34	60	60	0.17	0.03	5.33
IV	PMMA	15	84.5	104	60	240	0.23	0.03	5.33
V	PMMA	12	60.0	254	30	120	0.47	0.07	2.66

^{a)} Polymerization was performed using ethanol as solvent; ^{b)} Polymerization was performed using toluene as solvent; ^{c)} Estimated by ¹H NMR, T = 70 °C.

Synthesis of quasi-block copolymers. For the synthesis PDMAEMA-*q*b-P(DMAEMA-co-[BVBIM]Cl) (Figure 22) chain extension polymerizations of macroCTAs (**I** to **III**) was performed in one-pot procedures as follows: Right after the synthesis of the macroCTA,

up to a specific conversion of DMAEMA (ca. 60%), the reaction mixture was cooled to room temperature; then, pre-defined amounts of [BVBIM]Cl (considering the unreacted DMAEMA) and ACVA were added into this crude polymerization mixture (Table 7). Next, this new reaction mixture was degassed and heated again to 70 °C to re-initiate the polymerization. After 12h of reaction, samples were withdrawn to calculate the monomer conversion by ¹H NMR. Finally, *quasi*-block copolymers were purified by dialysis in deionized water (48 h, r.t., 1.0 kg mol⁻¹ MWCO). The final product was freeze dried for 24 h to obtain a yellowish solid.

Table 7 Experimental details and characterization of *quasi*-block precursors (PDMAEMA-*qb*-P(DMAEMA-*co*-[BVBIM]Cl)).

Entry	Remnant DMAEMA [mmol] ^{a)}	[BVBIM]Cl [mol %] ^{b)}	[BVBIM]Cl [mmol]	Conv [%] ^{a)}	
				[BVBIM]Cl	DMAEMA
D1	16	20	3.2	99	70
D2	21	20	4.2	99	58
D3	18.1	20	3.6	99	74
D4	18.1	40	7.2	99	83

^{a)} Estimated by ¹H NMR; ^{b)} Initial monomer mol feed ratio of [BVBIM]Cl with respect to remnant DMAEMA.

Synthesis of block copolymers PMMA-b-(P([BVBIM]Cl-co-DMAEMA)). For the synthesis of block copolymers chain extension polymerizations were performed using PMMA (**IV** and **V**) as macroCTA. The experimental procedure was as follows: The predetermined quantities of PMMA and DMSO were transferred to a round bottom flask and subjected to a vigorous stirring at 45 °C for 2 h. Once the macroCTA was dissolved, predetermined quantities of [BVMIM]Cl or [BVBIM]Cl, DMAEMA, initiator solution (ACVA in DMSO), and 1,3,5-trioxane were added into the flask (**Table 8**). The total reaction volume was 24.9 mL with an initial monomer concentration of 0.5 M. Then, the flask was septum sealed, and the mixture was degassed by sparging N₂ gas for 30 min. This reaction mixture was heated for 12 h. Aliquots were withdrawn at 0, and 12 h to estimate monomer conversion by ¹H NMR. Once the reaction time elapsed, the polymer was purified by dialysis in H₂O/EtOH (ratio = 80/20, 48 h, r.t., 1.0 kg mol⁻¹ MWCO) and subsequent freeze drying for 48 h.

Table 8 Experimental details for the synthesis of block copolymers precursors PMMA-*b*-(P([BVMIM]Cl-co-DMAEMA) (**D5**) and PMMA-*b*-(P([BVMIM]Cl-co-DMAEMA) (**D6**).

Entry	Time [h]	Conv [%] ^{a)}	[M/macroCTA]	V _T [mL]	Monomer [mmol]	MacroCTA [mmol]	ACVA [mmol]	Trioxane [mmol]
D5 ^{b)}	12	58	100	24.9	20.8	0.21	0.04	5.33
D6 ^{c)}	15	58	100	16.0	8.0	0.08	0.016	1.41

^{a)} Estimated by ¹H NMR; T = 85 °C; ^{b)} [BVBIM]Cl was used as comonomer; ^{c)} [BVMIM]Cl was used as comonomer.

2.5. Anion exchange reactions

Series of halometallate (co)polymers (P([BXMIM]MCl_n)) were obtained by fusing the corresponding (co)polymer precursor with metal halides at elevated temperature. A representative procedure is as follows: a septum sealed flask was charged with 0.150 g of P([BVMIM]Cl) and 4.0 mL of EtOH. Next, the mixture was stirred until complete dissolution and degassed by sparging N₂ for 20 minutes. Later, the mixture was immersed in a preheated oil bath at 80 °C. After heating the mixture for 30 minutes, anion exchange was performed by adding a solution of the corresponding metal salt in EtOH (previously degassed with N₂, 10 mg mL⁻¹). Heating and stirring continued for 12 h. Upon addition of the metal salt solution, a viscous precipitate was observed. The obtained heterogeneous mixture was purified by completing the precipitation of the polymer into acetone. Finally, the precipitate was washed three times with 10 mL of EtOH each to remove any excess of the salt. The same procedure was followed to perform the anion exchange of homopolymer P([BVBIM]Cl). The obtained solid was dried until constant weight in a vacuum oven (at 40 °C). The ratio of metallic salt was calculated according to **eq. 1**:

$$R = \frac{n_{MCl_n}}{n_{MCl_n} + n_{[BVXIM]Cl}} \quad \text{eq. 1}$$

Where n_{MCl_n} represents moles of metallic salt and $n_{[BVXIM]Cl}$ represents moles of the corresponding polymerized monomer [BVMIM]Cl or [BVBIM]Cl (estimated by ¹H NMR). The same procedure was followed for statistical, *quasi*-block and block copolymers.

2.6. General procedure for the glycolysis of post-consumer PET

The catalytic performance of the MPCs was evaluated in glycolysis experiments using a FORMAX platform from Chemspeed Technologies AG (Switzerland) (Figure 13B). As indicated in Figure 14, the platform is equipped with a formulation block composed of six reactors ($V = 100$ mL), each one provided with an independent thermal jacket, a thermocouple, mechanical stirring (anchor, disk-type, or disperser disc), and a reflux condenser (Figure 14A and inset). Every reactor can be independently heated up to 250 °C or cooled down with a heating/cooling system (Hüber cryostat -20 to 140 °C). For transferring solid and liquid materials, a 4-needle head (4-NH, (Figure 14B) and gravimetric dispensing units were available (Figure 14D). The 4-NH was connected to a block of 4 syringe pumps (Figure 14C, $V = 1$ and 10 mL) and a solvent reservoir bottle (ethanol) for needle rinsing after each liquid transfer.

Sets of up to 6 glycolysis reactions were carried out in open reactors. For this purpose, the corresponding amount of MPC and 35 mL of EG were charged into the reactors of the formulation block. Then, each reactor vessel was heated to 180 °C (set point 215 °C) with a stirring speed of 500 rpm. After reaching thermal equilibrium (*ca.* 20 min), the reaction was started by adding the corresponding amount of PET flakes (weight ratio PET/EG = 1/4 wt. %). The onset of the reaction was set upon the addition of PET flakes. Then, the heating and stirring continued for 4 to 8 h.

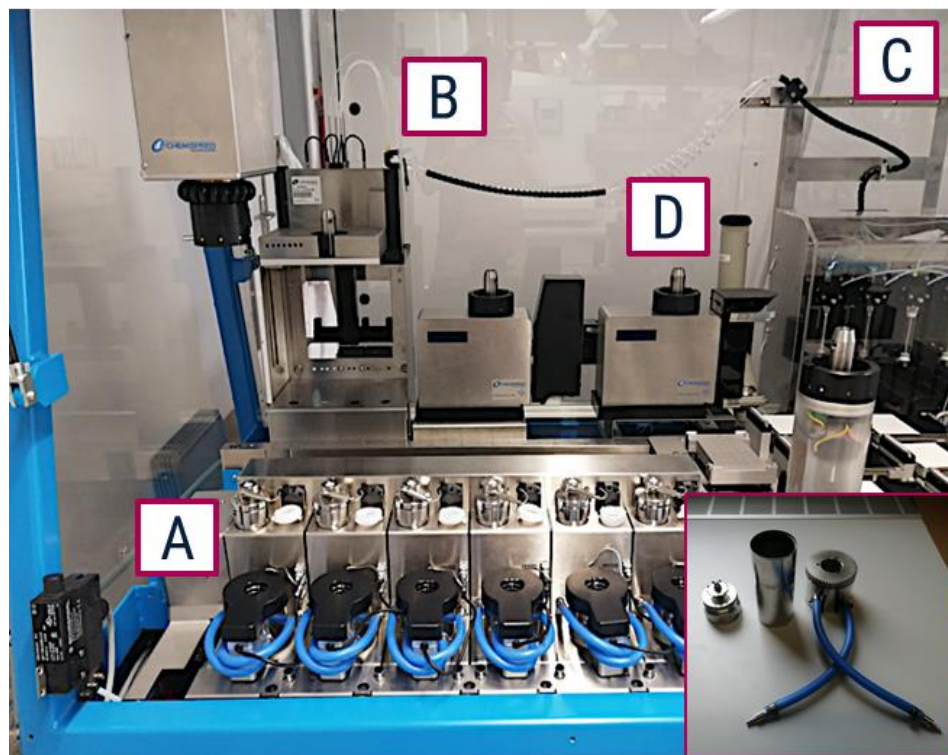


Figure 14 Front picture of the formulation block in the FORMAX platform. The inset shows a picture of the disassembled reactor, showing the mechanical stirrer used in this work.

After the reaction time elapsed, the mixture was cooled down to 50 °C (via a Hüber cryostat). Then, 100 mL of deionized water (at 60 °C) were added to the final mixture to wash and remove unreacted PET flakes, hydrophobic impurities, and oligomers from the product (see Figure SI 1 for details of the experimental procedure). The final mixture was heated ($T = 80$ °C) to solubilize the maximum amount of recycled monomer (BHET). Finally, the mixture was filtrated and washed three times with an excess of water (3 x 30 mL). The unreacted PET, hydrophobic impurities, and oligomers were collected, dried at 120 °C for 72 h, and weighed to estimate the conversion of PET using **eq. 2**:

$$\text{Conversion of PET} = \frac{W_0 - W_1}{W_0} \times 100\% \quad \text{eq. 2}$$

Where W_0 represents the initial weight of PET and W_1 represents the weight of unreacted PET and oligomers. The collected aqueous solution was concentrated to ca. 100 mL by vacuum evaporation at 50 °C. The concentrated filtrate was stored under

refrigeration at 4 °C for 24 h for crystallization. Next, white crystalline flakes were formed in the filtrate. Before filtration the solution was immersed in cold water to induce the complete crystallization of the product. The isolated crystalline product was dried at 80 °C for 48 h and characterized as BHET monomer. The selectivity of BHET was estimated gravimetrically using **eq. 3**:

$$\text{Selectivity of BHET} = \frac{n_{\text{BHET}}}{n_{f,\text{PET}}} \times 100\% \quad \text{eq. 3}$$

Where n_{BHET} represents the moles of BHET and $n_{f,\text{PET}}$ represents the moles of depolymerized PET. The obtained monomer was characterized by Elemental Analysis (Table 18), FTIR, ^1H NMR (Figure 43), TGA (Figure 44), and DSC (Figure 45).

After BHET isolation, the remaining mixture, containing EG, water, and the MPC, was concentrated by vacuum evaporation (at 55 °C) to remove water and yield the residual solution of MPC in EG solution (MPC/EG).

The reusability of the MPC was tested using the residual solution of MPC/EG as catalyst to perform new cycles of PET glycolysis. To this end, the amount of EG added to the new glycolysis reaction was subtracted from the volume of MPC/EG solution. Besides that adjustment, the new glycolysis cycles were carried out following the procedure described above. Therefore, the conversion of PET and selectivity of BHET was calculated for up to 6 cycles of catalyst reutilization tests. The screening of other halometallate PILs as catalyst was performed at a lower scale in septum-sealed flasks following the same procedure.

2.7. Kinetic studies of PET depolymerization

The following procedure was implemented to evaluate the effect of temperature and amount of catalyst in the production of BHET during the depolymerization of PET: In a reactor vessel of the FORMAX platform (Figure 14) the required amount of polymer catalyst, 350 mg of DS (used as internal standard for ^1H NMR analysis), and 35 mL of EG were added. The mixture was heated at different temperatures (160, 170, 180, and 190°C,

stirring speed = 500 rpm). Once the reactor vessel reached thermal stability, 2.25 g of post-consumer PET flakes (transparent coloration) were added, and the reaction continued for 4 to 6 h. The yield of BHET was measured by sampling during the depolymerization reaction with the robotic arm at different times. Then, the yield of BHET was estimated by ^1H NMR (using $\text{DMSO-}d_6$ as solvent) and by SEC using the RID signal and referring to a calibration curve (Figure 15).

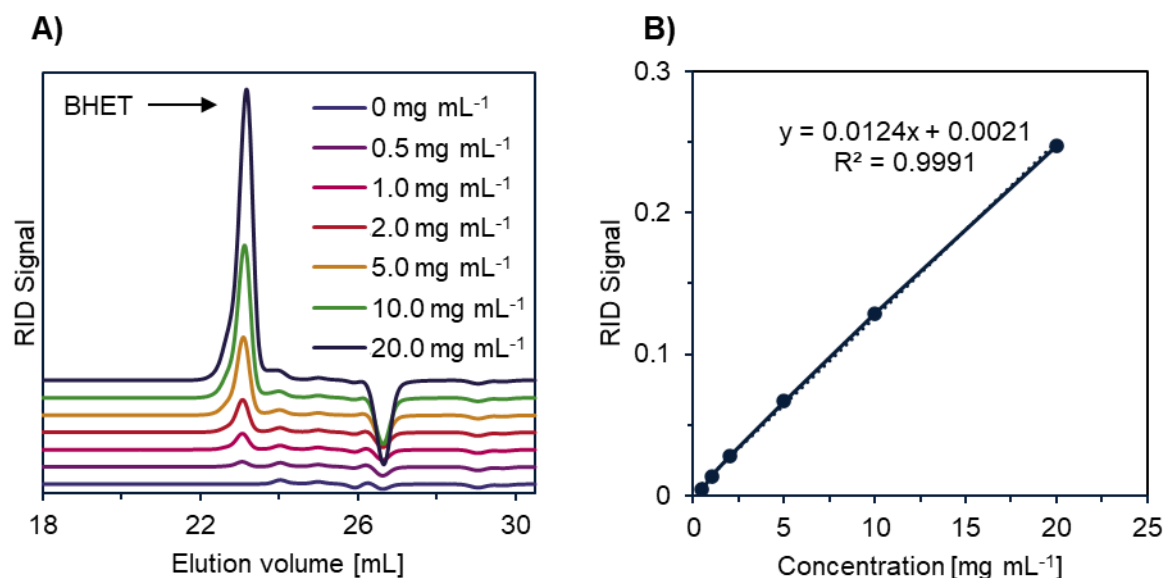


Figure 15 A) SEC traces of standard BHET solutions at different concentrations. B) Calibration curve, obtained by the intensity signal of BHET solutions in SEC.

The quantification techniques were validated by comparing the yield of BHET estimated by both techniques with the yield determined by gravimetry. The yield of the monomer was estimated by **eq. 4**:

$$\text{Yield of BHET} = \frac{n_{\text{BHET}}}{n_{i,\text{PET}}} \times 100\% \quad \text{eq. 4}$$

Where n_{BHET} represents the moles of BHET (calculated by ^1H NMR or SEC) and $n_{i,\text{PET}}$ represents the moles of initial PET.

2.8. Characterization methods

- Proton Nuclear Magnetic Resonance: (^1H NMR) spectra were recorded at room temperature on a Bruker Avance 300 MHz spectrometer using dimethyl sulfoxide ($\text{DMSO-}d_6$) as solvent. The chemical shifts are given in ppm. The monomer to polymer conversion was determined by comparing the integration resonance signal of the vinylic protons of the monomers to the internal standard (1,3,5-trioxane). The BHET conversion was estimated by comparing the integration resonance of BHET to the internal standard (DS).
- Diffusion Ordered Spectroscopy (DOSY) spectra of the obtained copolymers were recorded on a 400 MHz Bruker Avance III spectrometer at room temperature using $\text{DMSO-}d_6$ as solvent and tetramethylsilane (TMS) as an internal standard.
- Size Exclusion Chromatography (SEC). The number average molar mass (M_n) and molar mass distribution (\mathcal{D}) of the obtained (co)polymers were estimated using a Jasco system equipped with a PU-980 pump, an UV-975 detector, a RI-930 detector, and a PSS NOVEMA-MAX/100/100 Å columns, 5 μm particle size, at 30 °C, with aqueous solutions of trifluoroacetic acid (TFAA, 0.3%) and NaCl 0.1 M [pH < 2] as eluent at a flow rate of 1 mL min^{-1} . The system was calibrated with 2-polyvinyl pyridine (P2VP) standards ($M_p = 1.3$ to 81.0 kg mol^{-1} ; American Polymer Standards Corp., Mentor, OH, USA).
- Additional SEC measurements were carried out on an Agilent 1200 series system, equipped with a PSS degasser, a G1310A pump, and a G1329A autosampler. Data was collected by a G7162A RI detector. Samples were eluted in a GRAM guard/30/1,000 Å column, 10 μm particle size, using a dimethylacetamide (DMAc) + 0.21 wt.% LiCl solution as eluent at 1 mL min^{-1} flow rate, and 40°C. The system was calibrated with poly(methyl methacrylate) (PMMA) standards of narrow dispersity ($M_p = 0.4$ to 1,000 kg mol^{-1} ; PSS, Mainz, Germany).

- Raman spectra were recorded using a Raman microscope Senterra (Bruker Optics, Ettlingen, Germany) for depth-resolved measurements. A diode laser (532 nm, 50 mW) was employed as the excitation source. The excitation beam and the Raman backscattering radiation was guided through a 50-X objective and a CCD detector was used for signal collection. A typical integration time for recording the Raman spectra at high-resolution mode was 90 s on average. The spectral resolution was 4 cm^{-1} in the spectral range from 75 cm^{-1} to 1535 cm^{-1} . This spectral region was chosen since the most intensive Raman bands of halometallate anions were located here.⁹³
- Fourier transform infrared (FTIR) measurements were performed using a Nicolet IS-10 FTIR instrument equipped with an attenuated total reflectance (ATR) accessory.
- The thermogravimetric analysis (TGA) experiments were carried under nitrogen atmosphere with a heating rate of 10 K min^{-1} on a Netzsch TG 209 F1 Iris (Selb, Germany).
- Differential scanning calorimetry (DSC) was measured on a Netzsch DSC 204 F1 Phoenix instrument (Selb, Germany) under a nitrogen atmosphere with a heating rate of 20 K min^{-1} (first and second heating cycle) and 10 K min^{-1} (third heating cycle).
- Elemental analyses (EA) for carbon, hydrogen, nitrogen, were performed using a Leco CHNS-932 Elemental Chemical Analyzer, whereas EA of halogens (*i.e.*, chlorine) was measured in an Euro EA 3000 analyzer.
- Scanning Electron Microscope (SEM) images of unreacted PET obtained from glycolysis experiments were recorded using a TOPCON SM-510 (TopCon, Japan)

apparatus equipped with an Energy-dispersive X-ray spectrometer (EDX), at an acceleration voltage of 15 kV. Before SEM analysis, the corresponding sample was grinded with a mortar and coated with a thin layer of gold.

The sample pre-treatment for the analysis of copolymers in solution was as follows: First, the purified polymer was mixed with the corresponding solvent and heated ($T = 90\text{ }^{\circ}\text{C}$) in an ultrasonic bath for 30 minutes to enhance the polymer dispersion. After reaching a clear homogeneous solution, the solution was immediately passed through a $0.4\text{ }\mu\text{m}$ Nylon filter to remove any remnant solid. Next, the polymeric solution was let to cool down at room temperature for Transmittance, Dynamic Light Scattering (DLS) and Scanning Electron Microscopy (SEM) studies.

- Transmittance measurements were performed on an Avantium Crystal 16 (Technobis Crystallization Systems, Netherlands) platform composed of 16 wells designed to hold 2-mL vials and equipped with online turbidity (light transmission intensity) sensor. Each well is fitted with magnetic stirring at a fixed speed. The system is divided into four zones, with four wells each, that can be independently heated or cooled. The polymeric solutions (0.1 to 20 mg mL^{-1}) were subjected to three heating-cooling cycles in the temperature range from 0 to $90\text{ }^{\circ}\text{C}$ at a rate of $1\text{ }^{\circ}\text{C min}^{-1}$ and stirring of 500 rpm . The cloud point temperature (T_{CP}) was recorded when the transmittance signal of the apparatus reached 50%.
- Dynamic Light Scattering (DLS) measurements were performed on a Zetasizer Nano ZS (Malvern Instruments, Germany). Runs of $3 \times 30\text{ s}$ were carried out in a range of temperatures according to the T_{CP} of each sample, and an equilibration time of 180 s between each measurement (performed in triplicate). The counts were detected at an angle of 173° ($\lambda = 633\text{ nm}$). The mean particle size was approximated as the effective (Z-average) diameter and the width of the distribution as the particle polydispersity index (PDI) obtained by the cumulant method assuming spherical shapes.

- The SEM images of chlorozincate [PIL]ZnCl_n solutions were acquired using a Sigma VP Field Emission SEM, equipped with an Everhart-Thornley SE detector (Carl Zeiss AG, Germany) with an accelerating voltage of 10 kV. SEM samples were prepared by drop casting the polymeric solution onto a silicon wafer. Then, the solvent was evaporated by carefully applying a flux of air for at least 24 h. Before SEM analysis, the obtained films were coated with a thin layer of platinum via sputter coating (CCU-010 HV, Safematic, Switzerland). The average diameter was determined by particle size analysis in ImageJ software and by Gauss fitting function with the Origin software package.

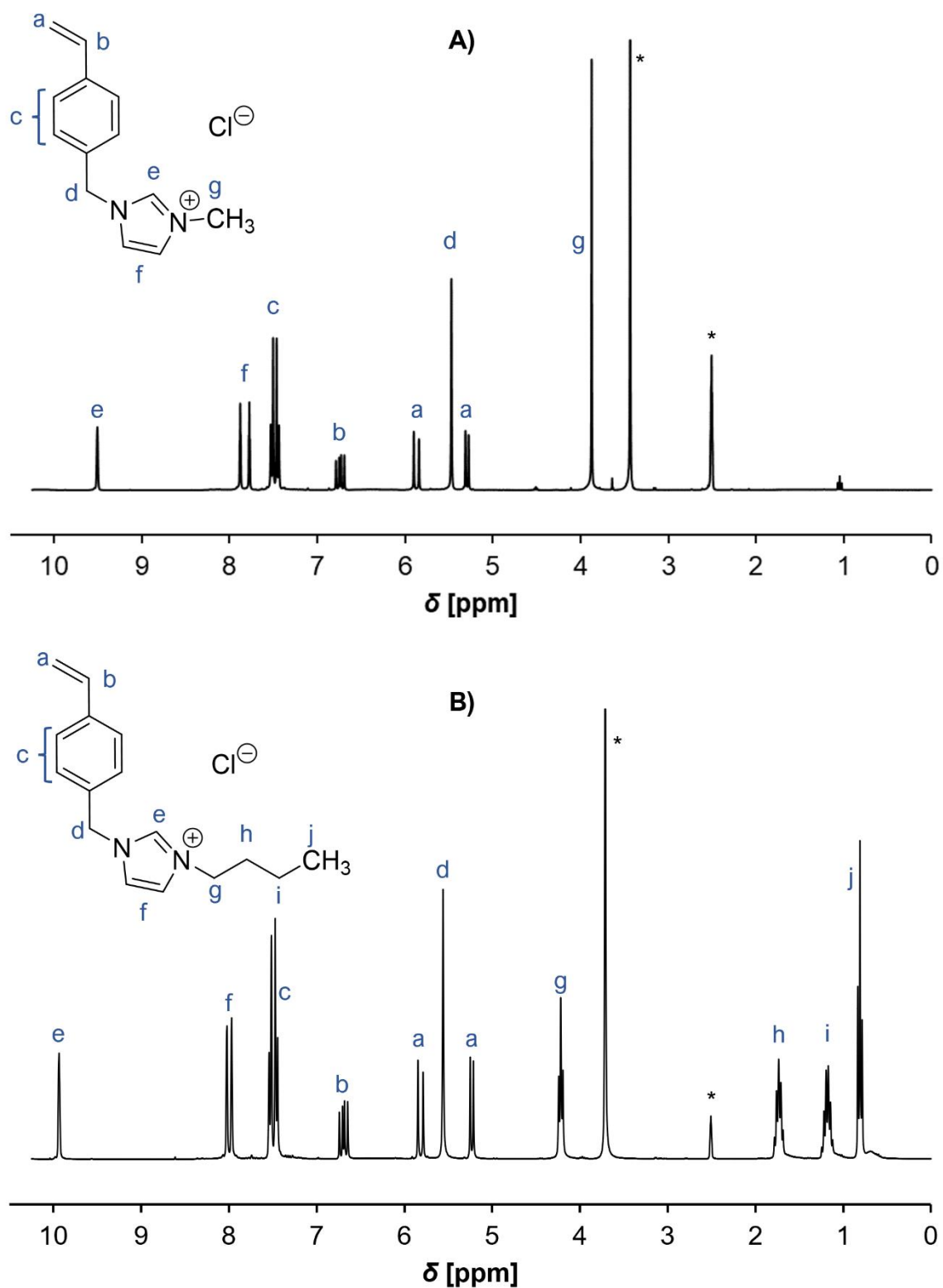
Chapter 3

Synthesis and characterization of MPCs

To discuss the demonstration of the hypothesis of this work, we summarized the results of this research in two main experimental phases. Firstly, Chapter 3 describes the synthesis and characterization of ionic monomers and a library of MPCs of variable structure and composition (homopolymers, statistical copolymers, *quasi*-block copolymers, and block copolymers) via RAFT polymerization and anion exchange reactions.

3.1. Synthesis of IL monomers

As discussed before, the highly specialized functionalization and versatile properties of ILs has attracted much attention in polymer science in the last decade. RAFT polymerization of IL-based monomers is a growing field, due to its effectiveness and high tolerance toward functional monomers. In this investigation, we undertook the synthesis of imidazole-containing styrenic monomers, with the objective to confer catalytic activity to polymer templates. Namely, [BVMIM]Cl and [BVBIM]Cl ionic monomers were designed through a simple substitution reaction. The monomers were obtained as a colorless viscous material with a yield of *ca.* 70%. Both monomers were characterized by ^1H NMR in $\text{DMSO-}d_6$ (Figure 16). Vinylic protons were identified at $\delta = 6.7$, 5.0 and 5.3 ppm (signals a and b). The characteristic single signal in the range of $\delta = 9.5$ to 9.8 ppm was attributed to the acidic proton in position two of the imidazole substituent (e). The signal at 5.50 ppm (d) was attributed to the methylene protons between the imidazole and the styrenic groups. Alkyl protons contribution from the imidazole moiety was identified at low fields (0.7 – 2.0 and 4.7 ppm). The experimental ^1H NMR data were consistent with published values.⁶⁹



3.2. Synthesis and characterization of homopolymer precursors derived from [BVMIM]Cl and [BVBIM]Cl

This section describes the synthesis and characterization of [PIL]Cl precursors of variable alkyl substituents, composition and structure. In a first approach, as depicted in Figure 17, we performed the synthesis of a library of homopolymers with variable alkyl substituents and counterions in two synthetic steps: (i) RAFT polymerization of ionic monomers [BVMIM]Cl or [BVBIM]Cl to produce precursor PILs with chloride counter anions (poly[1-methyl-3-(4'-vinylbenzyl)-1H-imidazol-3-ium chloride] (P([BVMIM]Cl)) and poly[1-butyl-3-(4'-vinylbenzyl)-1H-imidazol-3-ium chloride] (P([BVBIM]Cl))); and (ii) anion exchange reaction of [PIL]Cl precursors with a metal halide to yield halometallate polymers [PIL]MCl_n. We selected this strategy rather than performing the anion exchange of monomers as halometallate counter anions might cause undesirable side reactions during polymerization procedures and are difficult to dissolve in common solvents.⁸⁷

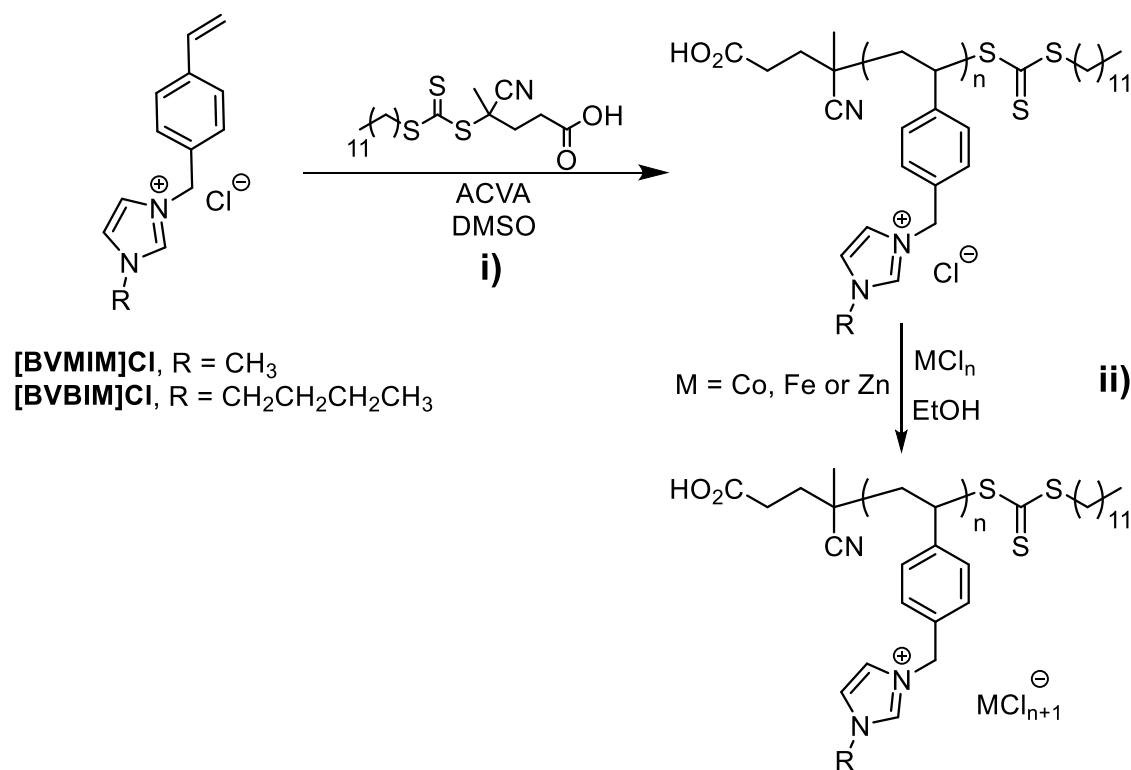


Figure 17 General synthetic scheme to produce [PIL]Cl precursors by RAFT polymerization (i) and anion exchange reaction to yield [PIL]MCl_n (ii).

The RAFT polymerizations were carried out using CDTPA as universal chain transfer agent (CTA) effective for the controlled polymerization of styrenic and methacrylate monomers.⁹⁴ Barner-Kowollik *et al.*, identified aprotic solvents as suitable media for the RAFT polymerization of ionic monomers;⁹⁵ thus, we used DMSO as aprotic solvent to ensure reasonable control over polymerization and optimal dissolution of the ionic monomer. The monomer conversion was calculated via ¹H NMR by analyzing the vinylic signals of the monomer at $\delta = 6.7$ and 5.0 ppm. Table 9 provides an overview of the homopolymer precursors synthesized in this investigation. As exemplified in Figure 18, ¹H NMR of the purified polymer showed the characteristic signals of the polymeric derivative and no presence of any residual vinylic protons from the monomer, initiator or internal standard. Hence, the reactants were effectively removed by the described synthetic approach. Moreover, as shown in Table 9, the M_n determined by ¹H NMR correspond closely to the theoretical values.

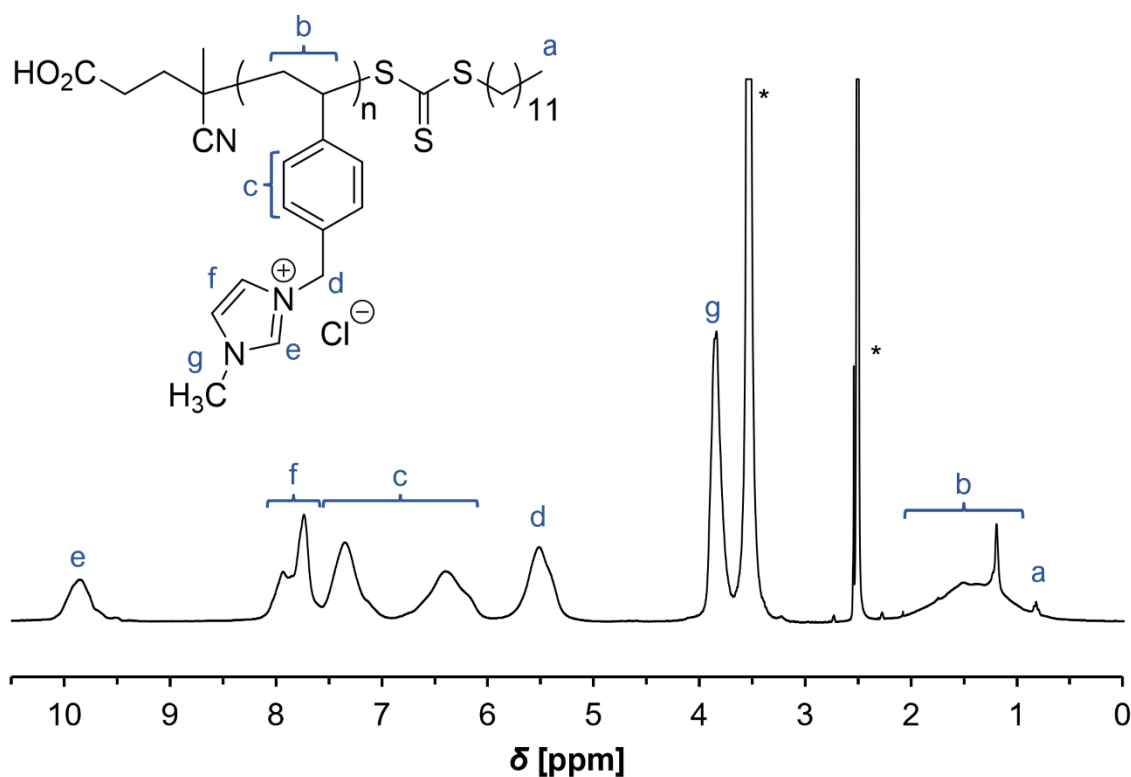


Figure 18 Representative ¹H NMR spectra (DMSO-*d*₆) of P([BVMIM]Cl) (**A2**).

The molar mass was challenging to estimate through SEC because of the ionic moieties in the copolymers; *i.e.*, hydrogen bonding and chloride counterions strongly interact with common SEC column materials.⁹⁵ Therefore, we used a specialized SEC system (H₂O/TFAA/NaCl) to characterize polymers with ionic character. As listed in Table 9, lower M_n experimental values than the theoretical values were obtained. This could be attributed to the different hydrodynamic properties between polymeric analytes and the utilized polymer standards;⁶⁹ additionally the presence of a separate counter ion (NaCl) in the SEC eluent contributed to the underestimation of the molar mass. As described elsewhere,⁹⁶ the ions in the SEC eluent should be similar to the analyte to improve SEC measurements of PIL derivatives. Thus, [PIL]Cl with relatively higher molar mass and derived from the monomer [BVBIM]Cl showed more significant discrepancies with the theoretical values. This effect could be further correlated to the decreasing solubility of the slightly more hydrophobic P([BVBIM]Cl) derivatives (series **B**). Nonetheless, as shown in Table 9, for most of the experiments, PILs with narrow \mathcal{D} were obtained, which indicated a good control during the RAFT polymerization of IL monomers. Thus, these results confirmed the successful fabrication of two series of P([BVMIM]Cl) (series **A**) and P([BVBIM]Cl) (series **B**) with variable M_n .

Table 9 Characterization of homopolymer [PIL]Cl precursors prepared by RAFT polymerization.

Entry	Functionalization	Time [h]	Conv. [%] ^{a)}	M_n , theo ^{b)} [kg mol ⁻¹]	M_n , NMR ^{c)} [kg mol ⁻¹]	M_n , SEC ^{d)} [kg mol ⁻¹]	\mathcal{D} ^{d)}
A1	P([BVMIM]Cl)	16	69.9	7.55	7.82	3.79	1.07
A2	P([BVMIM]Cl)	16	63.0	13.11	12.14	5.13	1.08
A3	P([BVMIM]Cl)	24	60.0	17.61	15.78	5.34	1.32
A4	P([BVMIM]Cl)	24	58.9	29.47	24.07	10.97	1.39
B1	P([BVBIM]Cl)	24	94.5	4.73	5.55	2.31	1.17
B2	P([BVBIM]Cl)	24	89.9	8.99	8.48	3.52	1.20
B3	P([BVBIM]Cl)	24	91.4	18.28	n.d. ^{e)}	5.49	1.20

^{a)} Estimated by ¹H NMR; ^{b)} determined by the formula $M_n = [([M]_{[BVXIM]Cl}]_0/[CDTPA]_0 \times \text{Conv.} \times M_{[BVBIM]Cl}] + M_{CDTPA}$; ^{c)} determined by ¹H NMR using as reference the signals of CDTPA ($\delta = 0.5$ to 0.8 ppm) and P([BVXIM]Cl) ($\delta = 10.1$ ppm); ^{d)} determined by SEC in aqueous solution containing TFAA and NaCl (RI detection, P2VP calibration); ^{e)} not determined due to insufficient intensity of the reference signal.

3.3. Synthesis and characterization of (co)polymer libraries derived from copolymers of [BVBIM]Cl and DMAEMA

According to the targeted application, numerous reports have documented the copolymerization of IL monomers to tune the physicochemical properties of the final materials.^{61,67,97} To prepare hydrophilic copolymers, with enhanced solubility in polar solvents, we employed DMAEMA as comonomer to copolymerize through conventional RAFT polymerization. Additionally, PDMAEMA is a thermo-responsive polymer,^{98–100} which, as shown later, was explored as an additional feature for MPCs in the glycolysis of post-consumer PET. Thus, a library and kinetic investigations on poly(1-butyl-3-(4'-vinylbenzyl)-1H-imidazol-3-ium chloride-co-2-(dimethylamino)ethyl methacrylate) (P(DMAEMA-co-[BVBIM]Cl)) copolymers were designed to search for insights of the copolymers structure and to find the optimal copolymers composition for their final application as catalysts. Table 10 summarizes the characteristics of the copolymers synthesized in this investigation.

Table 10 Properties of synthesized statistical copolymers P([BVBIM]Cl-co-DMAEMA)

ID	$M_{n, \text{theo}}$ [kg mol ⁻¹] ^{a)}	Conv [%] ^{b)}		Feed ratio [BVBIM]Cl: DMAEMA	Final Composition [BVBIM]Cl: DMAEMA ^{c)}	$M_{n, \text{SEC}}$ [kg mol ⁻¹] ^{d)}	\bar{D} ^{d)}
		[BVBIM]Cl	DMAEMA				
C1	10.54	0.6	0.54	0.8 : 0.2	0.72 : 0.28	2.09	1.8
C2	9.48	0.65	0.54	0.6 : 0.4	0.5 : 0.5	2.92	1.68
C3	9.31	0.65	0.59	0.4 : 0.6	0.42 : 0.58	3.50	1.71
C4	13.4	0.9	0.72	0.5 : 0.5	0.65 : 0.35	4.22	1.6
C5	8.56	0.66	0.55	0.2 : 0.8	0.26 : 0.74	4.08	1.84
C6	9.36	0.99	0.96	0.1 : 0.9	0.15: 0.85	5.82	1.49
C7	18.98	0.68	0.80	0.8 : 0.2	0.9 : 0.1	6.44	1.52
C8	19.96	0.73	0.67	0.6 : 0.4	0.7 : 0.3	18.08	1.31
C9	19.72	0.76	0.64	0.4 : 0.6	0.49 : 0.51	20.10	1.52
C10	18.27	0.80	0.61	0.2 : 0.8	0.16 : 0.84	24.50	1.58
C11	17.33	0.99	0.56	0.1 : 0.9	0.12 : 0.88	29.46	1.65

^{a)} Determined by the formula $M_{n, \text{theo}} = \{([M]_{[\text{BVBIM}]\text{Cl}}]_0 / [\text{CTA}]_0 \times \text{Conv.} \times M_{[\text{BVBIM}]\text{Cl}} + ([M]_{\text{DMAEMA}}]_0 / [\text{CTA}]_0 \times \text{Conv.} \times M_{\text{DMAEMA}}) + M_{n, \text{CTA}}\}$; ^{b)} determined by ¹H NMR in DMSO-*d*₆; ^{c)} determined after purification by ¹H NMR in DMSO-*d*₆. ^{d)} determined by SEC in aqueous solution containing TFAA and NaCl (RI detection, P2VP calibration).

We targeted two groups of copolymers with similar molar mass (10.0 to 25.0 kg mol⁻¹) and variable monomer composition. As listed in Table 10, a library of copolymers P([BVBIM]Cl-co-DMAEMA) was prepared showing good accordance between the final composition and the calculated values of molar mass. Figure 19 provides the assignment of the signals of the copolymer system, which correspond well to the reported data.^{63,69} The composition was calculated by comparing the integration resonance of PDMAEMA (signal **a**, 2H, $\delta = 3.9$ ppm) and P([BVBIM]Cl) (signal **h**, 2H, $\delta = 4.3$ ppm) of the purified copolymers. As shown in Table 10, the final composition of the copolymers exhibited certain differences to the theoretical values of monomer composition which could be attributed to the differences of monomer conversion during the polymerization reactions. This phenomenon could lead to compositional drifts in the copolymerization system. Additional discussion on this remark will be provided in the following sections.

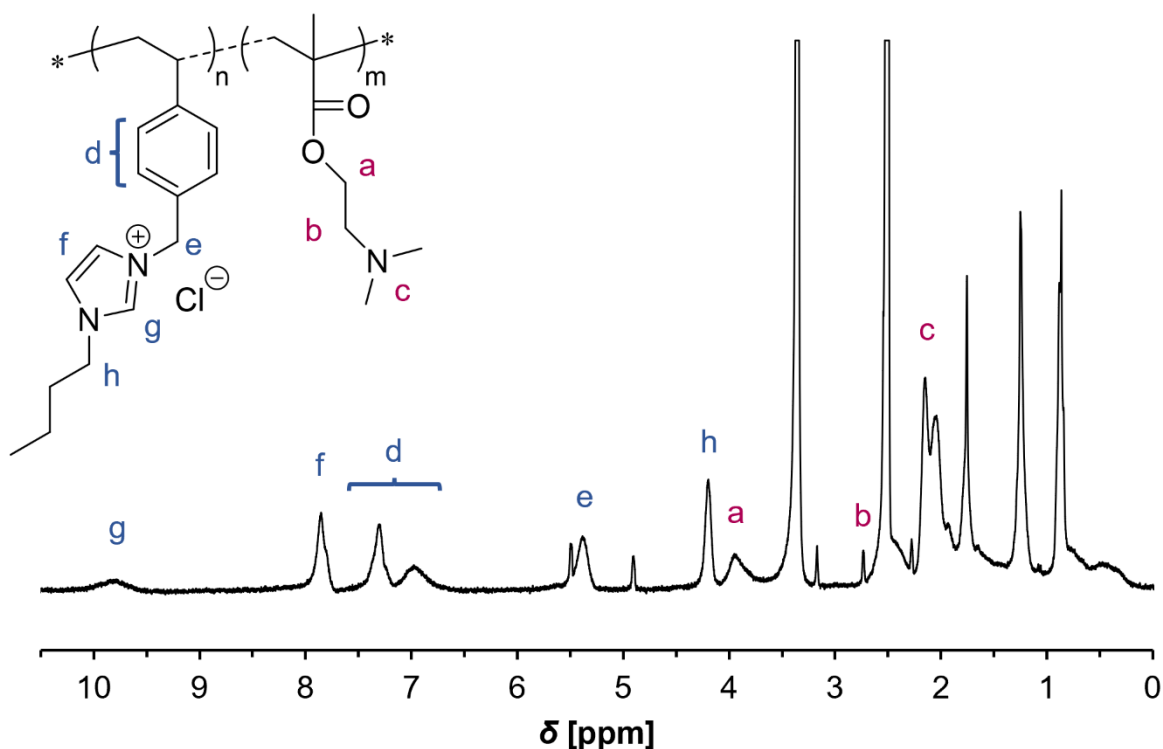


Figure 19 ¹H NMR spectrum of a representative example of P([BVBIM]Cl-co-DMAEMA).

To measure the experimental molar mass, we used the referred aqueous SEC system containing a stationary phase for positively charged polymers and an aqueous solution to minimize possible effects of interactions. This kind of system have been

recently proposed as effective alternatives for estimating the M_n of ionic polymers by SEC.^{63,96} As shown in Table 10, the experimental M_n values using the aqueous eluent were in general lower than the theoretical values. This fact was evident for low molar mass polymers with a high molar ratio of [BVBIM]Cl:DMAEMA (Samples **C1** to **C3** and **C7**). As shown in previous reports, the polyelectrolytes can interact with the stationary phase of the column.^{63,96} Such complex effects and the differences in the hydrodynamic volume between the utilized polymer references and the studied copolymers contributed to the bias between the experimental and the theoretical M_n values.

On the other hand, as the content of DMAEMA in the copolymers increased, a closer approximation in the M_n values was achieved (samples **C9** to **C11**, **Figure 20**). It is worth mentioning that the increase of the content of [BVBIM]Cl contributed to wide molar distribution, as revealed by the \mathcal{D} values. Nonetheless, as indicated in Table 10 most systems showed relatively narrow \mathcal{D} with control over the molar composition and M_n of the final copolymers.

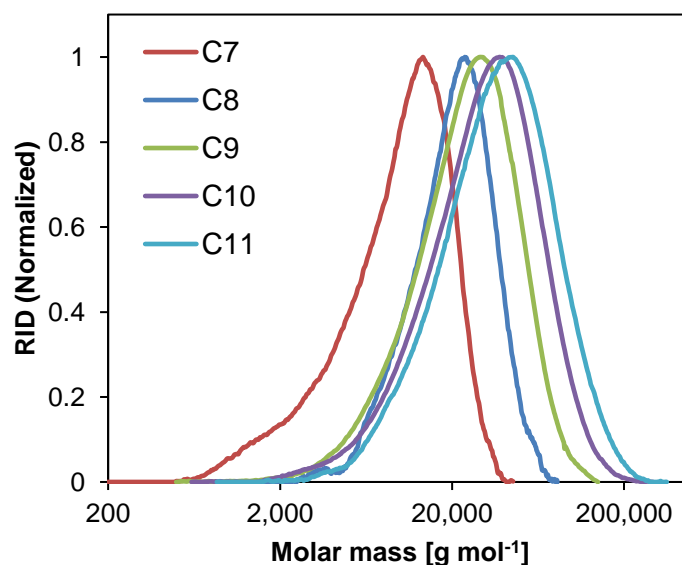


Figure 20 SEC traces of the series of P([BVBIM]Cl-co-DMAEMA) (**C7** to **C11**) in aqueous eluent.

Kinetic investigations of the copolymerization of the monomer pair DMAEMA:[BVBIM]Cl were performed to determine any significant compositional drift in this system. For this purpose, RAFT polymerizations with monomer compositions of DMAEMA:[BVBIM]Cl = 0.8, 0.6, 0.5, and 0.4 were performed in the automated parallel

synthesizer. Kinetic parameters were analyzed by withdrawing samples from the reactors at 1, 2, 3, 4, 6, and 8 h, and examining the evolution of monomer conversion in time. To the best of our knowledge, kinetic data for this copolymerization system has not been reported before. As shown in Figure 21, the plots of monomer conversion versus time, [BVBIM]Cl has slightly higher reactivity than DMAEMA in all studied systems. However, the increasing concentration of the IL monomer led to lower molar conversions, which could be attributed to the growing viscosity of the medium.⁶³ The linear relationship observed in the plots of $\ln([M]_0/[M]_t)$ versus time, indicates that the concentration of living free radicals remains unchanged and no detectable termination occurred after 6 to 8 h of polymerization. The obtained data will be useful in future reports to understand the microstructure these copolymer systems.

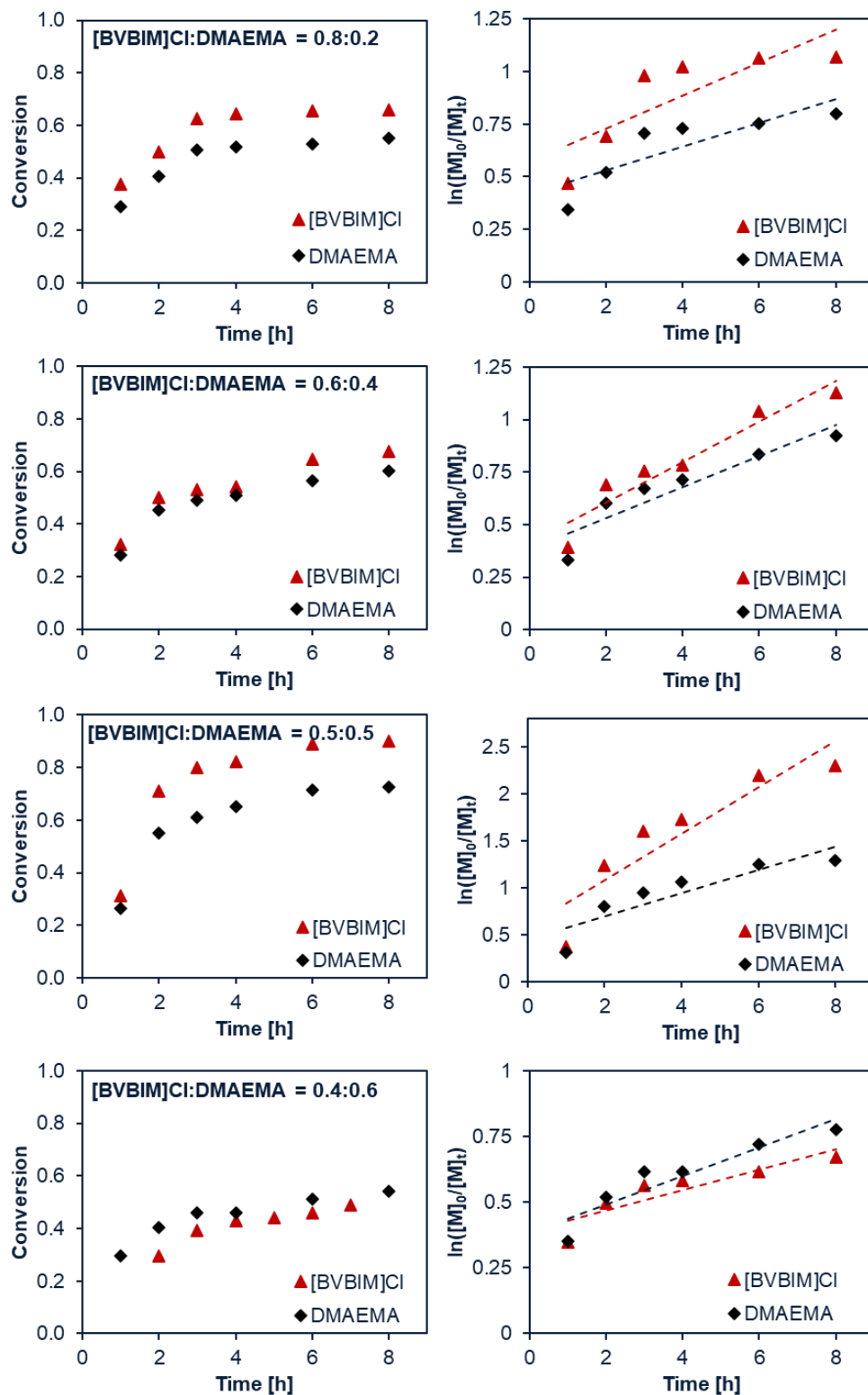


Figure 21 Monomer conversion and $\ln([M]_0/[M]_t)$ as a function of time for different compositions of a series of P([BVBIM]Cl-co-DMAEMA) (C1-C4).

3.3.1. Synthesis and characterization of *quasi*-block and block copolymer precursors

The design and selection of the copolymers reported in this section pursued the copolymerization of IL monomers and hydrophilic or hydrophobic monomers to yield block-like copolymers with thermo-responsive behavior, electrostatic interactions and hydrogen bonding in glycol and aqueous solutions. Thus, the targeted copolymers, with variable structure and thermo-responsive functionalities, were expected to show thermo-responsive properties in solution, such as Lower Critical Solution Temperature (LCST) and/or self-assembly behavior.¹⁰¹

As shown in Figure 22, the synthesis of block-like copolymers was performed via RAFT polymerization by two methodologies: (i) the conventional approach to produce block copolymers, and (ii) a one-pot synthesis procedure. The latter method represents a convenient strategy to confer self-assembly features to block-like copolymers in a straightforward approach.¹⁰² This procedure starts with the RAFT polymerization of a first monomer (M1 = DMAEMA) to produce a macroCTA precursor (PDMAEMA, monomer conversion < 70%). Next, a predetermined amount of a comonomer (M2 = [BVBIM]Cl) and initiator are added into the reactor mixture and the polymerization is re-initiated. Hence, a chain extension copolymerization reaction of residual monomer DMAEMA (from the first synthesis step) and freshly added [BVBIM]Cl is carried out to yield a second block composed of a statistical copolymer (P(DMAEMA-co-[BVBIM]Cl)). In general, based on the monomer reactivity ratios and feed protocol, the copolymer is composed of a “pure” first block and a second copolymer with the general structure of PDMAEMA-*qb*-P(DMAEMA-co-[BVBIM]Cl), which is herein referred as a *quasi*-block copolymer due to the mixture of comonomer in the second block of the copolymer.¹⁰²⁻¹⁰⁵

The described procedure has been useful to manufacture copolymers with block-like properties (e.g., self-assembly and thermo-responsive behavior) in a straightforward and cost-effective approach; thus, reducing the use of complex and time-consuming purification steps.^{102,105}

Additionally, as depicted in Figure 22, the complete procedure can be performed in an automated way by using an automated parallel platform (*i.e.*, Chemspeed ASW 2000) to transfer and/or withdraw reactants and samples at specific time intervals to produce libraries of *quasi*-block copolymer in a practical approach.

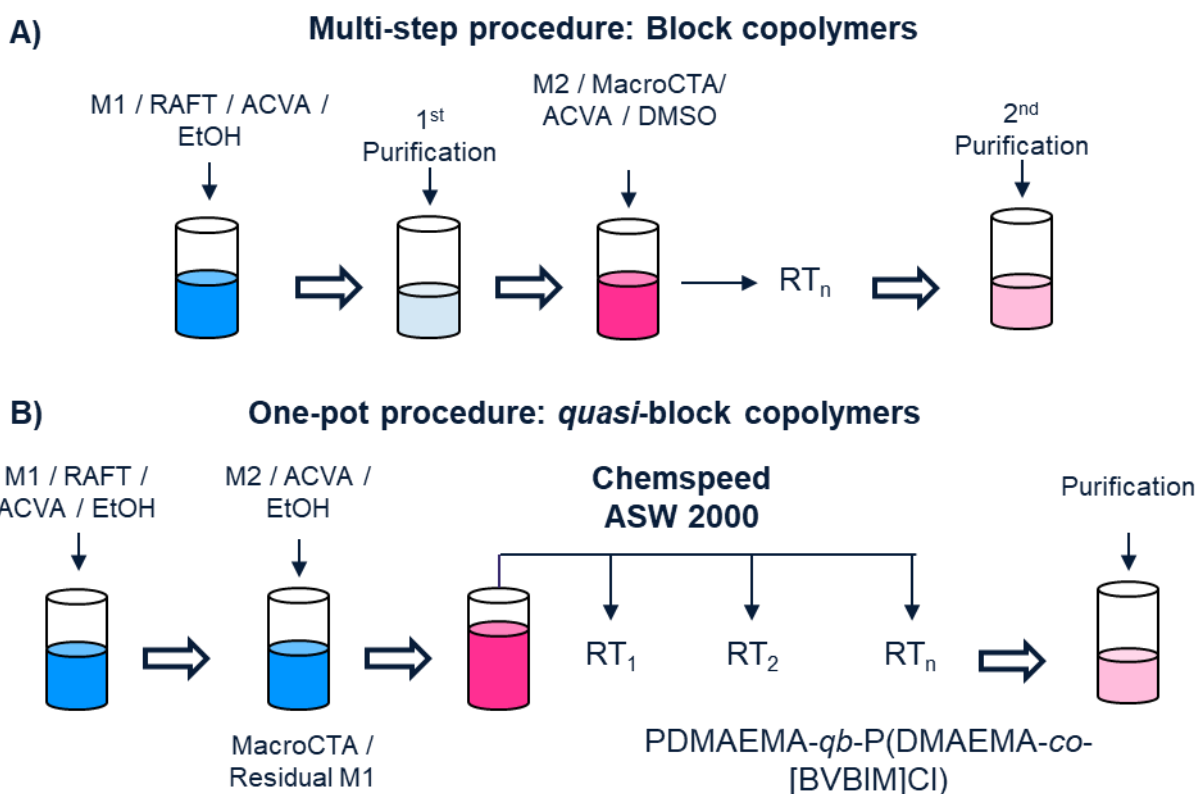


Figure 22 Methods for the synthesis of block-like copolymers: A) Synthesis of block copolymers in a conventional multi-step procedure. B) Synthesis of *quasi*-block copolymers in a one-pot procedure.

The described one-pot procedure is particularly beneficial for preparing copolymers with similar hydrophilicity, given that starting materials and polymer products should be soluble in the same solvent. Consequently, for the synthesis of amphiphilic block copolymers the conventional multi-step procedure was preferred to synthesize copolymers PMMA-*b*-P([BVBIM]Cl-co-DMAEMA).

Following up these strategies, the first synthetic step consisted of producing MacroCTA precursors derived from MMA or DMAEMA. Table 11 summarizes the MacroCTA obtained in the first step (see detailed information about the synthesis procedure in the Experimental Section). As shown, the \bar{D} values are low in all investigated

cases indicating a good control during RAFT polymerization. It is noteworthy that monomer conversion was maintained below 90% to avoid undesired termination reactions and to keep high RAFT end-group fidelity in the polymer chains.⁹⁴

Table 11 Properties of MacroCTA agents I to V.

MacroCTA	Polymer	Time [h]	Conv. [%] ^{a)}	$M_{n,theo}$ [kg mol ⁻¹] ^{b)}	$M_{n,exp}$ [kg mol ⁻¹] ^{c)}	\bar{D} ^{c)}
I	PDMAEMA	6	68	7.35	7.83	1.16
II	PDMAEMA	6	58	12.07	12.02	1.19
III	PDMAEMA	5	64.8	3.76	4.86	1.16
IV	PMMA	15	84.5	9.13	10.91	1.11
V	PMMA	12	60.0	15.5	15.84	1.16

^{a)} Determined by ¹H NMR; ^{b)} determined by the formula $M_{n,theo} = \{([M_1]_0/[RAFT]_0) \times Conv. \times M_1\} + M_{CDTPA}$; ^{c)} determined by SEC using a solution containing DMAc + 0.21 wt.% LiCl (RI detection, PMMA calibration).

As described in the Experimental Section, the obtained PDMAEMA precursors (I-III) were chain-extended in a one-pot reaction procedure, immediately after their synthesis. For the case of PMMA precursors (IV-V), the MacroCTAs were purified by precipitation for their subsequent chain extension via a conventional multi-step strategy. In this way, a library of hydrophilic *quasi*-block and amphiphilic copolymers was synthesized. Table 12 summarizes the properties of the copolymers obtained in this investigation.

Table 12 Properties of quasi-block (D1-D4) and block copolymers (D5-D6).

ID	$M_{n,theo}$ [kg mol ⁻¹] ^{a)}	Composition [%] ^{c)}			$M_{n,exp}$ [kg mol ⁻¹] ^{a)}	\bar{D} ^{d)}
		[BVBIM]Cl	DMAEMA	MMA		
D1	10.73	4.5	95.5	-	8.68	1.20
D2	18.65	8.5	91.5	-	13.5	1.30
D3	5.75	7.0	93.0	-	5.72	1.15
D4	5.82	14.1	85.9	-	5.85	1.15
D5	22.6	26.9	41.8	44.6	-	-
D6 ^{e)}	26.89	22.6	16.2	61.2	-	-

^{a)} Determined by the formula $M_{n,theo} = \{([M_{[BVBIM]Cl}]_0/[CTA]_0) \times Conv. \times M_{[BVBIM]Cl}\} + \{([M_{DMAEMA}]_0/[CTA]_0) \times Conv. \times M_{DMAEMA}\} + M_{n,CTA}$; ^{b)} determined by ¹H NMR in DMSO-*d*₆; ^{c)} determined after purification by ¹H NMR in DMSO-*d*₆. ^{d)} determined by SEC in DMAc/LiCl (RI detection, PMMA calibration); ^{e)} [BVMIM]Cl was used as comonomer.

The effective chain extension to yield *quasi*-block copolymers was validated by SEC in organic solvents. In these cases, the high composition of PDMAEMA allowed the characterization of the copolymers in common organic solvents. As indicated in Table 12 and Figure 23, in comparison to their MacroCTA precursors, a clear shift of the molar mass distribution is observed for the final *quasi*-block copolymers, along with a close correlation of the theoretical and experimental values of M_n . Thus, we could confirm that the initial macroCTA precursors were effectively chain extended by the described approach.

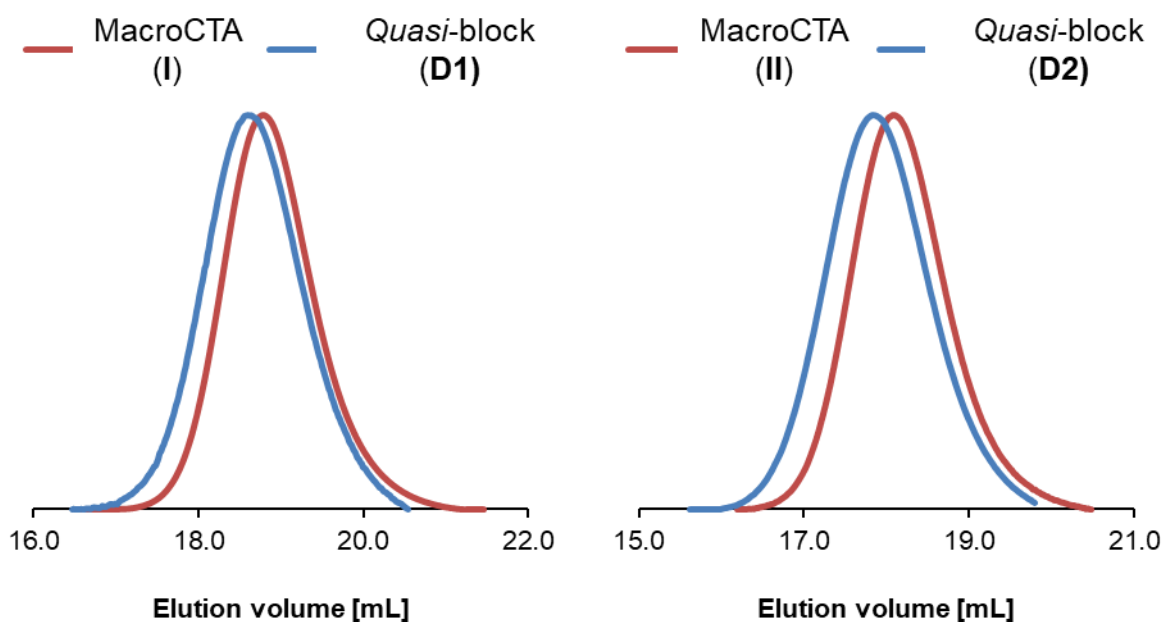


Figure 23 Representative SEC traces of MacroCTA I (left) and II (right) and their respective *quasi*-block derivatives.

The addition of the IL monomers was confirmed by identifying the characteristic signals of the imidazole moieties in ^1H NMR. Thus, the composition of copolymers was calculated by integrating the signals corresponding to P([BVBIM]Cl), as discussed for the series of statistical copolymers in Section 3.3. Hence, we could conclude that the chain extension of the MacroCTA precursors to yield *quasi*-block copolymers in a one-pot approach was successfully performed.

Concerning the block copolymers described in Table 12 (entries **D5** and **D6**), the characterization of the final materials was challenging to perform due to the amphiphilic nature of the copolymers. For instance, the final copolymers were insoluble in the utilized SEC solvent for the characterization of macroCTA precursors. Such disadvantage could be overcome by derivatization techniques (e.g., methylation, anion exchange, among others); however, the molar mass of the final copolymer and hydrodynamic behavior would be affected by such strategies.

Hence, the effective copolymerization was qualitatively corroborated by ^1H NMR and DOSY experiments. Figure 24A shows a representative DOSY spectra with the related ^1H spectra of a macroCTA precursor (PMMA, entry **V**). The signals of the solvent ($\text{DMSO-}d_6$) exhibited a diffusion coefficient (D) of $5.22 \times 10^{-10} \text{ m}^2 \text{ s}^{-1}$. As signaled by the dashed line the D of the macroCTA corresponds to ca. $2.53 \times 10^{-11} \text{ m}^2 \text{ s}^{-1}$. The DOSY map of the corresponding block copolymer (Figure 24B, entry **D6**) exhibited signals corresponding to the blocks of PMMA ($\delta = 3.5 \text{ ppm}$) and P([BVMIM]Cl) ($\delta = 7.3$ to 8.0 , and 10.0 ppm). Moreover, both polymer signals present the same diffusion coefficient ($D = 7.73 \times 10^{-11} \text{ m}^2 \text{ s}^{-1}$), lower than the precursor and consistent with an successful chain extension of the macroCTA precursor.

It is noteworthy that the DOSY map corresponding to the block copolymer showed no signals of residual PMMA or monomers, meaning that (i) the PMMA precursor was effectively copolymerized during the chain extension, and (ii) the purification procedure was achieved.¹⁰⁶ Hence, the addition of IL moieties in this set *quasi*-block and block copolymers was validated. Consequently, we applied the mentioned copolymers as models to enhance the features of MPCs, including hydrophobic and hydrophilic thermo-responsive segments.

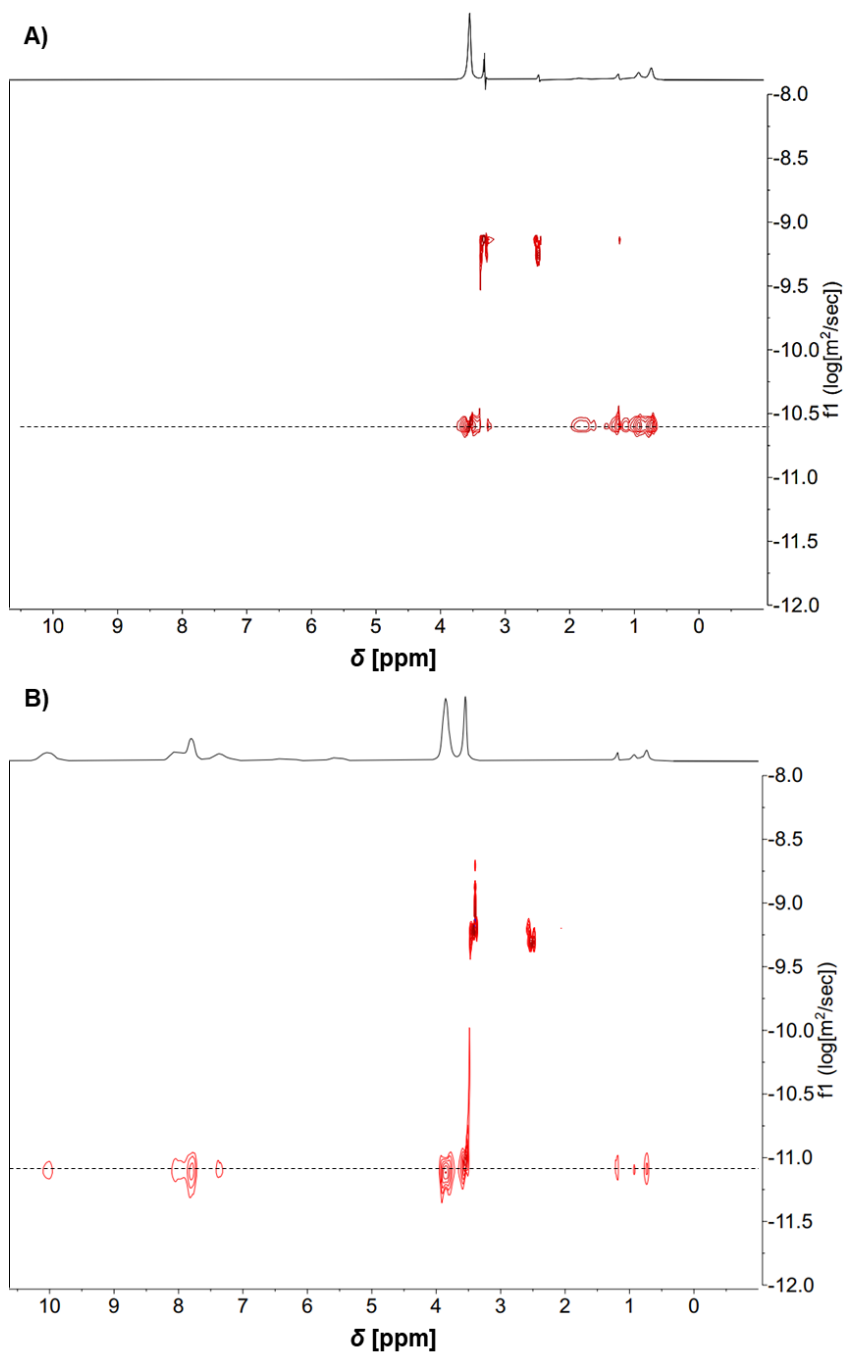


Figure 24 DOSY NMR spectra in DMSO- d_6 solution of A) PMMA (Sample **V**) and B) PMMA-*b*-P([BVMIM]Cl) (Sample **D6**).

3.3.2. Synthesis and characterization of halometallate [PIL]MCl_n

To prepare halometallate [PIL]MCl_n derivatives with catalytic activity in the glycolysis of PET, samples of the obtained [PIL]Cl precursors were subjected to anion exchange reactions with metal chlorides. Numerous reports have demonstrated the significance and complexity of the anion speciation in halometallate ILs.^{107–109} These equilibria, defined by the molar fraction (R or X_{MCl_n}) of metal chloride anions respect to cations, refers to the dynamic equilibrium between a well-defined cation, halide and one or more halometallate anions.¹⁰⁷ Thus, depending on the anion speciation, the generated halometallate [PIL]MCl_n may constitute monomer and/or oligomeric species with varying coordination number. Such a feature can be useful to develop polymer materials with tunable physicochemical properties, *e.g.*, viscosity, thermal stability, Lewis acidity, catalytic activity, among others.^{108,110} In this investigation we examined multiple metal chlorides with variable molar fractions to examine the influence of the counter ions, and their speciation, on the properties of the final halometallate (co)polymers and catalytic activity.

For all [PIL]MCl_n produced in this work, highly viscous liquids were generated. In cases where an excess amount of metal chloride was employed, insoluble polymers were formed (see experimental section 2.5). To assess the effect of the anion speciation on our polymeric systems, model polymers of P([BVMIM]Cl) (**A1**, Table 9) and P([BVBIM]Cl) (**B1**, Table 9)) were subjected to anion exchange reactions in different molar fractions of ZnCl₂. In all cases, white precipitates were observed, and the effect of the anion exchange was examined by ¹H NMR, Raman spectroscopy and Thermogravimetric Analysis.

Figure 25 and Figure SI 2 shows the ¹H NMR spectra of representative examples of Cl-type precursors and their anion exchanged derivatives. As expected, after subjecting P([BVMIM]Cl) and P([BVBIM]Cl) to anion exchange reactions, the signals of the protons in the imidazolium group, relative to those corresponding to the Cl-type precursor ($\delta = 10.1$, and 5.6 ppm), shifted upfield as a function of R ($\Delta\delta$ up to 0.9 ppm, $R = 0.8$). This evolution could be attributed to the shielding provided by the increasing electron density conveyed by chlorozincate anions, which consequently also decreased the hydrogen bond interactions between protons in the imidazolium group as R increased.^{111,112}

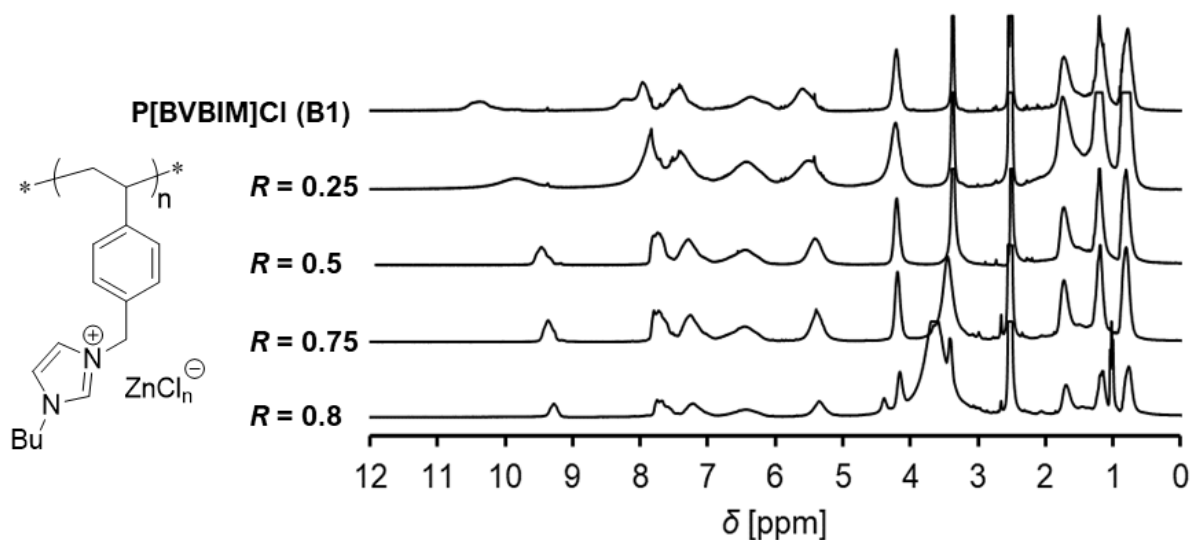


Figure 25 ^1H NMR spectra of $\text{P}([\text{BVBIM}]\text{Cl})$ (**B1**) and its anion exchanged chlorozincate derivatives.

Raman spectroscopy is a widely used technique to describe the speciation of halometallate species.^{93,110,112} These data have been used to assign the symmetry of the corresponding anions by analyzing the M-Cl vibrations, typically found within the 250 – 600 cm^{-1} range.¹⁰⁷ In this regard, the speciation effects on the physicochemical properties of macromolecular compounds have not been described before. In this study, we analyzed halometallates derived from $\text{P}([\text{BVBIM}]\text{Cl})$ (**B1**) with variable ZnCl_2 compositions ($R = 0.25, 0.5, 0.75$ and 0.8). Figure 26 shows the Raman spectra of the respective copolymers in the range of 200 to 1000 cm^{-1} .

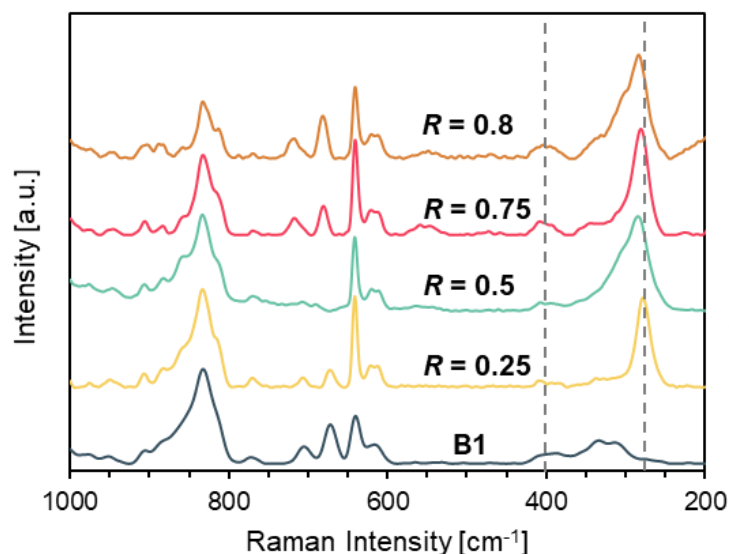


Figure 26 Raman spectra of P([BVBIM]Cl) (**B1**) and its anion exchanged chlorozincate derivatives at $R = 0.25, 0.5, 0.75,$ and 0.8 .

The spectrum corresponding to P([BVBIM]Cl) (**B1**, blue trace) shows only the characteristic signals of the polymeric chain, for instance, the C-C stretching vibrations of the aromatic groups at ca. 800 cm^{-1} . After anion exchange with $R = 0.25$ (yellow trace), the [PIL]ZnCl_n derivatives exhibited a new strong signal in the region of 279 cm^{-1} ; this signal was attributed to tetrahedral [ZnCl₄]²⁻ anions stretch vibrations (Zn-Cl), which are well described in the literature as chlorozincate ILs.^{93,111–113} Increasing the molar ratio R prompted a slight shift of the signal at 279 cm^{-1} to higher frequencies, and the emergence of an increasing shoulder signal around 380 cm^{-1} , which suggested the presence of doubly charged [Zn₂Cl₆]²⁻ anions. By increasing the molar ratio of ZnCl₂ ($R = 0.75$ and 0.8 , red and orange traces, respectively), the intensity of the signal at 380 cm^{-1} increased accordingly. These remarks suggested the formation of further oligomeric structures from [ZnCl₄]²⁻ to [Zn₄Cl₁₀]²⁻ under acidic compositions.¹¹⁴

Previous reports have described the declining of the signal at 279 cm^{-1} with the increasing molar ratio of ZnCl₂;⁹³ however, for our halometallate PILs the decrease of such signal remained unclear. Hence, we could hypothesize the coexistence of anions with variable symmetry within the copolymer systems. As shown in Figure 26, the signals in the range of 600 to 900 cm^{-1} were not affected after anion exchange reactions under the given conditions; thus, we could also conclude that the polymeric structure of the PILs was not

affected after anion exchange. These results suggest the formation of anionic cluster species within the polymeric system, with various types of symmetry as a function of R ; which are interacting with imidazolium cations in the polymeric chains through C–H...Cl hydrogen bonds.⁹³ These observations were also supported by the occurrence of precipitates during anion exchange reactions and the physical properties of the final halometallate PILs.

Since for halometallate ILs the ratio and symmetry of the anion represents a critical effect on the final properties of the material, we put forward a noticeable impact on the thermal properties of our halometallate PILs. Therefore, we performed TGA and DSC examinations to investigate the thermal behavior of model PILs. Figure 27 displays the TG traces of polymers P([BVBIM]Cl) (**A1**) and P([BVBIM]Cl) (**B1**), and their [PIL]ZnCl_n derivatives. The reference curve (Cl-type precursors, blue trace) shows two significant zones of mass loss: 1. The imidazole ring loss was found in the range of 200 to 350 °C,¹¹⁵ and 2. The styrenic group loss was found around 400-500 °C. After anion exchange ($R = 0.25$ and 0.5 , yellow and green traces, respectively) the thermal stability of the PIL was substantially increased. In such a case, the initial mass loss of the imidazole group was boosted by *ca.* 50 °C. The improved thermal stability exposes the effects of the shielding by anionic groups on the imidazole groups and forming a framework of anionic clusters within the structure of the polymer system. In this regard, the large area of the peak of decomposition of the styrenic backbone further suggested that the polymer chains are interconnected by the oligomeric anionic clusters.¹¹⁶ Thereafter, for $R = 0.75$ (red line), the thermal stability of the halometallate PILs was increased: up to *ca.* 320 °C.

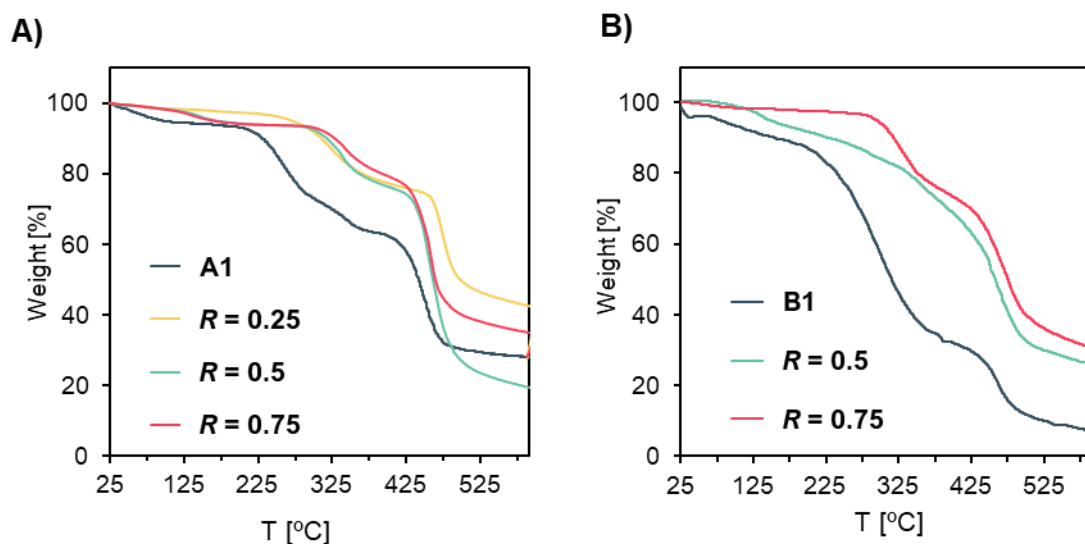


Figure 27 TGA curves of A) P([BVMIM]Cl) (**A1**) and B) P([BVBIM]Cl) (**B1**) and its anion exchanged chlorozincate derivatives.

As observed, after anion exchange, the thermal stability of the series of halometallate derivatives (Figure 27) only suffered a slight change of thermal stability between increments of molar ratio. As suggested by the Raman experiments, this fact could be attributed to the occurrence of a diversity of anions with variable symmetry in the systems.^{93,117} This hypothesis was corroborated by examining the glass transition (T_g) of a Cl-type precursor P([BVBIM]Cl) (**A1**) and its corresponding chlorozincate derivatives. In a representative example (Figure 28), DSC thermograms of **A1** showed a T_g of 41.8 °C, while its halometallate derivatives of $R = 0.25$ and $R = 0.5$ showed a net decrease of the T_g (31.9 and 5.5 °C, respectively). Hence the decreasing values of T_g as a function of R suggested changes in molecular mobility in the polymer systems. In this manner, along with the results observed by TGA and Raman Spectroscopy, we could hypothesize that the amorphous state in the polymeric systems was favored as the molar ratio of $ZnCl_2$ increased due to the growing variability of the symmetry of the oligomeric anionic species within ionic polymeric chains.

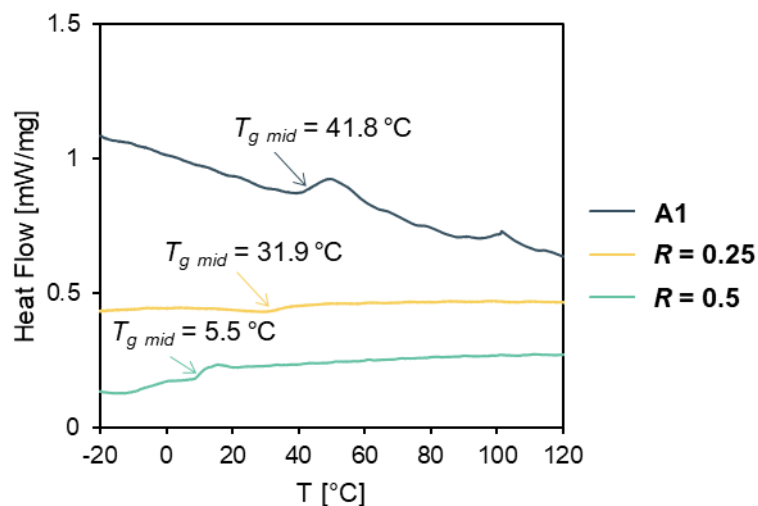


Figure 28 DSC thermograms of P([BVBIM]Cl) (**A1**) and its anion exchanged chlorozincate derivatives.^a

In this investigation, we described the synthesis of halometallate polymers and proved the effects of the anion exchange and speciation on the thermal stability of [PIL]ZnCl_n derivatives. Additionally, we disclosed the thermal stability of [PIL]ZnCl_n derivatives, which suggested that such materials could be used as catalysts for the chemical recycling of PET, without suffering degradation under typical glycolysis conditions (T = 160 to 190 °C). The described features could provide insights into further study since, in a similar fashion as halometallate ILs^{109,110} and as described here, more information on the speciation effects of complex halometallate macromolecular systems could pave the way to the discovery of a diversity of functional (co)polymers with tunable properties, such as thermo-responsive, magnetic or self-assembly properties, electrochemical properties, antimicrobial properties, and catalytic activity; as for the case described in this work.

^a DSC thermogram of sample **A1** could be described as a complex transition (involving multiples processes, e.g., melting, crystallization or relaxation enthalpy), which caused the T_g to look like a melting peak. This could be related to the storage conditions and physical aging of the sample in its glassy state.^{144,145} For more details on this complex process the reader is referred to Refs.¹⁴⁵⁻¹⁴⁷

3.3.2.1. Solution properties of [PIL]MCl_n

To follow up the study of the effect of anion exchange on the polymer properties, we examined the self-assembly capabilities of the obtained [PIL]MCl_n in EG and H₂O solutions (*i.e.*, the solvents used during the glycolysis reaction and purification, respectively) to get a better understanding of the phase separation behavior of the MPCs during and after glycolysis reactions. As previously reported for similar systems,^{85,87} the [PIL]Cl precursors (samples **A1** and **B1**, Table 13) were soluble in polar solvents such as water, ethanol, and EG even when a relatively hydrophobic butyl substituent (P[BVBIM]Cl, **B2**) was attached to the imidazolium group in the polymer backbone.

Table 13 Solubility properties of representative [PIL]Cl and their halometallate derivatives (**M** series) in EG, H₂O, and mixtures thereof (10 mg mL⁻¹ at 25°C).^{a)}

Entry	Precursor	MCl _n	R	EG : H ₂ O ratio							
				100:0	95:5	90:10	80:20	60:40	40:60	20:80	0:100
A1	-	-	-	S	S	S	S	S	S	S	S
M1	A1	ZnCl ₂	0.75	U	U	B	S	S	S	S	NS
M2	A2	ZnCl ₂	0.75	U	U	B	S	S	S	S	NS
M3	A2	ZnCl ₂	0.5	B	S	S	S	S	S	S	NS
M4	A2	ZnCl ₂	0.25	S	S	S	S	S	S	S	NS
M5	A2	ZnCl ₂	0.1	S	S	S	S	S	S	S	S
M6	A2	FeCl ₃	0.7	NS	NA	NA	NA	NA	NA	NA	NS
M7	A2	CoCl ₂	0.7	NS	NA	NA	NA	NA	NA	NA	NS
B2	-	-	-	S	S	S	S	S	S	S	S
M8	B2	ZnCl ₂	0.75	U	U	B	S	S	S	S	NS

^{a)} S: soluble; B: Tyndall effect; U: UCST-type phase separation; NS: non-soluble; NA: not applicable.

On the other hand, the series of chlorozincate derivatives were insoluble in EG and H₂O at room temperature (entries **M1** to **M5** and **M8**, Table 13). However, by heating a solution of P([BVMIM]ZnCl_n) (**M2**, R = 0.75) in EG the polymer could be solubilized to obtain a transparent solution at high temperature (*ca.* 90 °C). Remarkably, such solution became cloudy after cooling down to room temperature showing a reversible Upper Critical Solution Temperature (UCST) behavior (Figure 29A). As discussed before, this behavior could be attributed to the introduction of oligomeric halometallate counter ions,

which in a similar manner to BF_4^- anions in aqueous systems,^{118–120} induces UCST-type separation of PILs with chlorozincate anions in EG solutions by the interaction of polymer chains. In this respect, as reported before for halometallate ILs, the evolution of the structure of oligomeric halometallate anions can be triggered by the temperature, thus as a function of temperature the oligomeric halometallate counter anions can be reversibly dissociated to release MCl_n and Cl^- species.^{111,112} Regarding our chlorozincate (co)polymers, we hypothesized that anion dissociation of ZnCl_n anions also governs the association of polymer chains, and consequently, the phase transition of the polymer system in solution as a function of temperature

To investigate this premise, a sample of $\text{P}([\text{BVMIM}]\text{ZnCl}_n)$ (**M2**, $R = 0.75$) was subjected to transmittance experiments with temperature cycles (0 to 90 °C). As observed in Figure 29B, at the onset temperature of the test (black dotted line, 90 °C), the transmittance measured is 100 % (red line), indicating a clear solution and a fully solubilized polymer. Upon cooling down the transmittance curve shows a sharp decrease around 70 °C (cloud point temperature (T_{CP})), demonstrating that the solubility of the polymer decreased significantly to produce a cloudy solution (Figure 29A). As observed, the process is completely reversible; the transmittance curve recovers its values after three heating and cooling cycles (Figure 29B).

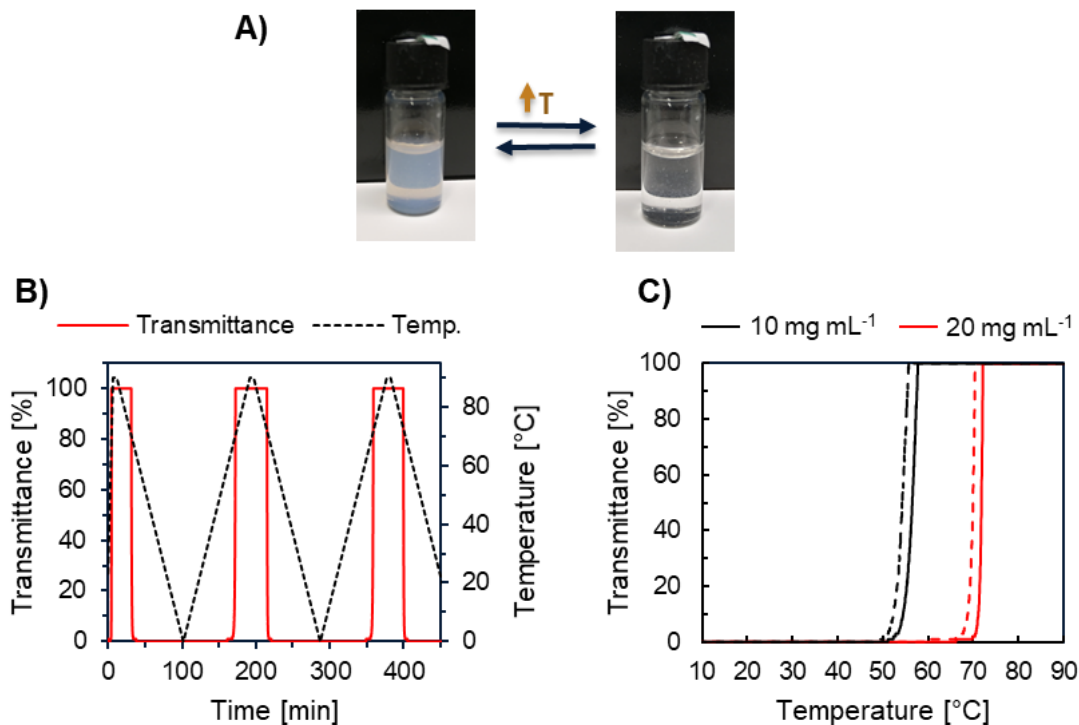


Figure 29 Representative pictures of the thermo-responsive behavior of a solution of P([BVMIM]ZnCl_n) (**M2**) in EG (20 mg mL⁻¹). B) Temperature and transmittance curves of a solution of P([BVMIM]ZnCl_n) (**M2**) in EG (20 mg mL⁻¹) as a function of time. C) Transmittance measurements of P([BVMIM]ZnCl_n) (**M2**) in EG solutions (10 and 20 mg mL⁻¹); solid line: heating; dotted line: cooling.

As reviewed by Kohno *et al.*,⁸⁰ polymeric systems with thermo-responsive behavior in organic solvents represent a distinctive phenomenon with several potential applications. This behavior might also be fine-tuned by multiple factors, such as: the concentration of the solution, molar mass and composition of (co)polymers, solvents, among others. In this regard, we identified that a two-fold increase of the concentration of P([BVMIM]ZnCl_n) **M2** in EG (10 to 20 mg mL⁻¹), promoted an increase of the T_{CP} of the solution by more than 10 °C (Figure 29C). On the other hand, after decreasing the polymer concentration to 5 mg mL⁻¹, the solubility of the polymer was significantly increased, yielding a solution with Tyndall effect (blue-transparent solution); therefore, the latter solution showed no phase transition as confirmed by transmittance experiments. The same behavior was observed for polymer solutions with 1 and 2 mg mL⁻¹, indicating clear transparent solutions.

For such cases, DLS measurements revealed that, by decreasing the polymer concentration, the mean hydrodynamic diameter (d_H) and PDI were modified (Table 14). It should be noted that polymer solutions with concentrations below 5 mg mL⁻¹ showed highly dispersed particle populations with a high PDI; thus, unstable particle populations with higher values of d_H were recorded at such conditions (Figure SI 3).

Table 14 Overview of the properties of P([BVMIM]ZnCl_n) (**M2**) in EG solutions, as a function of concentration, measured by DLS.

Concentration [mg mL ⁻¹]	d_H [nm]	PDI
1.0	154.3	0.415
2.0	233.9	0.524
5.0	94.8	0.382
10.0	128.9	0.044

In this series of experiments, we only observed defined populations of nanoparticles at 10 mg mL⁻¹ with $d_H = 128.9$ nm (PDI = 0.044). Further DLS experiments with temperature gradients revealed the thermal behavior of the polymeric nanoparticles. In a representative experiment, a solution of P([BVMIM]ZnCl_n) in EG (**M2**, $R = 0.75$, 10 mg mL⁻¹) was placed in the DLS setup, heated from 25 to 60 °C, with changes of 5 °C per step, and measurements were recorded in each step (in triplicate, Figure 30). As observed in Figure 30A, at the onset temperature, species with an average d_H of 128 nm are mainly present in the solution (blue line), as the nanoparticles are present in solution (below the T_{CP}). Subsequent measurements disclosed the gradual decreasing of d_H as the experiment reached the T_{CP} of the solution (55 °C, recorded by the transmittance tests). After that, when the solution became fully transparent, the DLS recorded the lowest d_H value (88.7 nm, red lines).

Moreover, as shown in Figure 30B, the recorded count rate of the solution as a function of temperature indicated a substantial decrease in value as the temperature increased in the studied range (40 to 60 °C), demonstrating that fewer particles are present in the solution after reaching the T_{CP} .¹²¹ Likewise, the PDI increased as a function of temperature, suggesting populations with a broader range of sizes due to the dissolution of nanoparticles in the system.

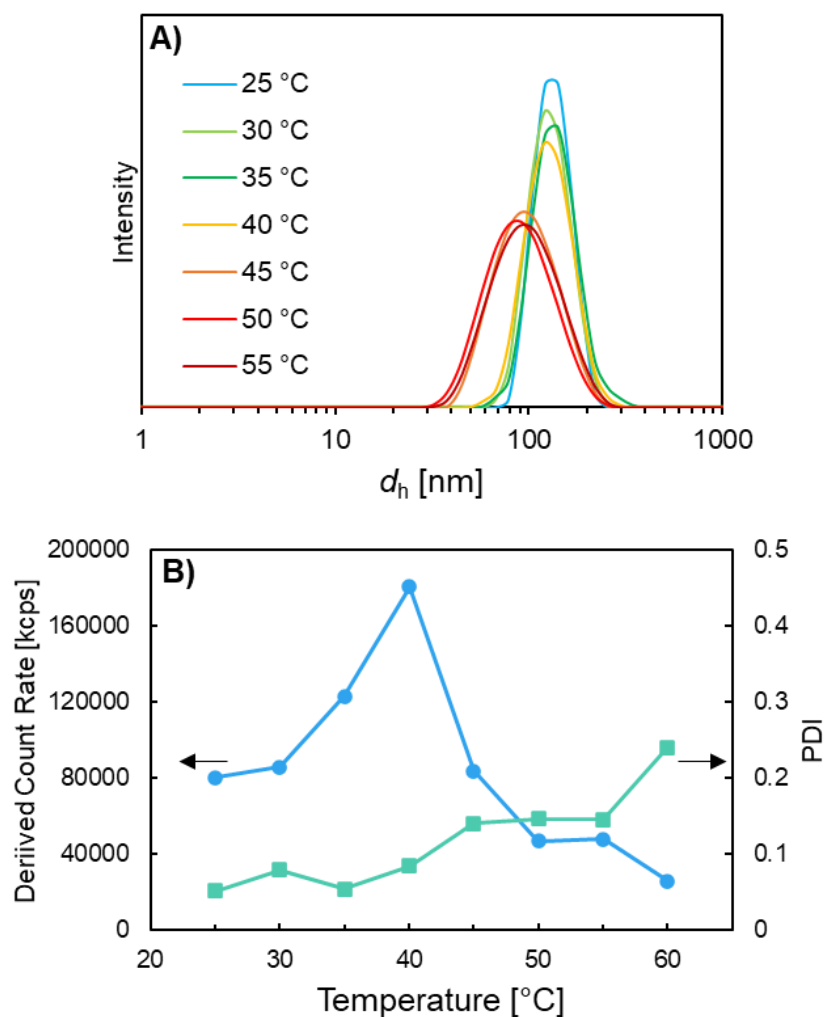


Figure 30 Plots of the A) d_H (nm) and B) derived count rate and PDI as a function of temperature, recorded by DLS, for a solution of **M2** in EG (10 mg mL⁻¹).

The effects of the molar mass were also investigated using the series of P([BVMIM]ZnCl_n) derived from precursor series **A** ($R = 0.75$). The T_{CP} as a function of the degree of polymerization (DP) is shown in Figure 31. In a similar trend as reported by Aoshima *et al.*,⁸⁷ the T_{CP} of P([BVMIM]ZnCl_n) in EG solutions is not exclusively dependent on the molar mass, specifically in the low molar mass range. However, and contrasting with those previous results, we noticed that higher values of DP induced lower values of T_{CP} , probably due to the higher concentration of halometallate anions and the strong dependence of the system on the formation of ionic clusters in solution. Thus, we hypothesized that the ionic interactions between oligomeric anions and cationic sites in the polymer chains promote their association and diminish the solubility of the entire system at low temperatures.

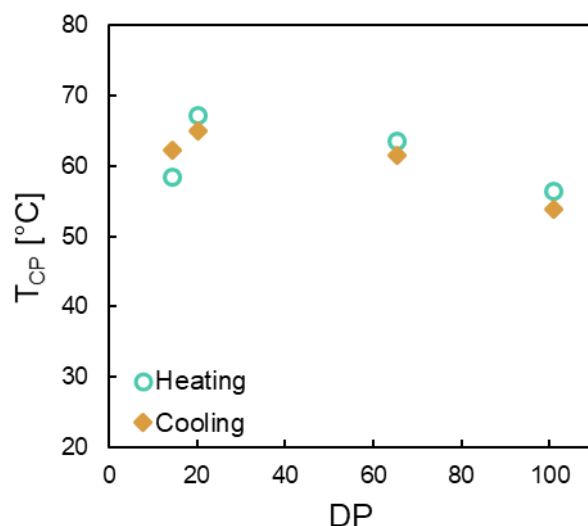


Figure 31 T_{CP} dependance on DP of solutions of [PVMIM]ZnCl_n derivatives in EG ($R = 0.75$, 10 mg mL⁻¹).

To test the dependance of the thermo-responsive behavior on the concentration of cluster ionic species, solutions of P([BVMIM]ZnCl_n) (**M2** to **M5**), with different molar ratios of ZnCl₂ ($R = 0.1$ to 0.75 , Table 13), in EG were also tested. We identified that systems with $R = 0.50$ revealed a solubility substantially increased, yielding blue-transparent solutions; subsequently, lower values of R generated transparent solutions ($R = 0.25$, and 0.1). Thus, no T_{CP} was observed for these set of experiments by transmittance examinations. Like the concentration experiments described before, DLS assays showed that decreasing the

molar ratio of anions in the system ($R = 0.1$ and 0.25) lead to form solutions with several populations and high PDI (Table 15 and Figure SI 4). Thus, under the examined conditions, the value of R should be > 0.5 to produce stable dispersion with low PDI in EG solutions. Such observations confirmed the tunable impact of the speciation effects in the final properties of chlorozincate PIL derivatives.

Table 15 Overview of the properties of P([BVMIM]ZnCl_n) (**M2 to M5**) in EG solutions, as a function of the molar ratio of ZnCl₂, measured by DLS.

Entry	R	d_H [nm]	PDI
M2	0.75	106.2	0.052
M3	0.5	94.8	0.207
M4	0.25	217.5	0.579
M5	0.1	127.6	1.000

The effect of the polymer structure on the thermo-responsive behavior was also examined by comparing [PIL]ZnCl_n derivatives **M1** and **M8** ($R = 0.75$, 10 mg mL^{-1}) with similar molar mass but different alkyl substituent in the imidazole group. As shown in Table 13, the precursors and anion exchanged derivatives showed similar solubility properties. The T_{CP} of both [PIL]ZnCl_n derivatives showed a slight difference in transmittance experiments under similar conditions (Figure 32). Therefore, alkyl substituents in the imidazole groups of chlorozincate PILs had only a slight effect (cooling cycles) on the solution properties of the described materials. Such variable could be more noticeable for longer alkyl chain substituents and/or higher values of molar mass, like other types of thermo-responsive polyelectrolytes.^{82,102,122,123}

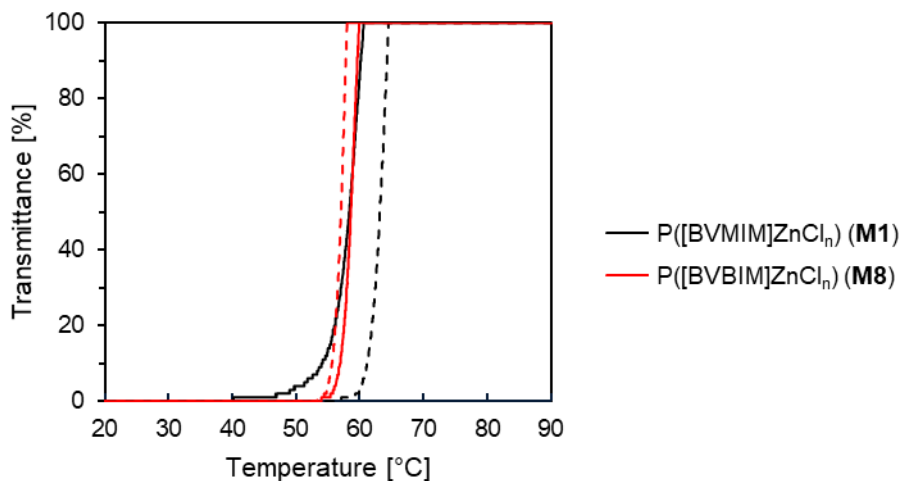


Figure 32 Transmittance measurements of halometallate PILs **M1** and **M8** (Table 13) in EG solutions (10 mg mL^{-1}); solid line: heating; dotted line: cooling.

In this manner, we disclosed the critical influence of the anion concentration on the solution properties of chlorozincate-type PILs. Thus, just like the oligomeric association between chlorozincate anions in ILs reported before,⁹³ we could assume that the ZnCl_n anions have a strong affinity to the imidazole groups in the polymer chains, which allowed to control the polymer-polymer interactions and hydrogen bonding ability, and consequently the association of polymer chains and stabilization of dispersions in EG solutions. Moreover, the dissociation of oligomeric anions and H-bonds can be triggered by increasing the temperature, creating an evolution of the structure of the ionic system;^{111,112} thus promoting UCST-type transitions by breaking the association of polymer chains at high temperatures.¹²⁴ Therefore, for our $[\text{PIL}]\text{ZnCl}_n$ derivatives, the interaction and structure of oligomeric anions varied as a function of concentration and temperature, leading to reversible solubility changes of the entire polymeric systems in solution.

In contrast, halometallate PILs derived from CoCl_2 and FeCl_3 metal chlorides showed low to null solubility in the tested solvents (**M6** and **M7**, Table 13); therefore, suggesting that interactions cation-anion were stronger for these systems and the formation of hydrogen bonds was less prominent in EG solutions. Studies aimed at establishing the systematic effect of the counter anions, substituents and polymer compositions on the solution properties of halometallate PIL derivatives are planned for subsequent investigations.

SEM measurements of casted solutions of P([BVMIM]ZnCl_n) in EG (**M2**, 10 mg mL⁻¹, Figure 33A), in silicon wafers at room temperature (see experimental section 2.8 for further details), confirmed the presence of spherically shaped nanoparticles with a mean particle diameter of 89.1 nm (SD = 22.7 nm). Moreover, as suggested by DLS experiments, SEM images of casted solutions with lower concentrations (5 mg mL⁻¹, Figure SI 5) exhibited the partial coalescence of nanoparticles in the system. These results demonstrated the stability of the formed nanoparticles of [PIL]ZnCl_n, and the strong dependence of the system on the polymer concentration. It is worth mentioning that the same casting procedure was performed at 80 °C. For this experiment, we hypothesized the dissolution of nanoparticles under these conditions. As shown in Figure SI 6, no particles were spotted by casting at increased temperatures; Thus, we could confirm the dissolution of nanoparticles of [PIL]ZnCl_n) in EG solutions as a function of temperature.

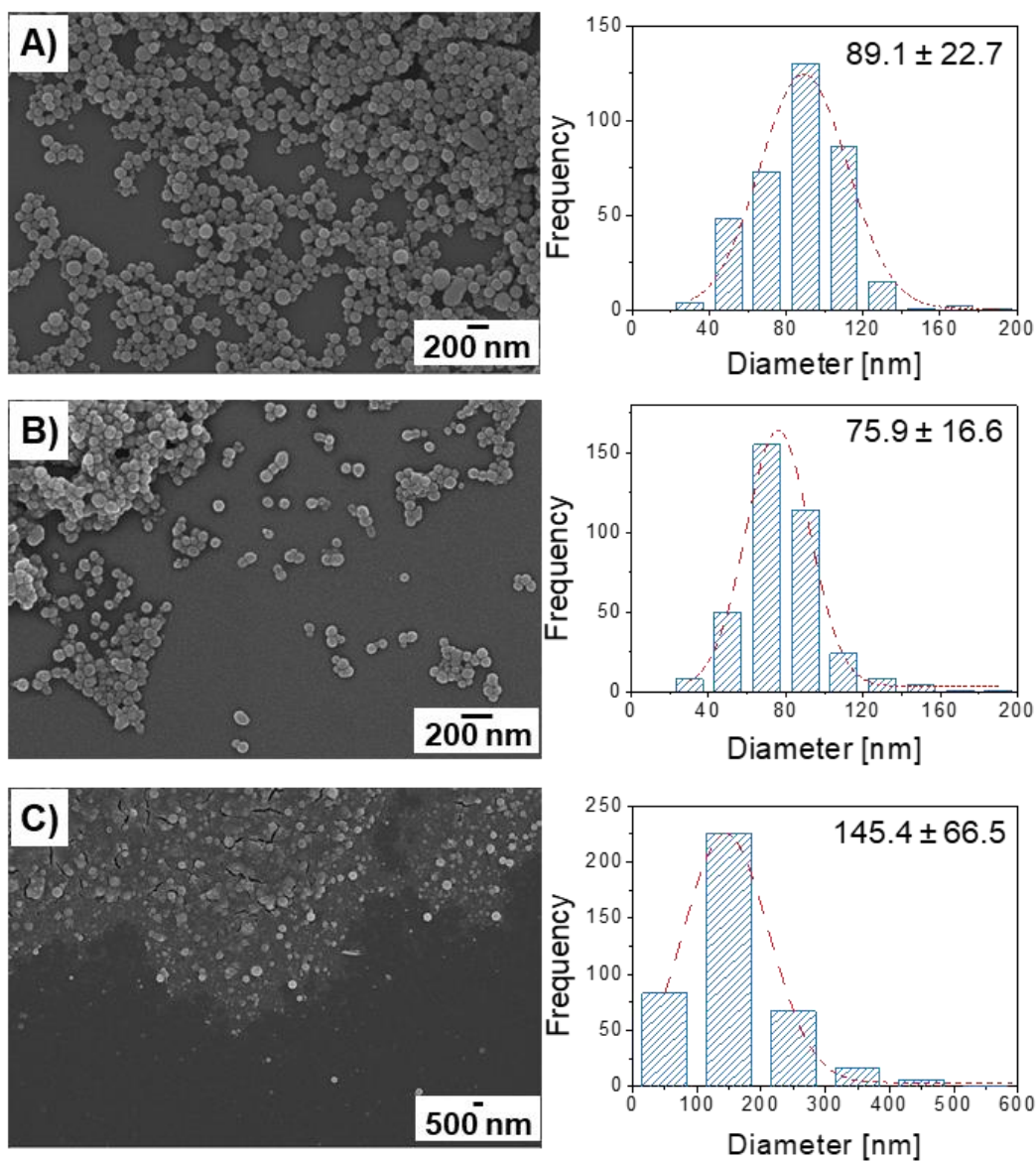


Figure 33 SEM images and particle size distributions of polymeric nanoparticles casted at room temperature from solutions of P([BVMIM]ZnCl_n) (**M2**, 10 mg mL⁻¹) in different solvents: A) EG, B) glycerol, and C) 1,3-propanediol.

Additional transmittance experiments revealed that the described UCST behavior (and Tyndall effect) of [PIL]ZnCl_n in EG was also observed for other types of glycols as solvents, such as 1,3-propanediol, diethylene glycol, and glycerol (Figure SI 7). SEM analysis of the corresponding casted solutions disclosed the existence of spherical nanoparticles with variable particle diameter according to the solvent used (Figure 33 B and C). Therefore, the chlorozincate anions were able to form H-bonds with other types

of glycols; thus, demonstrating the feasibility of the polymer system to be used in multiple kinds of glycolysis reactions with other glycols.

Interestingly, we also observed a UCST behavior for [PIL]ZnCl_n derivatives in mixtures of EG:H₂O. This finding is essential for the separation capacity of MPCs after the glycolysis of PET. As shown in Table 13, for [PIL]ZnCl_n derivatives with $R = 0.75$ (**M1**, **M2**, and **M8**), we observed a UCST behavior in EG and mixtures of EG:H₂O = 95:5. Then, increasing the ratio of H₂O diminished the phase separation by temperature (EG:H₂O = 90:10) diminished the phase transition by temperature, showing only the Tyndall effect, and no T_{CP} was recorded by transmittance analyses. Subsequently, the phase separation behavior was completely vanished at higher ratios of H₂O. This effect could be due to the moderate solubility of ZnCl₂ in H₂O: at fixed conditions of pH and ionic strength, ZnCl₂ can be solubilized in aqueous solutions; however, an excess of water promotes the formation of zinc oxychloride precipitates.^{125,126} Thus, concerning our [PIL]ZnCl_n systems, the presence of oxychloride species could hinder the formation of stable nanoparticles with the increasing ratio of H₂O, and consequently the solubility of the polymeric system. Thus, taking advantage of the UCST-type behavior of [PIL]ZnCl_n derivatives, we could suggest favorable conditions for recovering the MPCs after the glycolysis reaction.

In summary, these analyses confirmed that the features of halometallate ILs can be extrapolated to halometallate PILs to tune the properties of macromolecular systems.¹¹⁰ The molar ratio of the anion had a substantial effect on the final properties of the PIL systems. Furthermore, we examined the solution behavior of the copolymer systems under the conditions during and after the glycolysis reaction. Therefore, we could expect a different separation capacity of the MPC from the depolymerization reaction according to the type of the copolymer.

3.3.2.2. Solution properties of halometallate [PIL]MCl_n copolymers

The design and selection of the copolymers reported in this work had as a basis the copolymerization of hydrophilic and ionic monomers to yield thermo-responsive materials with electrostatic interactions and hydrogen bonding in solution. Thus, copolymers of P([BVBIM]ZnCl_n-co-DMAEMA) and derivatives were expected to show a Lower Critical Solution Temperature (LCST) behavior in aqueous solutions.¹⁰¹ Nonetheless, these series of halometallate copolymers exhibited low to null solubility in water (entry **M9**, Table 16). This effect could be ascribed to the formation of zinc oxychloride solids, which have low to null solubility in water, and possible complexation effects of the amino groups in the polymer backbone and the salt in aqueous solutions, which can form non-soluble copolymer complexes.¹²⁶ Furthermore, as discussed before, the speciation effect, observed for halometallate type ILs,⁹³ contributed to form oligomeric ZnCl_n species, which could decrease the solubility of the entire system in aqueous solutions under standard conditions. In contrast, Cl-type copolymer precursors, showed good solubility in aqueous solutions (Entries **C12**, **D3**, and **D4**, Table 16).

Table 16 Solubility properties of selected copolymers with variable structure and compositions in solutions of EG, H₂O, and mixtures thereof. ^{a)}

Entry	Polymer/Solvent	Composition [%] ^{b)}					EG:H ₂ O ratio				
		([BVBIM])	DMAEMA	100:0	95:5	90:10	80:20	60:40	40:60	20:80	0:100
C12	P([BVBIM]Cl-co-DMAEMA)	36.8	63.2	S	S	S	S	S	S	S	S
M9	P([BVBIM]ZnCl _n -co-DMAEMA)	36.8	63.2	U	U	S	S	S	S	S	NS
D3	PDMAEMA- <i>qb</i> -P([BVBIM]Cl-co-DMAEMA)	7.0	93.0	S	S	S	S	S	S	S	L
M10	PDMAEMA- <i>qb</i> -P([BVBIM]ZnCl _n -co-DMAEMA)	7.0	93.0	B	B	B	S	NS	NS	NS	NS
D4	PDMAEMA- <i>qb</i> -P([BVBIM]Cl-co-DMAEMA)	14.1	85.9	S	S	S	S	S	S	S	L
M11	PDMAEMA- <i>qb</i> -P([BVBIM]ZnCl _n -co-DMAEMA)	14.1	85.9	U	B	B	B	NS	NS	NS	NS

^{a)}S: soluble; I: insoluble; U: UCST-type phase separation; L: LCST-type phase separation; NS: non-soluble; 1 wt. % solutions; ^{b)} determined by ¹H NMR in DMSO-*d*₆.

After anion exchange, the solubility of the copolymers was significantly altered; for instance, statistical copolymers comprising further hydrophilic compositions showed a tunable UCST behavior in EG solutions as a function of the monomer composition. In this regard, Figure 34A shows that adding the hydrophilic DMAEMA in the copolymers induced a gradual increase of the T_{CP} of the corresponding solutions in EG. For instance, the transmittance curves (heating and cooling) of the reference homopolymer (**M8**, Table 13) showed a T_{CP} of *ca.* 40 °C. Such values increased for copolymers with an increasing ratio of DMAEMA:BVBIM (variable T_{CP} up to 16 °C). Copolymers with greater PDMAEMA content were also tested; however, although a thermal transition was visible for such solutions of copolymers, a sharp transition from cloudy to transparent solution could not be recorded by transmittance experiments. As discussed before, this fact could be attributed to the decreased concentration of ionic sites and anion concentration in the system. Thus, we could conclude that the ionic interactions and H bonding between anions and ionic sites enhance the association of polymer chains in EG, reducing the solubility and yielding turbid solutions at low temperatures.

The solution behavior of *quasi*-block copolymers was also modified as a function of the composition of the final materials. For instance, Cl-type *quasi*-block copolymer precursors were soluble in EG, H₂O, and mixtures thereof (entries **D3** and **D4**, Table 16). As expected, these samples showed a LCST-type phase separation in aqueous solutions because of the “pure” PDMAEMA segment in the polymer chain. Such phenomenon was vanished by the addition of EG to the solvent mixture, which promoted the solubility of the copolymers. On the other hand, *quasi*-block copolymers with chlorozincate anions (entries **M10** and **M11**, Table 16) showed low to null solubility in aqueous solutions. Thus, the complexation effects (Zn–N) became more prominent for copolymers with a high content of PDMAEMA. Consequently, chlorozincate *quasi*-block copolymers only showed solubility for solutions with EG:H₂O ratios greater than 80:20. For the latter examples, bluish solutions were observed, and a clear UCST transition was only observed for EG solutions of the statistical and *quasi*-block copolymers with the highest composition of P([BVBIM]ZnCl_n) (Entries **M9** and **M11**, Table 16). The decreasing d_H , PDI, and count rate

measured by DLS ($d_H = 136$ nm and 65 nm, in solutions of EG:H₂O = 100:0 and EG:H₂O = 80:20, respectively) confirmed the increasing dissolution of the studied *quasi*-block copolymers by the addition of water to the solution.

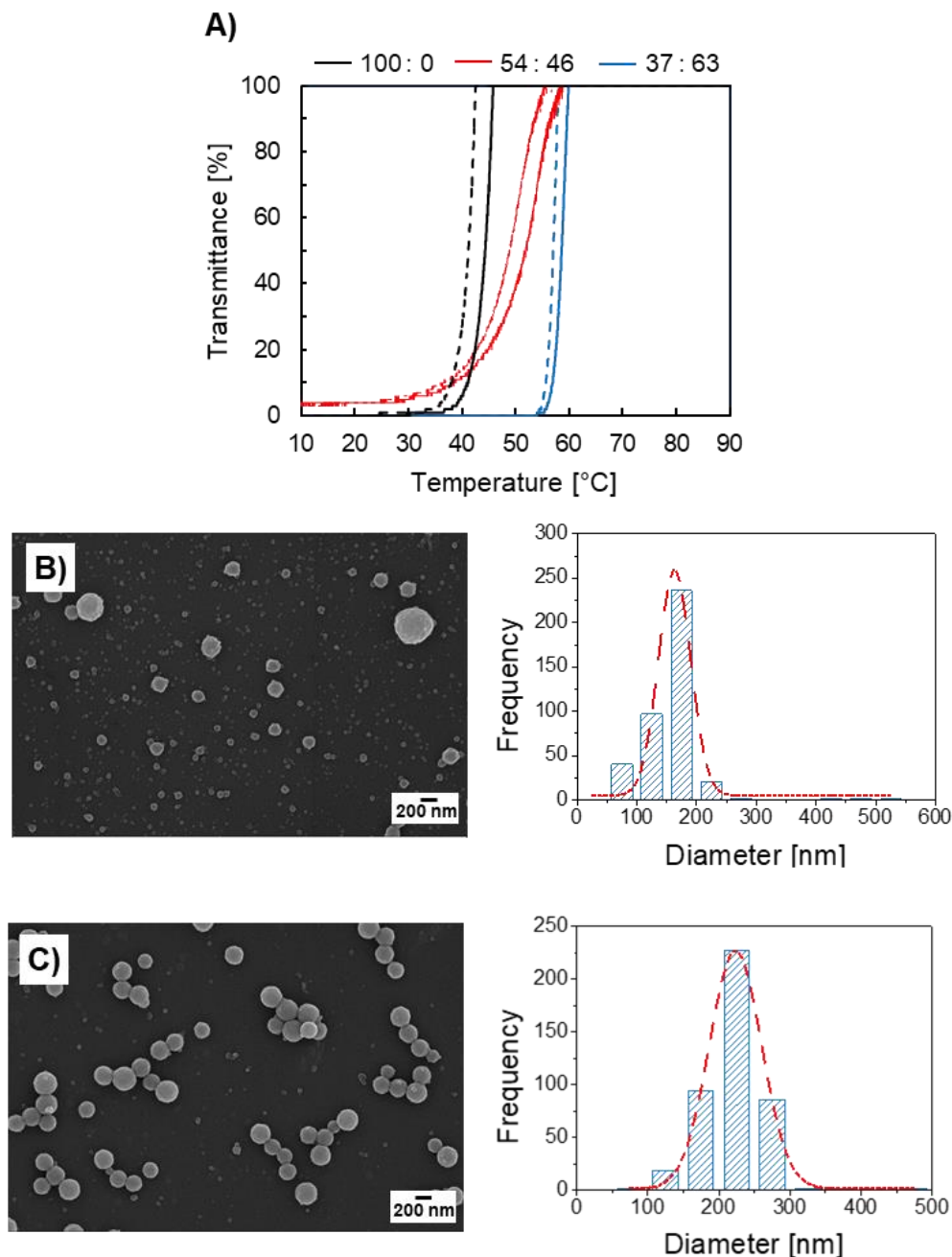


Figure 34 A) Transmittance measurements solutions of [PIL]ZnCl_n (P([BVBIM]ZnCl_n), **M8**) and copolymers P([BVBIM]ZnCl_n-*co*-DMAEMA) with variable molar composition [BVBIM]Cl_n:DMAEMA = 54:46 and 37:63 in EG (10 mg mL⁻¹); solid line: heating; dotted line: cooling. SEM images and particle size distributions of polymer nanoparticles casted at room temperature from solutions of [PIL]ZnCl_n B) PDMAEMA-*qb*-P([BVBIM]ZnCl_n-*co*-DMAEMA) (**M10**) and C) PDMAEMA-*qb*-P([BVBIM]ZnCl_n-*co*-DMAEMA) (**M11**) in EG (10 mg mL⁻¹).

As seen in Figure 34B and C, SEM confirmed the presence of spherical-shaped nanoparticles in EG solutions of *quasi*-block copolymers (**M10** and **M11**) with homogeneous populations. As shown, the presence of hydrophilic sites in the copolymer system supported the stabilization of well-defined nanoparticles in EG solution. Moreover, as revealed by the analysis of the nanoparticle populations in both examples, the d_H and stability of the obtained nanoparticles were effectively fine-tuned by modifying the composition of [BVBIM]ZnCl_n in the system.

In this manner, we demonstrated that copolymers could also be tailored with additional solubility features, for instance to fine-tune the T_{CP} or to add LCST behavior in aqueous solutions. As exemplified, such characteristics were helpful to stabilize nanoparticles under the described conditions. The examples described confirmed the prominent effect of the molar ratio of MCl_n on the physicochemical properties of the copolymers. The solution behavior of the copolymer systems revealed that, as a function of temperature, [PIL]ZnCl_n derivatives formed homogeneous solutions in glycol solvents at high temperatures (above the T_{CP} of the solution) and cloudy solutions below the T_{CP} of the system. Well-defined and stabilized particles with nanometric size were observed under the described conditions. As shown next, such features benefit the catalytic performance, and the capability of separation and removal of impurities of the polymer catalyst. Mainly, homopolymers and statistical copolymers with chlorozincate anions were valuable candidates as catalyst in the depolymerization of polyesters under glycolytic conditions.

Chapter 4

Glycolysis of post-consumer PET using MPCs

The following sections describe the investigations on the glycolysis of post-consumer PET using MPCs as catalyst comprising: (i) the screening of the catalytic performance of a series of MPCs with variable composition, molar mass, counter ions, and structure; (ii) the selection of optimal MPCs with superior catalytic performance; (iii) the optimization of the glycolysis procedure using an automated parallel platform and screening the effect of variable PET feedstocks (different type and coloration) as a function of catalytic performance; (iv) tests regarding the removal of catalyst are presented and subsequent catalyst reuse; and (v) the evaluation of the removal capacity of colorants by the selected MPCs.

4.1. Preliminary experiments - Selection of catalyst

We first tested a series of halometallate PILs with variable anions. According to previous reports,^{19,47,49,55,127,128} several factors govern the catalytic glycolysis of PET using ILs (*e.g.*, reaction time, temperature, and PET:catalyst:EG ratio, IL symmetry, anions, etc.). A PET:catalyst:EG weight ratio of 1:0.1:4, reaction temperature between 170 to 190 °C and 4 to 6 h of reaction has been proposed as starting conditions for the highest selectivity of the recycled monomer BHET.⁴⁷ Therefore, in the following series of preliminary experiments, we used similar reaction conditions. The catalytic performances of halometallate PILs were tested as a function of the conversion of PET and selectivity of isolated BHET (see experimental section for further details).

Initially, we carried out a screening of $[\text{PIL}]\text{MCl}_n$ catalysts by modifying the structure, molar mass, and composition of the polyelectrolyte chains and the type and molar ratio of anions. According to previous reports,⁴⁸ the selection of anion has a crucial effect on the catalytic activity of the ionic system. Thus, we tested series of halometallate homopolymer with similar molar mass but comprising variable alkyl substituents in the polymer chain and different counteranions. As raw material, we used post-consumer PET of transparent bottles.

As observed in Figure 35, we corroborated the effect of the anions on the conversion of PET and selectivity of BHET. The glycolysis reaction using a [PIL]Cl precursor (**B1**) as catalyst yielded a conversion of PET <10%. This result could be attributed to the low Lewis acidity of chloride anions. Thus, the conversion of PET remained low for such types of (co)polymers.

The conversion of PET was increased by using anion exchanged PIL derivatives. For example, P([BVBIM]ZnCl_n) derivatives from **B1** and **B2** promoted the conversion of PET up to 20%; however, the selectivity of BHET remained low in both experiments (< 10%). P([BVMIM]ZnCl_n) derivatives from **A1** and **A2** showed a higher conversion and selectivity of PET (up to 50%) and BHET (< 30%) in both cases. The limited conversion of PET in the former experiments suggests that the growth of alkyl chain substituents in the polymer backbone (butyl substituents in P([BVBIM]ZnCl_n)) increased steric effects and diminish the formation of hydrogen bonds (H-bonds) —between the carbonyl groups of PET chains and cationic moieties.¹²⁹ Thus, halometallate derivatives P([BVMIM]ZnCl_n), with less voluminous methyl substituents on the polymer backbone, showed higher interactions with PET chains and consequently better catalytic performance. However, as shown later for MPCs based on statistical copolymers, it should be noted that additional functionalities in the polymer catalyst can enhance the catalytic performance, as this strategy was also effective to reduce steric effects and increase the formation of H-bonds of the catalytic systems.

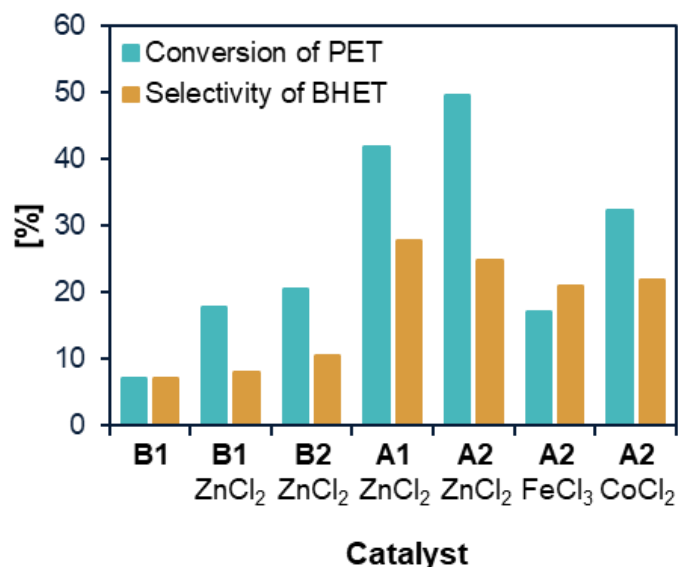


Figure 35 Effect of halometallate PIL catalysts (precursors and metal chloride indicated, $R = 0.7$) on the glycolysis of post-consumer PET and selectivity of BHET.

As expected, halometallate derivatives of FeCl₃ and CoCl₂ also showed good catalytic activity, however, for such cases the conversion of PET remained below the values obtained by using [PIL]ZnCl_n derivatives. This result was in good accordance to previous reports, where the Lewis acidity of species derived of ZnCl_n was higher relative to other halometallate derivatives.^{48,130} Furthermore, as discussed before, the distinctive evolution of the speciation of chlorozincate anions, as a function of temperature, triggered the dissociation of voluminous chlorozincate anions to form of ionic species during the glycolysis reaction. This remark considerably improved the interaction of Lewis acidic sites with PET chains. Consequently, the depolymerization mechanism occurred aided by the synergic effect of cationic and dissociated anionic species to yield improved catalytic performance; in a similar fashion as homogeneous catalysts.^{48,131}

From this results and the examination of the properties of halometallate (co)polymers in solution, we could conclude that chlorozincate PILs could be the most suitable catalyst aiming to optimize the catalytic activity of the MPCs. For this purpose, these catalysts were evaluated in glycolysis experiments on a larger scale utilizing an automated parallel platform.

4.2. The parallel platform for the glycolysis of post-consumer PET

To perform a more extensive screening of (co)polymer catalysts and optimize the glycolysis of post-consumer PET, we implemented a HTE procedure to rapidly evaluate a library of MPCs using a robotic system. For this purpose, we used an automated parallel platform (FORMAX, Chemspeed) provided with a formulation block adapted to perform catalyzed glycolysis reactions (**Figure 14**, see experimental section 2.6 for further information). Hence, a set of up to 6 glycolysis reactions could be carried out in open reactors with the possibility of sample taking to follow up conversion (by SEC or ^1H NMR).

Preliminary glycolysis experiments were carried out using a reference catalyst to prove the viability of the glycolysis reaction using the automated platform. The reference catalyst consisted of ILs supported on superparamagnetic nanoparticles (NPs).⁶⁰ Therefore, we compared the catalytic performance between reactions performed in the robotic platform and the conventional procedures using oil baths and magnetic stirring. The conditions of glycolysis were kept the same in all cases: PET:catalyst:EG weight ratio: 1.0: 0.04 – 0.08 :4.0, reaction temperature of 180 °C, and reaction time of 4h. In the case of the reactions performed in the FORMAX platform, the reactions were performed using mechanical stirring with a disperser disc at 500 rpm. Figure 36 shows the results of PET conversion and BHET selectivity after purification by crystallization.

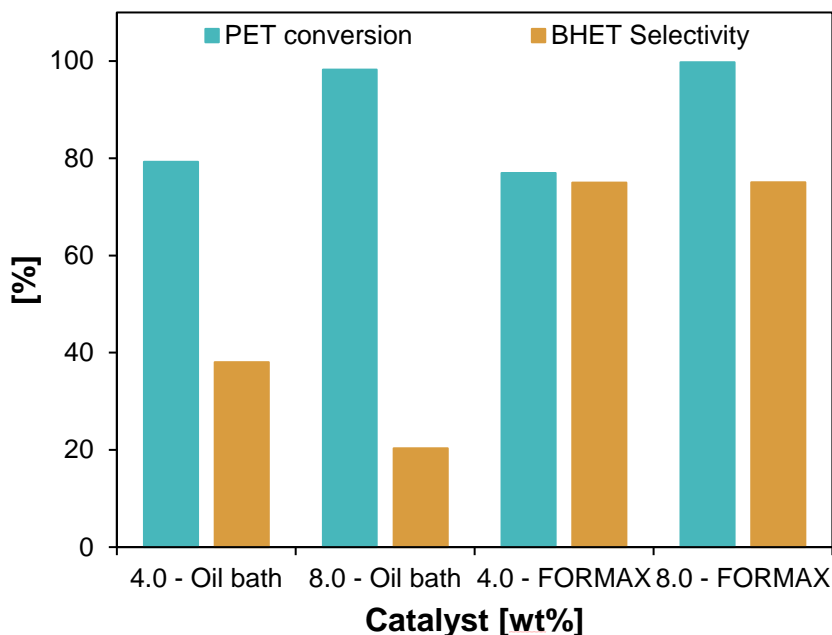


Figure 36 Effect of the amount of standard catalyst on the conversion of PET and selectivity of BHET using different procedures (oil bath and FORMAX platform).

As observed, the conversion of PET was $> 80\%$ using both procedures. Remarkably, concerning the selectivity of BHET, we detected an increase in the selectivity for the experiments performed in the FORMAX platform. For example, the glycolysis in an oil bath with the catalyst:PET ratio = 4.0 wt.% reached a selectivity of 38%; meanwhile using the mechanical stirring of the FORMAX the selectivity of BHET was increased to 75%. The same tendency was reproduced in the case of a higher catalyst:PET ratio (8.0 wt.%). In these cases, the conversion of PET was enhanced to reach 99% and up to 75% of selectivity. These results could be attributed to the effective control of temperature and mechanical stirring provided by the automated platform; which contributed to enhance the catalyst diffusion and subsequent catalyst adsorption and interaction with PET flakes.⁴⁹

Additionally, as the reactions were carried out in open reactors, water coming from humid feedstocks and/or water possibly formed during transesterification reactions could be removed by simple evaporation, which avoided competing hydrolysis reactions to hydroxylated oligomers or terephthalic acid.^{132,133} Therefore, using a reference catalyst, we could conclude that the conditions used on the FORMAX platform were beneficial for our

glycolysis procedure. In the following sections, we present screening and optimization studies using MPCs and the described automated parallel procedures.

4.3. Screening of MPCs as catalysts

To follow up the selection of MPCs with optimal structure and functionalities, we evaluated the effect of the molar ratio (R) of ZnCl_2 in the MPC. This feature dominates the Lewis acidity and consequently the catalytic activity.¹¹⁷ As shown in Figure 37, we performed glycolysis reactions of post-consumer PET flakes and evaluated the catalytic performance as a function of R . When the value of R was in the range of 0 to 0.25, the catalytic performance did not exceed 50% PET conversion. As discussed earlier the low Lewis acidity of Cl^- anions diminished the catalytic activity of the MPCs.

Thereafter, for polymers with $R = 0.5$ and 0.75 the catalytic performance was increased to reach high conversion of PET and a selectivity of BHET in the range of 65 to 72%. These data allowed us to confirm that the increasing concentration of oligomeric chlorozincate anions, and therefore increasing Lewis acidity of the system, helped the overall catalytic activity of the polymeric systems.¹¹⁷ Additionally, in comparison with preliminary results, the conditions employed in this series of experiments ($T = 180\text{ }^\circ\text{C}$, $t = 4\text{ h}$, 500 rpm, FORMAX platform) boosted the efficiency of the process to yield a conversion of PET of up to 93% and selectivity of BHET of 72%. In this way, we confirmed the catalytic activity of $[\text{PIL}]\text{ZnCl}_n$ derivatives and found an optimal molar ratio of ZnCl_2 in our catalytic systems for the efficient chemical upcycling of PET.

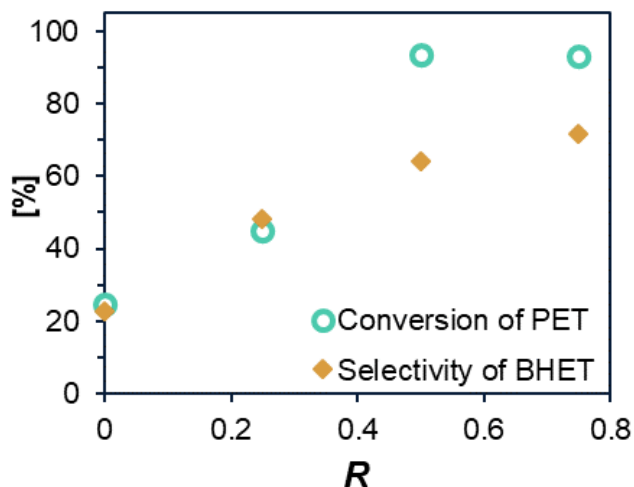


Figure 37 Effect of the molar ratio (R) of the $[\text{PIL}]\text{ZnCl}_n$ (**M2** to **M5**, Table 13) on the glycolysis of PET and selectivity of BHET (isolated).

These examinations showed the crucial role of the composition, anions, and anion molar ratio in the catalytic performance of the MPCs. The following discussion describes the catalytic activity on PET glycolysis of a series of copolymers with variable composition and structure. Table 17 summarizes the properties and catalytic activity of the copolymers utilized in this investigation. We targeted a series of statistical, *quasi*-block and block copolymers with similar monomer compositions, including hydrophobic and hydrophilic thermo-responsive segments.

To explore the effect of adding hydrophilic segments to MPCs, the first set of experiments consisted of testing a library of chlorozincate statistical copolymers ($\text{P}([\text{BVBIM}]\text{ZnCl}_n\text{-co-DMAEMA})$), with M_n in the range of 10 to 25 kg mol^{-1} and variable content of $[\text{BVBIM}]\text{ZnCl}_n$:DMAEMA ranging from 90:10 to 80:20%, as catalyst for the glycolysis of PET in an automated platform. Figure 38 shows the PET conversion and BHET selectivity as a function of the composition of copolymers and M_n . As observed, the conversion of PET was relatively low ($< 71\%$) for the series of low molar mass copolymers (10 kg mol^{-1} , samples **C1** to **C6**, Table 10) in all polymer compositions. As expected, the catalytic performance decreased as a function of the proportion of ionic sites in the system. Thus, for this series of copolymers the catalytic performance was directly proportional to the content of $[\text{BVBIM}]\text{ZnCl}_n$ in the polymer. It is worth mentioning that

MPCs with lower content of $[\text{BVBIM}]\text{ZnCl}_n$ also showed acceptable catalytic activity under these experimental conditions (ca. 80% PET conversion and 67% BHET selectivity).

Compared to the halometallate homopolymers ($\text{P}[\text{BVBIM}]\text{ZnCl}_n$, **B1**, Figure 35), tested during the preliminary studies (Section 4.1), the hydrophilic fractions PDMAEMA in the copolymers increased the interaction and H-bond formation between polyester chains and the corresponding catalysts.¹²⁹ In this way, the copolymers with a high content of $[\text{BVBIM}]\text{ZnCl}_n$, in the range of 80 to 90 %, yielded good conversion of PET; however, the selectivity for the monomer remained low due to the lower composition of hydrophilic sites. In contrast, we observed better results of BHET selectivity for copolymers with a content of $[\text{BVBIM}]\text{ZnCl}_n$ in the range of 35 to 90% . These results also suggest that a lower content of catalytic sites could be used in the copolymers, yielding a system with acceptable catalytic performance.

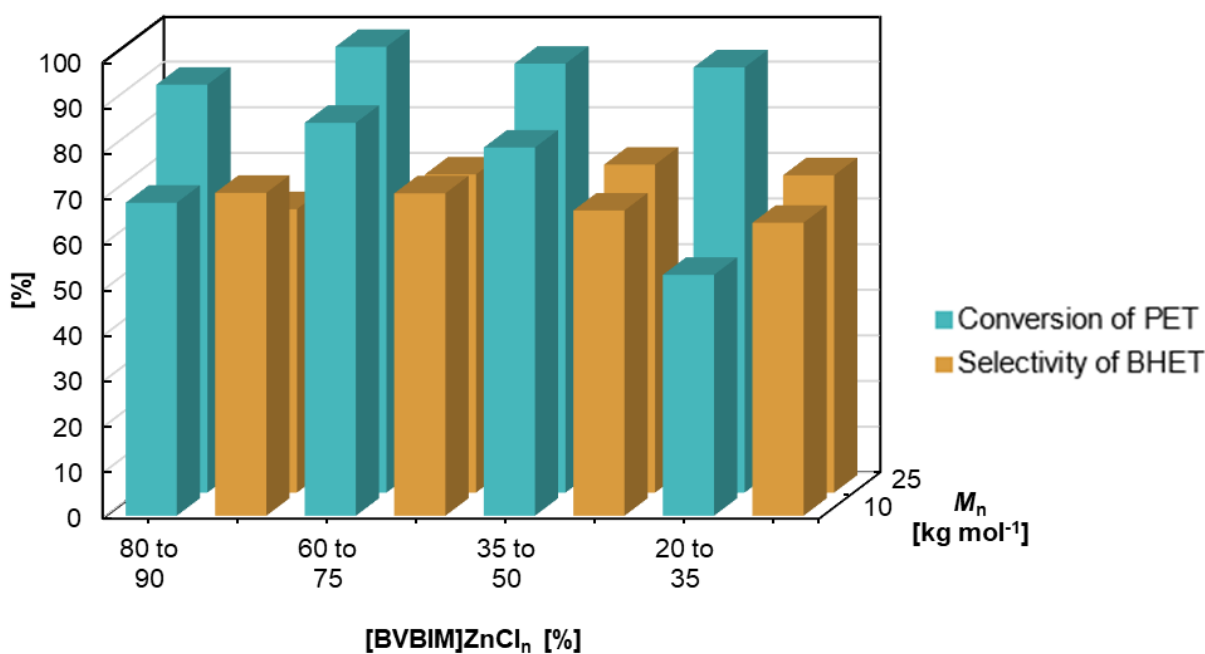


Figure 38 Effect of the molar ratio of MPCs ($\text{P}[\text{BVBIM}]\text{ZnCl}_n\text{-co-DMAEMA}$), series **C**) on the conversion of PET and selectivity of BHET (FORMAX platform, 1 atm, 180 °C, and 4h).

Such trend was consistent for copolymers of higher molar mass (25 kg mol^{-1} , **C7** to **C11**, Table 10). Remarkably, as observed in Figure 38, even the copolymers with a relatively low composition of ionic sites (20 to 35 and 35 to 50% of $[\text{BVBIM}]\text{ZnCl}_n$ content) delivered an excellent conversion of PET (up to 93%) and selectivity of BHET (up to 69%).

The molar mass did not reveal a critical influence on the catalytic performance; however, we could notice a slight increase of catalytic activity for high molar mass copolymers (conversion of PET and selectivity of BHET up to 97% and 72%, respectively). Such observation could be attributed to the higher hydrophilicity conveyed by the polymer chains of higher molar mass and the content of hydrophilic comonomer, which might contribute to the dissolution and diffusion of catalytic sites.

As observed, the copolymers of higher molar mass showed the best catalytic performance with a composition of [BVBIM]ZnCl_n between 35 to 90 %; consequently, we could confirm the predominant effect of the hydrophilicity of the copolymers and proposed this range of composition and molar mass as the optimal composition for the synthesis of MPCs. Interestingly, we also tested a copolymer obtained by conventional radical polymerization with similar composition; however, for this case, we observed a relatively low conversion of PET (53%) and selectivity of BHET (42%). Thus, the catalytic performance of such catalyst was similar to bulk or supported catalysts; showing steric effects hindering the interaction of ionic sites and ester bonds in PET chains.⁴⁹ These experiments allowed us to demonstrate the effect of the controlled molar mass and hydrophilicity of the copolymers, as these characteristics aided the MPC to surmount the steric effects, observed for homopolymers and copolymers obtained by free radical polymerization, to yield high catalytic activity in the glycolysis of PET.

Altogether, screening this library of P([BVBIM]ZnCl_n-co-DMAEMA copolymers as catalyst allowed us to find an effective molar composition and parallel system of PET glycolysis using an automated protocol. In addition, the catalytic activity of statistical copolymers opened the door to integrate different segments in the polymer structure and increase the functionalities of the copolymers. For instance, we proposed employing *quasi*-block copolymers to add thermo-responsive segments to the copolymer system in aqueous solutions. As listed in Table 17, using these series of MPCs, we found comparable catalytic performance to that obtained with statistical copolymers (see entry **1** for comparison with statistical copolymers). Nonetheless, we observed a slight decrease in the reaction performance (see for instance entries **2** to **5**). Similarly to previous results of low molar mass copolymers, the decrease of the [BVBIM]ZnCl_n catalytic sites per chain in

the MPCs resulted in the decline of catalytic activity. Therefore, for these series of copolymers, the steric effects were more predominant than the hydrophilicity effects of the MPCs.

Table 17 Properties and catalytic performance of the MPCs used in this study.

Entry	Polymer	Polymer ^{e)}	$M_{n, \text{theo}}$ [kg mol ⁻¹] ^{a)}	Composition [%] ^{b)}			PET conversion [%] ^{c)}	BHET selectivity [%] ^{d)}
				[BVBIM]Cl	DMAEMA	MM		
1	<i>Statistica I</i>	P([BVBIM]ZnCl _n -co-DMAEMA)	15.2	36.8	63.2	-	96.0	79.6
2	<i>Quasi-block</i>	PDMAEMA- <i>qb</i> -P([BVBIM]ZnCl _n -co-DMAEMA)	7.4	4.5	95.5	-	74.8	50.8
3	<i>Quasi-block</i>	PDMAEMA- <i>qb</i> -P([BVBIM]ZnCl _n -co-DMAEMA)	12.1	8.5	91.5	-	90.9	62.6
4	<i>Quasi-block</i>	PDMAEMA- <i>qb</i> -P([BVBIM]ZnCl _n -co-DMAEMA)	3.8	7.0	93.0	-	70.7	68.1
5	<i>Quasi-block</i>	PDMAEMA- <i>qb</i> -P([BVBIM]ZnCl _n -co-DMAEMA)	3.8	14.1	85.9	-	86.1	68.3
6	<i>Block</i>	PMMA- <i>b</i> -P([BVBIM]ZnCl _n -co-DMAEMA)	26.9	13.6	41.8	44.6	57.9	42.8
7	<i>Block</i>	PMMA- <i>b</i> -P([BVMIM]ZnCl _n -co-DMAEMA)	22.6	20.4 ^{f)}	18.4	61.2	95.2	64.6

^{a)} Determined by the formula $M_{n, \text{theo}} = \{([M]_{\text{[BVBIM]Cl}}/[CTA]_0 \times \text{Conv.} \times M_{\text{[BVBIM]Cl}}) + ([M]_{\text{DMAEMA}}/[CTA]_0 \times \text{Conv.} \times M_{\text{DMAEMA}}) + M_{n, \text{CTA}}\}$; ^{b)} determined by ¹H NMR in DMSO-*d*₆; ^{c)} Estimated by gravimetry and eq. 2 ; ^{d)} Isolated yield determined by eq. 3 ^{e)} $R = 0.75$; ^{f)} [BVMIM]Cl was used as comonomer.

In this regard, the catalytic performance could be enhanced by simply increasing (i) the composition of catalytic sites in the polymer (see for instance entries **2** and **3** and **4** and **5**, respectively) or (ii) the concentration of catalyst during the depolymerization reaction.¹³⁴ On the other hand, as assessed before, steric and solubility effects attributed to the modification or addition of alkyl substituents and hydrophilic and hydrophobic

segments to the MPCs could reduce the formation of hydrogen bonds between MPCs and the PET chains during the glycolysis.¹²⁹ Such premise was more evident for amphiphilic block MPCs (entry **6**). Nevertheless, a slight increase in the composition of catalytic sites and a decrease of the alkyl side chain of the ionic sites (entry **7**) benefited the catalytic activity. In this manner, we could conclude that, adding different hydrophilic or hydrophobic segments and maintaining a standardized composition of catalytic sites in the MPCs allowed to obtain polymer catalysts without considerably affecting their catalytic performance. This study could be extended to provide the MPCs with additional features according to the requirements of the procedure or feedstocks and/or to reduce the manufacture expenses of the catalyst; for instance, by using common comonomers that could increase the hydrophilicity of the copolymers and at the same time reduce expenses of manufacture. Therefore, as shown later, we used the specific properties and functionalities of the MPCs according to the requirements of the glycolysis system.

4.4. Optimization of PET glycolysis using MPCs

As demonstrated in previous experiments, we could expect variable catalytic performance according to the composition and structure of the MPCs. Furthermore, the examination of the MPCs solution properties allowed us to get more insights regarding their possible separation capacity from the glycolysis products, by-products, and impurities; according to the structure of the corresponding MPC. Moreover, the observed results showed that [PIL]ZnCl_n derivatives were suitable catalysts for the glycolysis of PET due to: (i) ZnCl₂ is an inexpensive and non-toxic compound,¹³⁵ (ii) in comparison with other halometallate PILs, [PIL]ZnCl_n derivatives revealed the highest catalytic activity, and (iii) these materials showed an UCST behavior, even with solutions with a small percentage of H₂O. Therefore, as shown in subsequent results, we could hypothesized the quasi-homogeneous glycolysis of PET to yield high catalytic performance and the heterogeneous separation of the MPC after the glycolysis reaction.¹³⁵ The following discussions analyze the optimization of the quasi-homogeneous system to perform the glycolysis of post-consumer PET and the separation of catalyst via the UCST-type behavior of the catalyst. Next, we introduce kinetic studies of PET depolymerization to find the optimal conditions of glycolysis

reactions. Finally, we analyze the influence of post-consumer PET coloration in the catalytic performance, as well as the reusability capabilities of the catalyst.

4.4.1. Kinetic investigations on PET glycolysis using MPCs

To evaluate the effect of the temperature and the amount of catalyst on the production of BHET during the glycolysis PET, we performed kinetic studies of the glycolysis reaction using a statistical copolymer as catalyst and transparent post-consumer PET. To assess the effect of temperature, time of reaction, and amount of catalyst, we used two different techniques to estimate the instantaneous yield of BHET. For this purpose, Dimethyl Sulfone (DS) was added to the reaction mixtures as an internal standard for ^1H NMR analysis. We chose DS as internal standard due to its stability at high temperatures (b.p. = 238 °C); moreover, this standard did not overlap with the BHET signals in ^1H NMR measurements (Figure SI 8). Therefore, the yield of BHET was estimated by sampling the glycolysis reaction with the robotic platform every hour and analyzing the corresponding samples by two analytical techniques (^1H NMR and SEC). The instantaneous yield of BHET was estimated via ^1H NMR by comparing the signal intensity of the internal standard ($\delta = 3.0$ ppm) and the signals of BHET ($\delta = 3.9$ and 4.2 ppm)

The yield of BHET was also estimated via SEC using a calibration curve constructed with standards solutions of BHET (Figure 15). First, we compared both analytical techniques to evaluate the viability of kinetic studies for our glycolysis system. As shown in Figure 39, the yield of BHET was similar when estimated by both techniques at low conversions (0 to 20 %). Nevertheless, when the yield of BHET increased to 30 to 50%, the estimation of monomer by SEC showed an increasing deviation from the results of ^1H NMR. In this way, we could notice two detrimental conditions for the estimation of BHET by SEC with the glycolysis setup used in this investigation: (i) the consumption of the solvent (EG) during the glycolysis reaction, and (ii) the partial evaporation of the solvent under the reaction conditions (the glycolysis setup in the robotic system does not comprise sealed reactors). Therefore, although SEC is a reliable technique that should not be discarded for other depolymerization systems,¹³⁶ ^1H NMR was selected as consistent

analytical technique to calculate the yield of BHET in the kinetic investigations, as this technique was less affected by concentration and dilution effects.

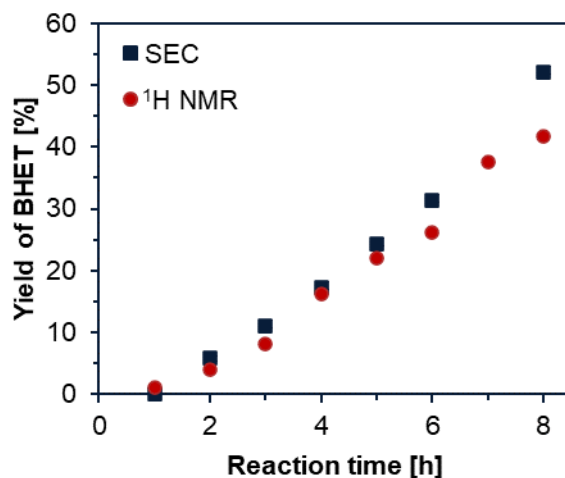


Figure 39 Comparison of BHET yield during the glycolysis of PET (170 °C, 8 wt.% catalyst) using SEC and ¹H NMR techniques.

Thus, we performed a series of kinetic experiments with variable temperatures in the range of 160 to 190 °C using copolymer (**M9**, Table 16) as catalyst. From this experimental data (Figure 40A), we confirmed that the transformation of PET into BHET was favored by the MPC and the increasing temperature.^{47,132} For instance, temperatures ranging from 160 to 170 °C revealed a maximum yield of BHET of 41% after 8 h of reaction. By increasing the temperature to 180 °C, the yield of BHET was considerably enhanced, this effect was evident after 5 to 6 h of reaction time, when the BHET yield reached *ca.* 95%. Then, the depolymerization reached near completion after 7 h of reaction (97%).

Increasing reaction temperature to 190 °C further accelerated the rate of depolymerization to reach a maximum 90% of BHET yield after 4 h of reaction. However, as indicated in previous reports,^{4,47,136,137} such temperature and high concentrations of catalyst might lead to the complete depolymerization of PET and reversible reaction of the monomer to produce oligomers in the mechanism depicted in Figure 41. Due to this remark, a decrease of yield of BHET was observed after 5 to 6 h for the glycolysis performed at 190 °C. Thereafter, the yield of BHET increased again (7 h, 87%), suggesting the equilibria between the formation of BHET and reverse reaction to produce oligomers.

Thus, to avoid the formation of a significant fraction of oligomers, we determined that the glycolysis reaction could be performed at 180 °C in an interval of 5 to 6 h of reaction. Hence, we assessed more precisely the influence of the temperature in the glycolysis of PET in the presence of a MPC.

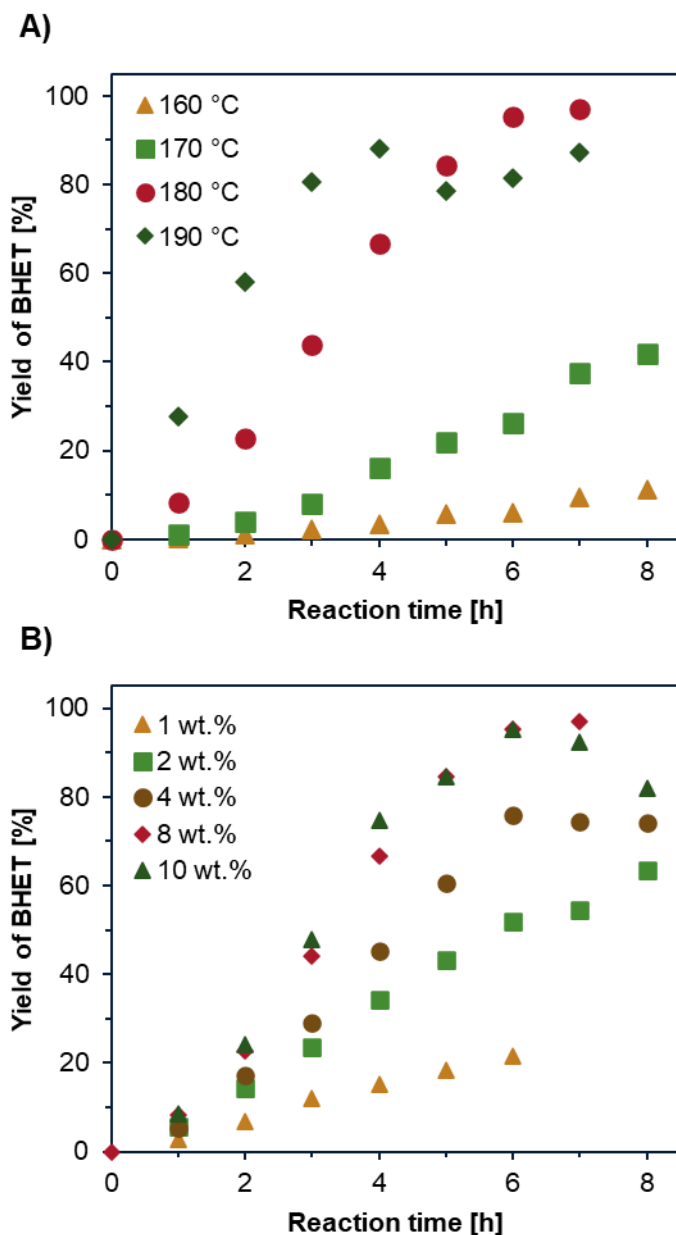


Figure 40 Effect of A) temperature (8 wt.% catalyst), and B) MPC:PET weight ratio (180 °C), as a function of time, on BHET yield during the depolymerization of waste PET using MPCs.

To further optimize the conditions of glycolysis, the yield of BHET was also analyzed by varying the MPC:PET weight ratio. Figure 40B shows the kinetic experiments as a

function of the amount of MPC (1 to 10 wt.% concentration) and time. A clear correlation was identified between the increasing catalyst concentration and the reaction rate; for instance, after 6 h of reaction, the yield of BHET increased from 21% to 95% by increasing the amount of catalyst from 1 wt.% to 10 wt.%.

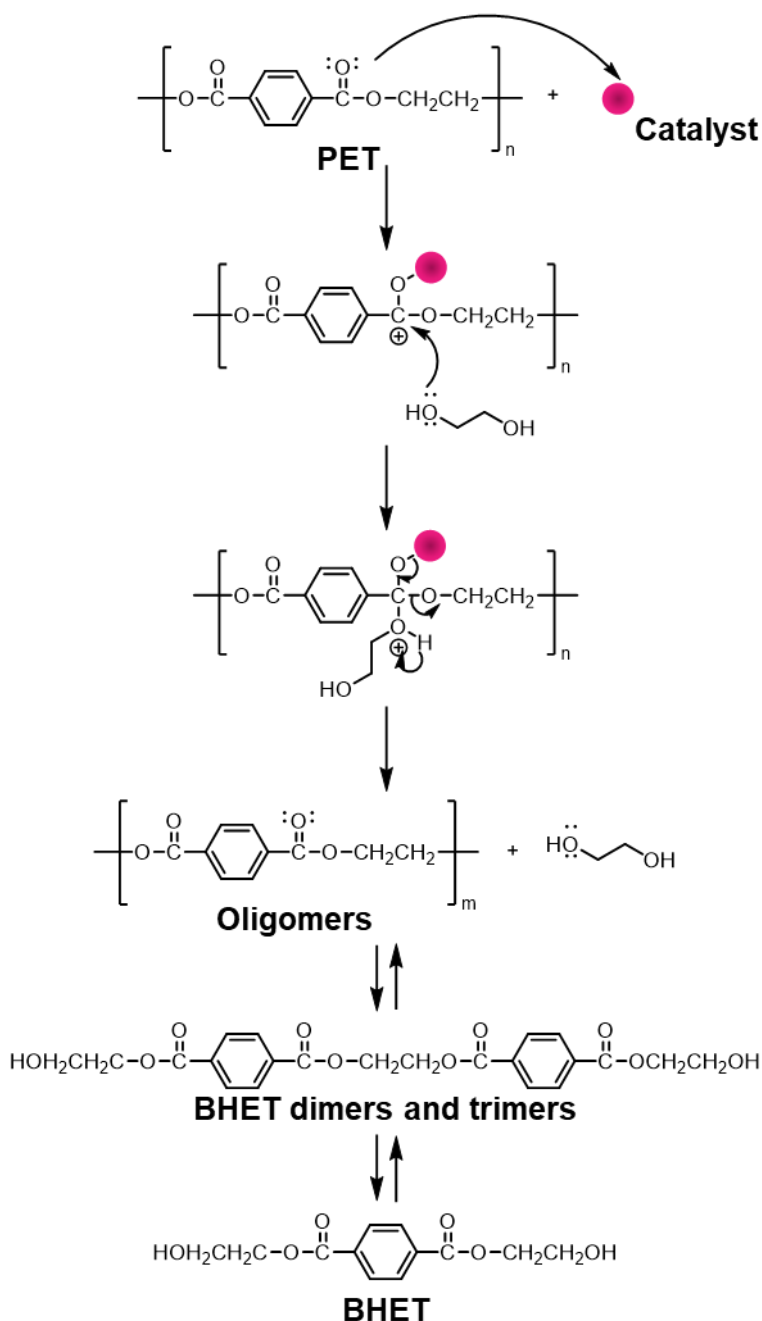


Figure 41 Scheme of the proposed mechanism for glycolysis reaction catalyzed by MPCs.

In addition, increasing the catalyst concentration also reduced the time to reach high yield of BHET; for example, the reaction with a MPC concentration of 4 wt.% required 6 h to reach 75% yield, whereas, to reach similar values, the reactions with catalyst concentration of 8 and 10 wt.% required only 5 and 4 h of reaction, respectively. Remarkably, we observed that after 5 h, the reactions with 8 and 10 wt.% of catalyst concentration reached a similar yield of BHET. Next, for the 6 to 7 h of reaction, the glycolysis with 8 wt.% of catalyst kept a steady increase of yield of BHET (97%). On the other hand, the additional increase of catalyst concentration was detrimental to the selectivity; as shown, the glycolysis with a catalyst concentration of 10 wt.% produced excellent yields of BHET (up to 95%) after 5 to 6 h of reaction, however continuing with the reaction time contributed to the decline of concentration of BHET monomer (8 h, 81% of yield). In sum, under such conditions, the reversible formation of BHET into oligomers was favored.

From these results, sought to optimize the yield of monomer, we could conclude that the amount of catalyst and reaction time could be established at 8 wt.% and 4 to 6 h of reaction. This study is applicable for copolymers with the described composition and could provide insights about the behavior of polymer catalysts with different characteristics. Systematic studies could further comprehend the analysis of libraries of copolymers with variable composition under the same glycolysis conditions; thus, focusing on a high throughput study of catalytic activity of MPCs. In summary, these data allowed us to further enhance the features and catalysis rate of the PET glycolysis by selecting a prime MPC, a suitable characterization technique to calculate the yield of monomer, as well as suitable conditions of catalyst concentration, temperature, and time of reaction.

4.4.2. Influence of the type of post-consumer PET

Once the type of MPC and parameters of depolymerization were analyzed, we performed a further study to evaluate the catalytic performance during the depolymerization of post-consumer PET of different colorations. This study was conducted to examine any possible variation during the glycolysis reaction caused by colorants or dyes and other additives in PET feedstocks; commonly added to food containers and soft drink bottles of PET. Figure

42 shows conversion of PET and selectivity of BHET using feedstocks of different colorations (blue, black, green, transparent and a mixtures thereof); a statistical chlorozincate copolymer (**M9**, Table 16) was employed as control catalyst.

As observed, the conversion of PET and selectivity of BHET, using the optimized MPC and glycolysis parameters, revealed values ranging from 95 to 99% of PET glycolysis and about 80% of BHET selectivity (isolated selectivity, determined by gravimetry) regardless of the feedstock coloration. A slight decrease of BHET selectivity (76%) was observed for blue-colored feedstocks. As suggested in previous reports,¹³⁸ these kinds of dyes might cause a poisoning effect on ionic catalysts. Nevertheless, for black, green, and mixtures of waste PET, similar results of catalytic performance were obtained compared to those experiments performed with transparent post-consumer PET; such results show that the catalytic activity of the MPC was not significantly influenced by using different types of post-consumer PET feedstocks.

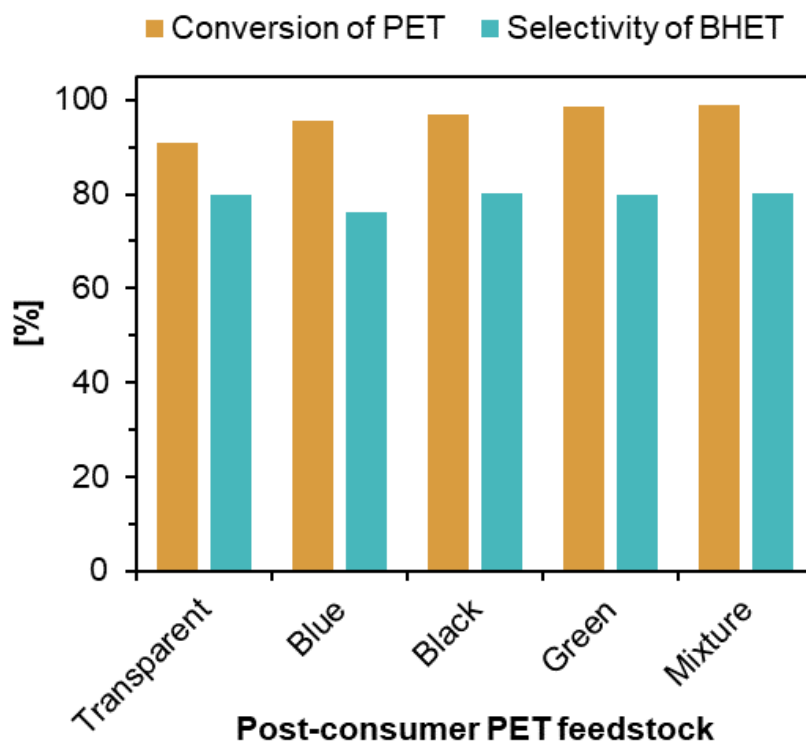


Figure 42 Effect of the coloration of post-consumer PET on catalyzed glycolysis using MPC **M9** as catalyst (T = 180 °C, t = 4h, 500 rpm).

The removal of colorants, side products and other impurities was achieved through two main steps of purification. First, the addition of water to the reaction mixture (see Figure SI 1 for an example on the experimental procedure) aided to remove hydrophobic impurities; such as unreacted PET, oligomers, and hydrophobic colorants. Thus, these impurities were removed from the reaction media by simple filtration of non-soluble materials.

The second purification step consisted of crystallization in aqueous solutions at low temperatures (4 °C) to isolate BHET as a white crystalline product. After filtration and drying, the analysis of the purity of the crystalline product, obtained from different PET feedstocks, demonstrated the high purity of the final product. Firstly, the structure of BHET was confirmed by FTIR and ^1H NMR (Figure 43). FTIR showed the characteristic signals of $-\text{OH}$ (3350 cm^{-1} and 1135 cm^{-1}) and $\text{C}=\text{O}$ (1710 cm^{-1}) stretch bands (Figure 43A).⁴⁷ Furthermore, signals at 2850 and 2910 cm^{-1} evidenced the $\text{C}-\text{H}$ stretch bands from the alkyl chain. The set of signals at $1350\text{-}1450\text{ cm}^{-1}$ and 700 cm^{-1} , showed the characteristic $\text{C}=\text{C}$ stretch and $\text{C}-\text{H}$ bend signals corresponding to the *p*-disubstitued aromatic ring, respectively. The bands at 1250 and 1050 cm^{-1} were attributed to the $\text{C}-\text{O}-\text{C}$ of the ester group and the $\text{C}-\text{O}$ of the hydroxy group of the primary alcohol.

An exemplary ^1H NMR spectrum of the crystalline product is reproduced in Figure 43B. The singlet signal at $\delta = 7.9$ ppm demonstrates the presence of the four aromatic protons of the *p*-substituted aromatic group. The triplet at $\delta = 5.1$ ppm was assigned to the hydroxyl protons from the $-\text{OH}$ group. Finally, the two triplet signals at $\delta = 5.0$ and 4.3 ppm, characteristic of methylene groups $\text{COO}-\text{CH}_2$ and $\text{HO}-\text{CH}_2$, corresponded well to the data reported in the literature.³⁸ As observed, the calculated signal integrals fit very well with the chemical structure of BHET; in addition, ^1H NMR spectra showed no substantial contribution from impurities, side products or reaction solvents, indicating that the followed procedure helped removing impurities from the main glycolysis product.

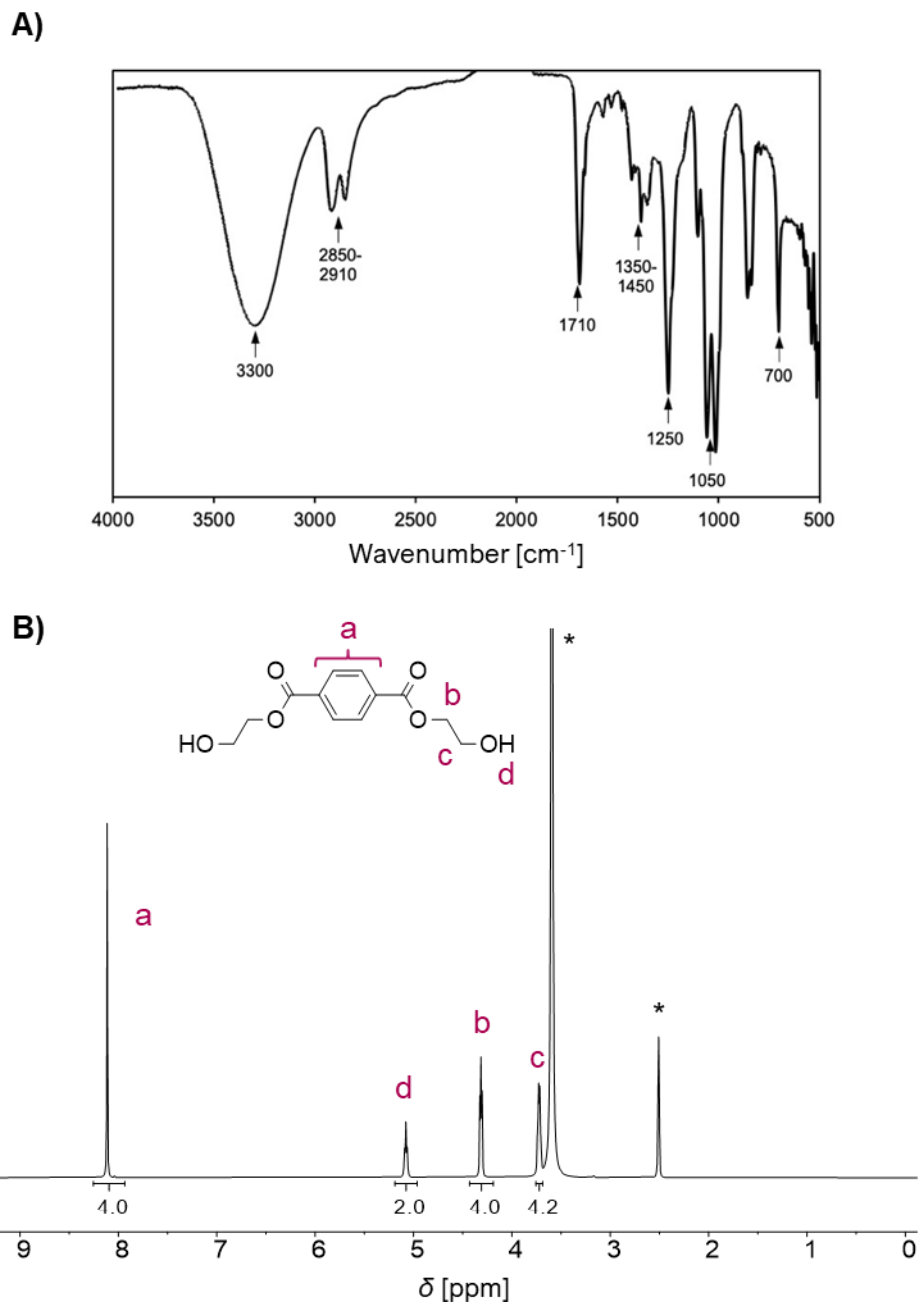


Figure 43 A) FTIR and B) ^1H NMR spectra (DMSO-d_6) of the main product of glycolysis (BHET) after purification by crystallization.

The absence of any additional impurities or side products in the BHET obtained from post-consumer PET of different colorations was further examined by TGA and DSC analysis. The TGA traces of BHET obtained from different PET feedstocks are displayed in Figure 44. Thermal analysis shows the characteristic weight losses of 30% at 226 °C, and 55% at 420 °C corresponding to the decomposition of BHET, whereas the second

weight loss is attributed to the thermal decomposition of the repolymerized BHET during the temperature increase in the thermogravimetry analysis.⁴

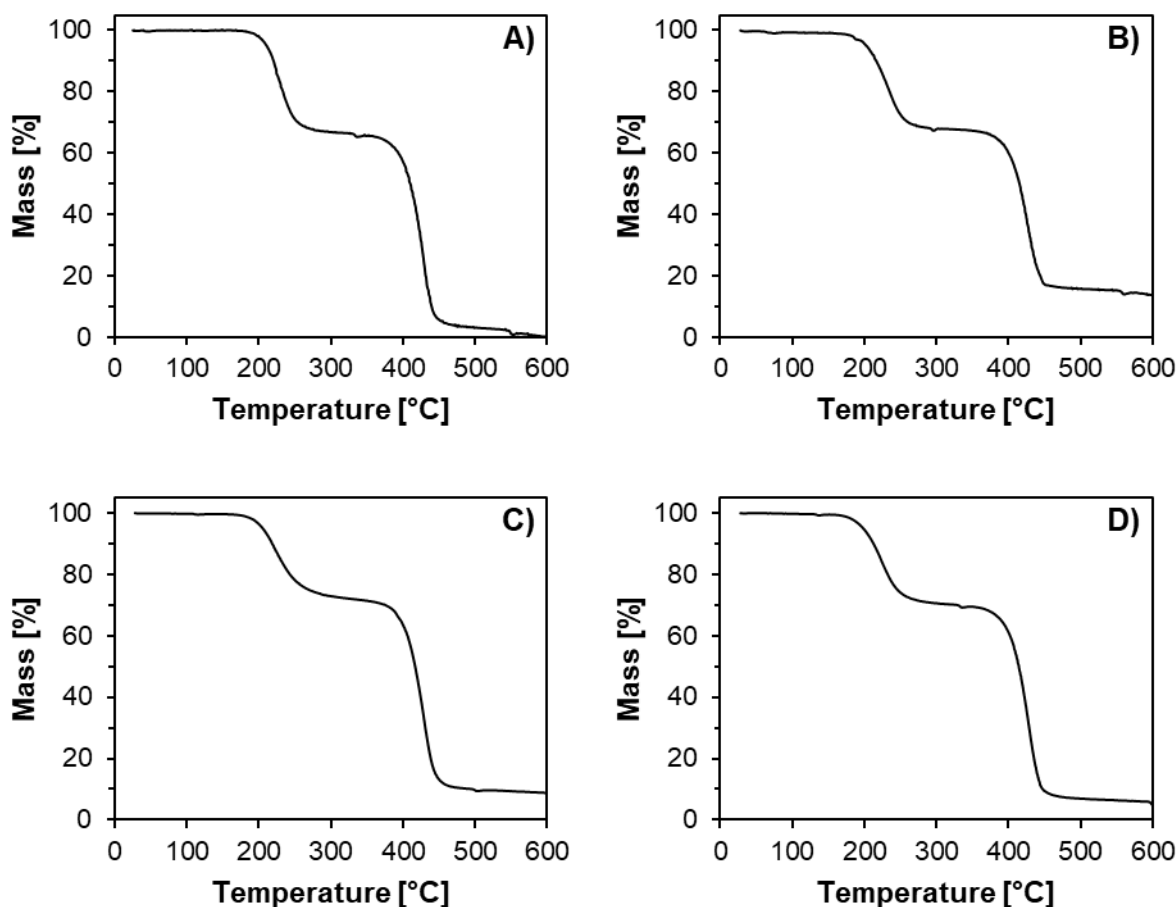


Figure 44 TGA curves of BHET obtained from the glycolysis of A) blue PET, B) black PET, C) green PET, and D) Mixture of blue, black, green, and transparent PET.

DSC curves of the main glycolysis products are displayed in Figure 45. All DSC curves exposed a sharp endothermic signal at 110 °C that corresponds to the melting point of BHET.⁴⁷ These results confirmed the absence of dimers and/or oligomers of BHET in the final product, which display melting points in the range of 173 to 220 °C.²⁶ It is worth mentioning that an additional signal was observed in the DSC curve of Figure 45A, which could be attributed to a small fraction of BHET contaminated with impurities. Thus, further crystallization and/or purification steps could be implemented to remove such contaminated products. As shown later in section 4.4.2.1, a MPC with additional

characteristics could aid to remove remnant colorants from the products after glycolysis reactions.

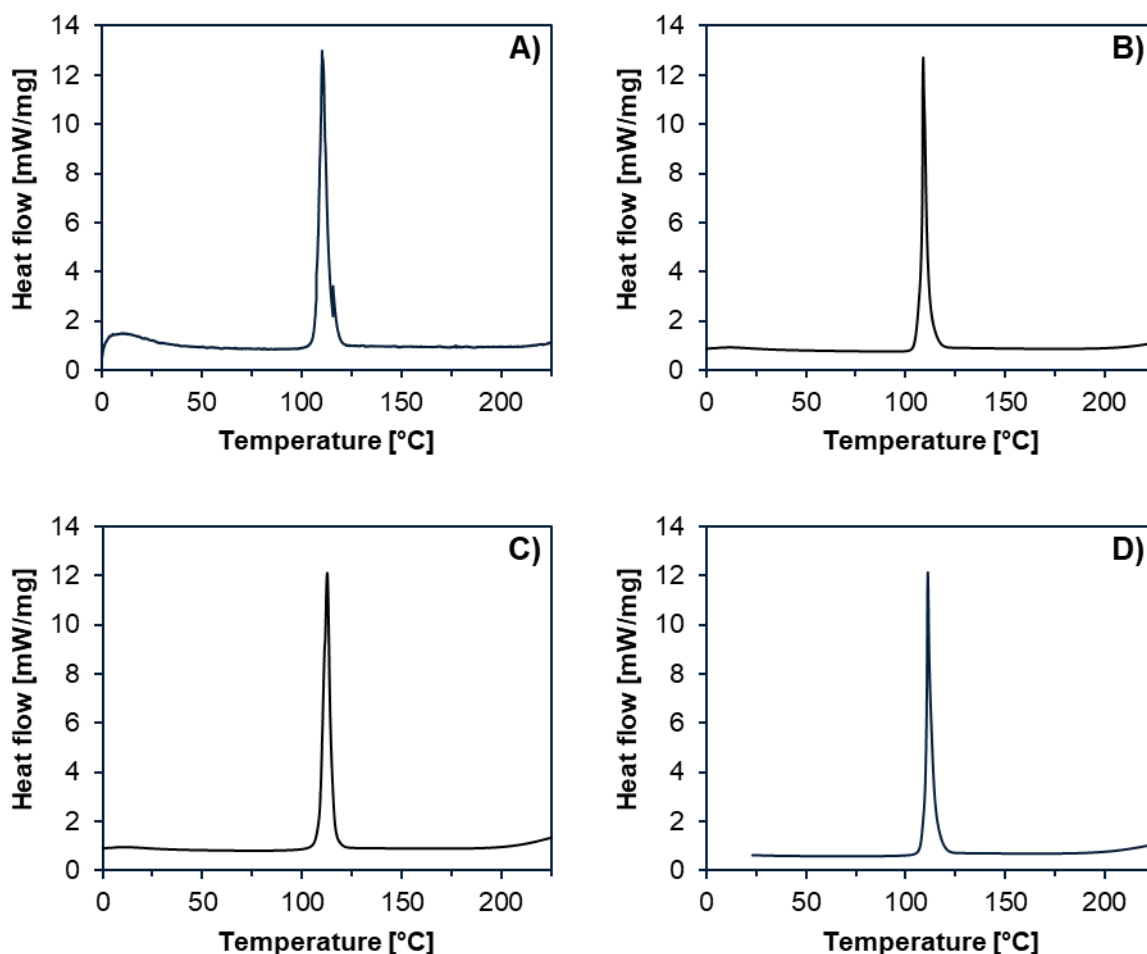


Figure 45 DSC curves of BHET obtained from A) blue PET, B) black PET, C) green PET and D) Mixture of blue, black, green, and transparent PET.

The absence of remnant catalyst and/or zinc chloride salts or derivatives of the depolymerization mixture was verified by Elemental Analysis (EA). As noted in Table 18 (entries **1** and **2**), the examples provided of post-consumer PET revealed contents of C and H in agreement with the calculated values. As shown in entries **3** to **5**, the content of C and H of exemplary glycolysis products are in good accordance to the calculated values for the monomer BHET. Likewise, the observed content of N and Cl for such samples strongly suggests the absence of colorants and/or remnant catalyst in the glycolysis products.

Table 18 Elemental Analyses of post-consumer PET feedstocks and BHET obtained from glycolysis reactions using MPCs.

Entry	Compound	Source	% C (Found / Calcd.)	% H (Found / Calcd.)	% N (Found / Calcd.)	% Cl (Found / Calcd.)
1	PET	Pink bottle	62.5 / 62.57	4.2 / 4.3	0 / 0	0 / 0
2	PET	Blue bottle	62.5 / 62.61	4.2 / 4.31	0 / 0	0 / 0
3	BHET	Black container	56.7 / 56.85	5.60 / 5.60	0 / 0	0 / 0
4	BHET	Mixture of PET	56.7 / 56.85	5.60 / 5.60	0 / 0	0 / 0
5	BHET	Mixture of PET	56.7 / 56.69	5.60 / 5.56	0 / 0	0 / 0
6	Residual Dimers	Black container	59.2 / 60.13	4.9 / 5.09	0.45 / 0	0 / 0

Additionally, as shown in entry **6**, the EA results of the residual filtrate were in good accordance to the calculated values for dimers of BHET; thus, we could also confirm the isolation of dimers after the glycolysis reaction. In this manner, as described in the experimental section, the addition of water to the crude mixture and subsequent filtration provided an adequate approach to separate residual dimers, oligomers, and hydrophobic impurities from the product. These results validated the production and isolation of the monomer BHET from glycolysis side products, impurities, and catalysts. Hence, we could conclude that BHET of high purity could be obtained by the catalytic system reported in this work.

4.4.2.1. Removal of hydrophobic impurities

To improve the purity of BHET obtained from blue-colored post-consumer PET, an additional glycolysis reaction using a specialized polymer catalyst was implemented. A MPC containing an additional hydrophobic block was used to enhance the separation of hydrophobic impurities that remained in the aqueous solutions, such as colorants and dyes.

As shown in Table 17, entry **7**, using an amphiphilic catalyst, with a sufficient content of ionic sites, also yielded results of PET conversion and BHET selectivity comparable to those obtained by using statistical copolymers (entry **1**, Table 17).

Moreover, using such catalyst a white crystalline final product could be obtained; which for the specific case of blue-colored PET was difficult using statistical copolymers as catalyst. Thus, as shown in Figure 46, after glycolysis procedure and employing an amphiphilic MPC, most of the remnant impurities remained in the aqueous solution of MPC/EG/H₂O after isolating the final BHET monomer by crystallization and filtration. After that, the remaining solution was washed with organic solvents to remove the colorants from the catalyst. Finally, the organic solution with impurities was discarded, and the aqueous solution was evaporated under reduced pressure to obtain a final MPC/EG solution. As discussed later, this solution was readily available to perform more glycolysis cycles.

In summary, this experiment showed that the purity of the recycled monomer could be further improved by modifying the structure and composition of the MPC; avoiding additional crystallization and/or time-consuming purification steps that could detriment the yield of BHET and the overall the economic viability of the chemical recycling development.^{139,140} This improvement represent an advantage over earlier strategies, which have exhibited a significant decrease in monomer yield caused by the presence of dyes and/or impurities in post-consumer PET.¹³⁸ Therefore, MPCs with fine-tuned properties could be implemented to depolymerize specific types of post-consumer polyesters and overcome possible poisoning effects and/or enhance the purity of the final product.

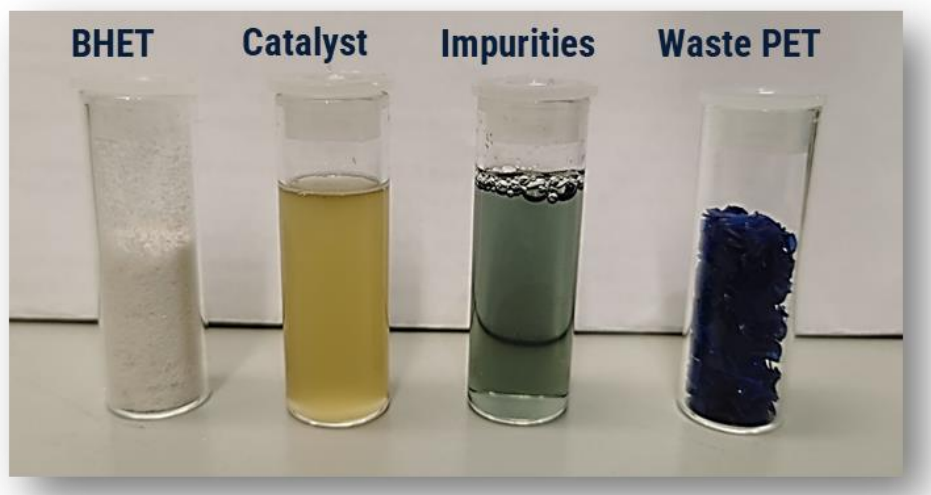


Figure 46 Image of the blue-colored post-consumer PET flakes used in this work (right) and products of glycolysis reaction using a MPC. BHET was obtained as a white crystalline solid (left). The aqueous solution of MPC/EG (yellow solution) was washed with fractions of hexane/diethyl ether (X3) to isolate an organic mixture with remnant dyes (impurities).

4.5. Reusability of the MPCs

Following up the examination of glycolysis reactions using MPCs, after isolation of unreacted PET and pure BHET, the MPC remained dispersed in the final EG/H₂O solution. In good accordance with our previous analysis of chlorozincate (co)polymers in EG and aqueous solutions, after removing H₂O and keeping the solution of MPC/EG in refrigeration for 24 h ($T = 4^{\circ}\text{C}$), we observed a biphasic solution at low temperature (Figure SI 9A). Thus, we could put forward that the MPC remained in solution and preserved its UCST behavior after the glycolysis procedure. Accordingly, the MPC could be isolated and recovered for subsequent glycolysis cycles. However, it should be noted that such phase was easily redispersed at room temperature, probably due to the low concentration of MPC, the occurrence of water traces in solution, and the increasing temperature. Thus, the isolation of the precipitated MPC from solution was a challenging procedure by means of common filtration or centrifugation techniques (Figure SI 9B). Therefore, to avoid any additional procedures that could result in loss of MPC, we decided to test a new cycle of

glycolysis using the final solution of MPC in EG (details can be found in the experimental section).

We explored the reusability of the MPCs in solution by using two types of copolymer structures, which showed excellent catalytic activity in the experiments described in sections 4.1 and 4.3. Figure 47A shows the reusability of the MPC P([BVMIM]ZnCl_n) (**M2**, Table 13) in EG solution in glycolysis reactions of mixtures of post-consumer PET. As demonstrated before, the first glycolysis reaction yielded an excellent catalytic performance by using the described reaction conditions. Afterwards, using only the MPC/EG solution that remained after purification procedures, the second cycle of glycolysis yielded 96 % PET conversion and 85% BHET selectivity (isolated selectivity). Therefore, we could confirm that the MPC remained in EG solution after the glycolysis and purification procedures, thereafter, the MPC/EG solution could be further used as catalyst; avoiding additional washing and/or separation steps that could detriment the catalytic performance.¹⁴¹ As shown the catalytic reaction was performed for 5 cycles exhibiting that the activity of the MPC remained practically unaffected. Remarkably, compared to the first two cycles of glycolysis, the catalytic performance of the system increased from the third up to the fifth cycle. We could attribute this observation to the increasing dispersion of the MPC in solution which, as shown during the study of their properties in solution, was improved after heating, and cooling the catalyst in EG solution. Accordingly, in the last catalytic cycles, the conversion of PET and selectivity of BHET ranged as high as 94% and 95%, respectively.

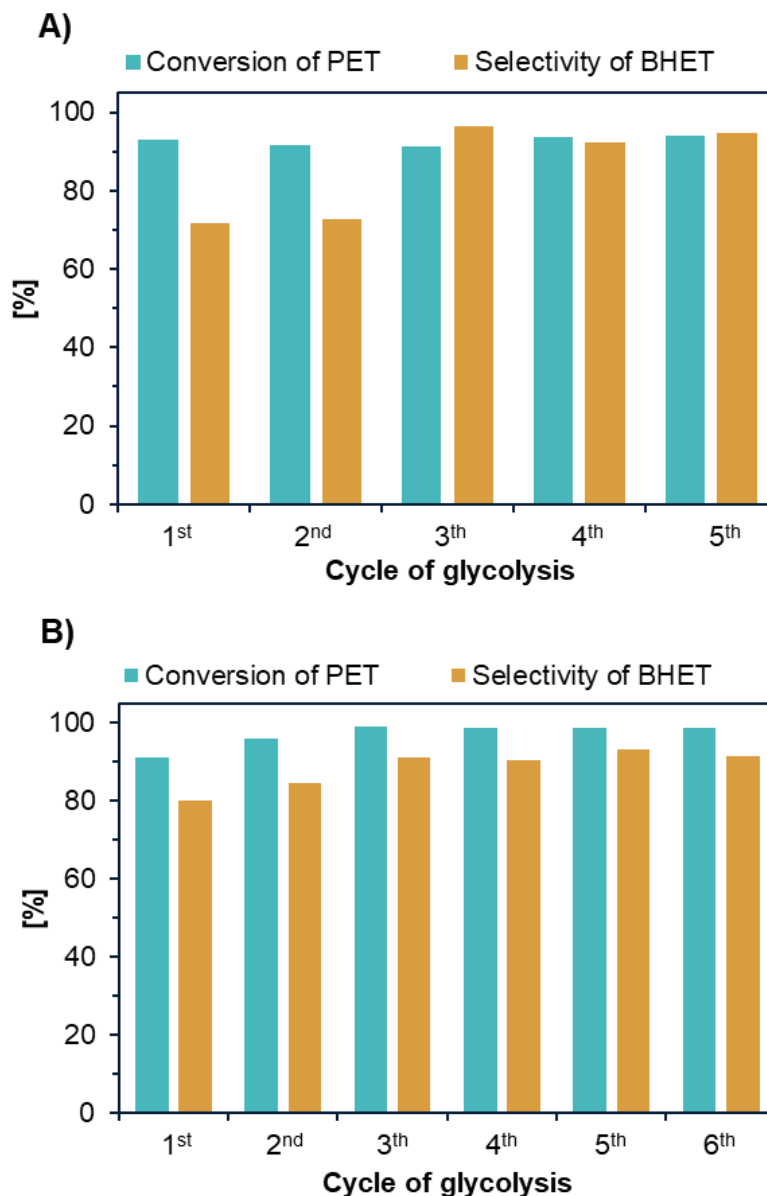


Figure 47 Effect of the reusability of MPCs on the glycolysis of PET and selectivity of BHET (isolated): A) Catalyst P([BVMIM]ZnCl_n) (**M2**) and B) Catalyst P([BVBIM]ZnCl_n-co-DMAEMA) (**M9**); $R = 0.75$ / $T = 180$ °C / $t = 4$ h / 500 rpm.

The same experiments of catalyst reusability were implemented for a MPC based on a statistical copolymers (**M9**, Table 16). As shown in Figure 47B, a similar trend of conversion and selectivity was observed by using such catalyst. For these series of glycolysis reactions, in comparison to the homopolymer (**M2**) we could observe a slight increase on the values of conversion of PET, which, as described in previous sections, could be attributed to the lower steric effects and higher hydrophilicity conferred by the

additional hydrophilic segments in the MPC. On the other hand, the values of BHET selectivity achieved up to 93% for the last cycles of glycolysis. Additionally, we could extend reusability tests of this MPC for 6 glycolysis cycles; thus, demonstrating the high viability of this approach and the good catalytic activity of the MPC after several glycolysis cycles. In conclusion, the MPCs reported in this work are effective and reusable catalyst for the glycolysis of various types and grades of post-consumer PET.

Representative SEM micrographs of unreacted PET flakes, isolated after glycolysis reactions (Figure 48A and B), evidenced the degradation of the materials and the indication of porous surfaces. These findings encompass the documented PET glycolysis mechanism: (1) diffusion of EG into PET, (2) adsorption of catalyst and PET swelling, and (3) glycolysis of ester bonds in PET chains.⁴⁹ Therefore, under glycolysis conditions, we could confirm that the MPCs were readily soluble in EG and adsorbed to react on the external surface of PET and later enter into the porous structure.⁴⁹ From these results, we could settle that the following factors enhanced the catalytic performance of chlorozincate polymer catalyst in the glycolysis of PET: (i) The reversible evolution of the structure of oligomeric chlorozincate anions, as a function of temperature, releases $ZnCl_n$ and Cl^- anions; which improved the dispersity of the catalyst and the concentration of catalytic sites in the medium,¹¹² and (ii) as recently reported by Coleman *et al.*,¹⁴² the adsorption of PET by MPCs could increase the interaction of catalytic sites and PET chains.

Additional EDX analysis of the remnant materials (Figure 48C) revealed only the signals corresponding to the binding energies of C and O (0.4 and 0.6 KeV, respectively) of the ester groups of PET. This supplementary result, along with EA of isolated BHET (Table 18), evidenced that the MPCs could be effectively recovered from the products and side glycolysis products.

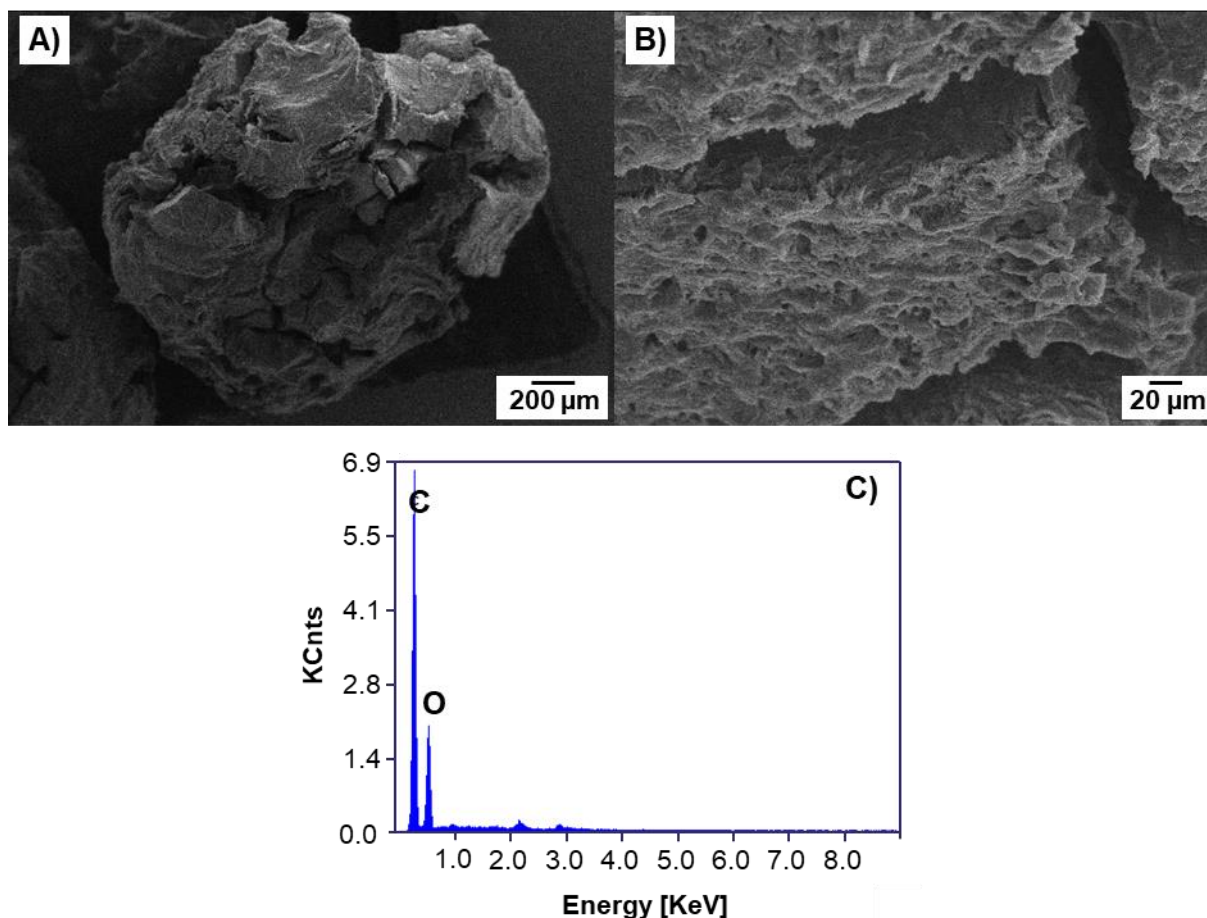


Figure 48 SEM images of residual PET after glycolysis catalyzed by MPC **C2**: **A)** shows the overall image of the degraded PET and **B)** shows the porous surface of PET after the diffusion of the solvent and catalyst. **C)** EDX spectrum of residual PET after glycolysis (using MPC) and isolation.

In summary, after isolating pure BHET and unreacted PET, the MPC could be recovered similarly to heterogeneous catalysts; triggered by the UCST behavior described for chlorozincate polymeric derivatives in EG solutions. The outcomes of this investigation allowed us to confirm the quasi-homogeneous mechanism of PET glycolysis (Figure 49), consisting of MPCs featured by the advantages of homogeneous catalysts to perform the glycolysis reaction (for high catalytic performance) and heterogeneous catalysts to perform the separation of the catalyst along with impurities. Furthermore, the MPCs could be highly cost-efficient as they can be either recovered (for instance, to replace spent catalyst with a fresh catalyst), or directly reused in EG solution to perform more glycolysis cycles, without dropping the catalytic performance with additional procedures. Finally, embedding additional functionalities to MPCs enhanced the depolymerization rate, the

selectivity for the monomer, and allowed the separation of catalyst and colorants to produce BHET of high purity.

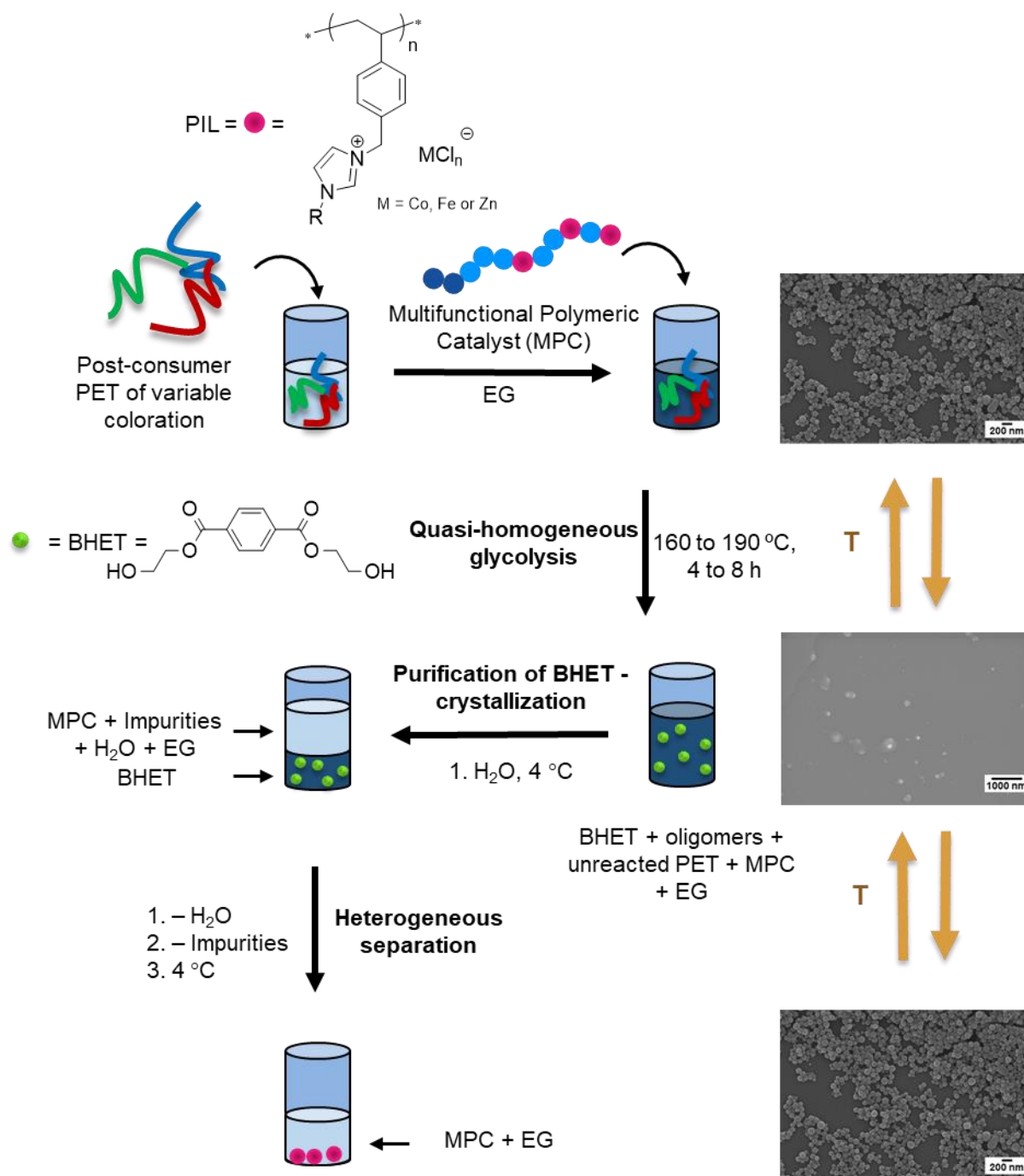


Figure 49 Schematic representation of the proposed system for the glycolysis of post-consumer PET, catalyzed by a thermo-responsive MPC, to obtain highly pure monomer BHET.

Chapter 5

Conclusions and outlook

5.1. Conclusions

This research described the development of an efficient chemical method for recycling post-consumer PET of variable coloration. By introducing structure-specific polymers as catalyst, the developed method tackles the current limitations of PET chemical recycling, providing an effective glycolysis procedure with high catalytic performance along with a separation procedure for the removal of impurities (*i.e.*, colorants or dyes) and recovery of the catalyst.

In the first phases, we covered the synthesis and characterization of poly(ionic liquids) via RAFT polymerization to design copolymers with IL functionalities and self-assembly features in aqueous and glycol solutions. The functional groups of the copolymers were carefully designed to accomplish the following functions: 1. Catalyze the glycolysis of post-consumer polyesters, 2. Remove impurities from the products, and 3. Recover the MPC from depolymerization mixtures. Thus, the obtained copolymers were tested in PET glycolysis to prove the central hypothesis of this project, *i.e.*, removing the catalyst and impurities from the final reaction mixture by adding water and subsequently applying an external stimuli (*i.e.*, temperature). Therefore, the thermo-responsive MPCs could be recovered from the reaction mixture for its reuse. Additionally, the study of the physicochemical properties of the MPCs demonstrated their UCST behavior in glycol solutions. As shown by transmittance studies, DLS and SEM experiments, the UCST behavior was completely reversible and could be fine-tuned by varying the concentration, molar mass, and composition of the (co)polymers, or solvents. Moreover, the effect of the anion molar ratio was assessed, showing the crucial role of the anion in the structure of the polymer and its impact on the MPCs solution properties.

Such studies were essential to choose the optimal MPCs in the second phase of this project, where we performed the screening and optimization of the glycolysis procedure using an automated parallel platform and ^1H NMR for the estimation of instantaneous BHET yield. In this manner, we analyzed the influence of MPCs (molar mass, composition, structure, anions, and anion molar ratio) and the glycolysis conditions (temperature, time of reaction, and amount of catalyst) to define optimal conditions of

temperature (180 to 190 °C), time of reaction (4 to 6 h), and catalyst concentration (8 to 10 wt.%). The developed catalytic approach allowed a PET depolymerization up to 99% with a selectivity of BHET above 92%. Moreover, we showed the influence of the post-consumer PET coloration over the catalytic performance. While the catalytic activity was scarcely affected, hydrophobic colorants were effortlessly removed using the developed technology and novel MPCs.

On the other hand, impurities that remained in the final solutions of MPC/BHET/EG/H₂O were effectively removed from the products of glycolysis using a tailored MPC. To remove colorants, this strategy was grounded on copolymers containing additional hydrophobic functionalities. Therefore, we showed that balancing the functionalities of the polymers allowed the modification of the glycolysis catalytic system to recycle specific types of post-consumer PET.

Indeed, a remarkable feature of the MPCs is their reusability. After reaction and product purification, the soluble MPCs could be spontaneously separated from the EG solution by decreasing the temperature for their isolation or reuse for following cycles of glycolysis. Thus, under optimized conditions, the MPCs are easily recyclable in EG solution yielding over 90% selectivity of BHET and demonstrating similar catalytic activity after several reactions. In summary, the MPCs described in this work represent a system combining the advantages of homogeneous catalytic reactions and heterogeneous separation of catalysts from the products. The benefits of the MPCs represent highly desirable features in the chemical industry as they could be designed and handled on demand, according to specific procedures or raw materials (*e.g.*, different grades post-consumer PET with variable coloration).¹⁴³ This development integrating chemical glycolysis, catalyst recovery, and colorant removal for PET recycling is projected to be applicable to the upcycling of a wide variety of post-consumer polyesters.

5.2. Outlook

Considering the versatility and the wide-selection of polymer synthesis strategies, studies aimed at designing (co)polymers, with precise compositions and architectures, improved catalytic performance, and enhanced separation capabilities in the chemical recycling of polyesters could follow up this investigation —as the possibilities to find more polymer compositions suitable for this process are infinite. The development of fully automated and high-throughput chemical recycling procedures could accelerate discoveries in the field, which would help to develop highly specific MPCs, and overall, chemical recycling protocols with more sustainable approaches for different types and grades of PET or other polyesters.

Furthermore, developing a continuous process integrating glycolysis, catalyst recovery, and colorant removal for PET chemical recycling is projected to broaden the success possibilities to the upcycling of post-consumer PET at the commercial level.

Finally, the esterification-transesterification reactions using highly specific MPCs could be further extended for the chemical recycling of other types of polyesters or materials. For instance, the esterification/transesterification of oils or waxes to produce value-added materials such as biodiesel or similar derivatives, highly desired in the chemical industry.

5.3. References

- 1 F. Awaja and D. Pavel, *Eur. Polym. J.*, 2005, **41**, 1453–1477.
- 2 P. . Subramanian, *Resour. Conserv. Recycl.*, 2000, **28**, 253–263.
- 3 J. M. Harris, in *Dimensions of Sustainable Development*, eds. R. Seidler and K. Bawa, Island Press, 2000, pp. 21–41.
- 4 H. Wang, Z. Li, Y. Liu, X. Zhang and S. Zhang, *Green Chem.*, 2009, **11**, 1568.
- 5 L. Biermann, E. Brepohl, C. Eichert, M. Paschetag, M. Watts and S. Scholl, *Green Process. Synth.*, 2021, **10**, 361–373.
- 6 E. M. Aizenshtein, *Fibre Chem.*, 2007, **39**, 355–362.
- 7 A. Gent and G. Bierwagen, Major Industrial Polymers, <https://www.britannica.com/topic/industrial-polymers-468698> (Accessed November 2021).
- 8 J. E. McIntyre, in *Modern Polyesters: Chemistry and Technology of Polyesters and Copolyesters*, eds. T. E. Long and J. Scheir, John Wiley & Sons, Ltd, Chichester, 2003, pp. 3–24.
- 9 D. Morrison and C. Tyree, Invisibles - The plastic inside us, https://orbmedia.org/stories/Invisibles_plastics/multimedia (Accessed November 2021).
- 10 C. Tyree and D. Morrison, Plus Plastic - Microplastics found in global bottled water, <https://orbmedia.org/stories/plus-plastic> (Accessed November 2021).
- 11 X. Zhou, X. Lu, Q. Wang, M. Zhu and Z. Li, *Pure Appl. Chem.*, 2012, **84**, 789–801.
- 12 H. Webb, J. Arnott, R. Crawford and E. Ivanova, *Polymers (Basel)*, 2012, **5**, 1–18.
- 13 D. . Suh, O. . Park and K. . Yoon, *Polymer (Guildf)*, 2000, **41**, 461–466.
- 14 T. Astrup, J. Møller and T. Fruergaard, *Waste Manag. Res.*, 2009, **27**, 789–799.
- 15 S. Xu, H. Zhang, P. He and L. Shao, *Environ. Technol.*, 2011, **32**, 1269–1277.
- 16 Petcore/Europe, What is PET? Processing, <https://www.petcore-europe.org/processing> (Accessed November 2021).
- 17 J. J. Benvenuta Tapia, J. A. Tenorio-López, A. Martínez-Estrada and C. Guerrero-Sánchez, *Mater. Chem. Phys.*, 2019, **229**, 474–481.
- 18 L. Bartolome, M. Imran, B. Gyoo, W. A. and D. Hyun, in *Material Recycling - Trends and Perspectives*, InTech, 2012.
- 19 A. M. Al-Sabagh, F. Z. Yehia, G. Eshaq, A. M. Rabie and A. E. ElMetwally, *Egypt. J. Pet.*, 2016, **25**, 53–64.
- 20 D. S. Achilias and G. P. G. Karayannidis, *Water, Air, Soil Pollut. Focus*, 2004, **4**, 385–396.
- 21 D. Paszun and T. Spychaj, *Ind. Eng. Chem. Res.*, 1997, **36**, 1373–1383.
- 22 Vreinigte Glanzstoff-Fabriken, A.-G. "Conversion of Poly(ethylene terephthalate) into dimethyl

- terephthalate" Brit. Patent **755,071**, 1956.
- 23 F. L. Mantia, *Handbook of Plastics Recycling*, Rapra Technology Limited, Telford UK, 2002.
- 24 N. George and T. Kurian, *Ind. Eng. Chem. Res.*, 2014, **53**, 14185–14198.
- 25 D. Carta, G. Cao and C. D'Angeli, *Environ. Sci. Pollut. Res.*, 2003, **10**, 390–394.
- 26 G. Güçlü, T. Yalçinyuva, S. Özgümüş and M. Orbay, *Thermochim. Acta*, 2003, **404**, 193–205.
- 27 J. R. Campanelli, D. G. Cooper and M. R. Kamal, *J. Appl. Polym. Sci.*, 1994, **53**, 985–991.
- 28 M. Genta, T. Iwaya, M. Sasaki, M. Goto and T. Hirose, *Ind. Eng. Chem. Res.*, 2005, **44**, 3894–3900.
- 29 V. Sinha, M. R. Patel and J. V. Patel, *J. Polym. Environ.*, 2010, **18**, 8–25.
- 30 J. Scheirs, *Polymer Recycling: Science, Technology and Applications*, Wiley, Chichester, UK, 1998.
- 31 G. Xi, M. Lu and C. Sun, *Polym. Degrad. Stab.*, 2005, **87**, 117–120.
- 32 M. Y. Abdelaal, T. R. Sobahi and M. S. I. Makki, *Constr. Build. Mater.*, 2011, **25**, 3267–3271.
- 33 D. E. Nikles and M. S. Farahat, *Macromol. Mater. Eng.*, 2005, **290**, 13–30.
- 34 Z. Helwani, M. R. Othman, N. Aziz, J. Kim and W. J. N. Fernando, *Appl. Catal. A Gen.*, 2009, **363**, 1–10.
- 35 N. D. Pingale, V. S. Palekar and S. R. Shukla, *J. Appl. Polym. Sci.*, 2010, **115**, 249–254.
- 36 U. R. Vaidya and V. M. Nadkarni, *J. Appl. Polym. Sci.*, 1987, **34**, 235–245.
- 37 U. R. Vaidya and V. M. Nadkarni, *J. Appl. Polym. Sci.*, 1988, **35**, 775–785.
- 38 M. Ghaemy and K. Mossaddegh, *Polym. Degrad. Stab.*, 2005, **90**, 570–576.
- 39 M. Imran, K. Lee, Q. Imtiaz, B.-K. Kim, M. Han, B. G. Cho and D. H. Kim, *J. Nanosci. Nanotechnol.*, 2011, **11**, 824–828.
- 40 R. Wi, M. Imran, K. G. Lee, S. H. Yoon, B. G. Cho and D. H. Kim, *J. Nanosci. Nanotechnol.*, 2011, **11**, 6544–6549.
- 41 K. Troev, G. Grancharov, R. Tsevi and I. Gitsov, *J. Appl. Polym. Sci.*, 2003, **90**, 2301–2301.
- 42 S. R. Shukla and K. S. Kulkarni, *J. Appl. Polym. Sci.*, 2002, **85**, 1765–1770.
- 43 S. R. Shukla and A. M. Harad, *J. Appl. Polym. Sci.*, 2005, **97**, 513–517.
- 44 S. R. Shukla, A. M. Harad and L. S. Jawale, *Waste Manag.*, 2008, **28**, 51–56.
- 45 F. R. Veregue, C. T. Pereira Da Silva, M. P. Moisés, J. G. Meneguín, M. R. Guilherme, P. A. Arroyo, S. L. Favaro, E. Radovanovic, E. M. Giroto and A. W. Rinaldi, *ACS Sustain. Chem. Eng.*, 2018, **6**, 12017–12024.
- 46 H. Wang, Z. Li, Y. Liu, X. Zhang and S. Zhang, *Green Chem.*, 2009, **11**, 1568.
- 47 Q. F. Yue, C. X. Wang, L. N. Zhang, Y. Ni and Y. X. Jin, *Polym. Degrad. Stab.*, 2011, **96**, 399–403.
- 48 Q. F. Yue, H. G. Yang, M. L. Zhang and X. F. Bai, *Adv. Mater. Sci. Eng.*, 2014, **2014**, 1–6.

- 49 A. M. Al-Sabagh, F. Z. Yehia, G. Eshaq and A. E. ElMetwally, *Ind. Eng. Chem. Res.*, 2015, **54**, 12474–12481.
- 50 Q. Suo, J. Zi, Z. Bai and S. Qi, *Catal. Letters*, 2017, **147**, 240–252.
- 51 Z. Wang, Y. Wang, S. Xu, Y. Jin, Z. Tang, G. Xiao and H. Su, *Polym. Degrad. Stab.*, 2021, **190**, 109638.
- 52 N. V. Plechkova and K. R. Seddon, *Chem. Soc. Rev.*, 2008, **37**, 123–150.
- 53 J. Yuan and M. Antonietti, *Polymer (Guildf.)*, 2011, **52**, 1469–1482.
- 54 S. Mallakpour and Z. Rafiee, *J. Polym. Environ.*, 2011, **19**, 447–484.
- 55 H. Wang, Y. Liu, Z. Li, X. Zhang, S. Zhang and Y. Zhang, *Eur. Polym. J.*, 2009, **45**, 1535–1544.
- 56 A. Pawlak, M. Pluta, J. Morawiec, A. Galeski and M. Pracella, *Eur. Polym. J.*, 2000, **36**, 1875–1884.
- 57 C. Davies, H. F. Naoush and G. J. Rees, *Polym. Int.*, 1996, **41**, 215–225.
- 58 M. García, J. I. Eguiazábal and J. Nazábal, *J. Appl. Polym. Sci.*, 2001, **81**, 121–127.
- 59 Ioniqa Technologies, PET Cradle-to-Cradle solution, <http://www.ioniqa.com/pet-recycling/>, (Accessed November 2021).
- 60 M. Vilaplana Artigas, L. Mestrom, R. De Groot, V. Philippi, C. Guerrero-Sanchez, T. Hooghoudt, "Polymer degradation" Int. Patent **WO 2014/209117 A1**, 2014.
- 61 J. Yuan, D. Mecerreyes and M. Antonietti, *Prog. Polym. Sci.*, 2013, **38**, 1009–1036.
- 62 O. Green, S. Grubjesic, S. Lee and M. A. Firestone, *Polym. Rev.*, 2009, **49**, 339–360.
- 63 J. Steinkoenig, F. R. Bloesser, B. Huber, A. Welle, V. Trouillet, S. M. Weidner, L. Barner, P. W. Roesky, J. Yuan, A. S. Goldmann and C. Barner-Kowollik, *Polym. Chem.*, 2016, **7**, 451–461.
- 64 Y. Gu and T. P. Lodge, *Macromolecules*, 2011, **44**, 1732–1736.
- 65 H. He, S. Averick, E. Roth, D. Luebke, H. Nulwala and K. Matyjaszewski, *Polymer (Guildf.)*, 2014, **55**, 3330–3338.
- 66 H. Mori, M. Yanagi and T. Endo, *Macromolecules*, 2009, **42**, 8082–8092.
- 67 J. Yuan, H. Schlaad, C. Giordano and M. Antonietti, *Eur. Polym. J.*, 2011, **47**, 772–781.
- 68 J. Texter, V. A. Vasantha, R. Crombez, R. Maniglia, L. Slater and T. Mourey, *Macromol. Rapid Commun.*, 2012, **33**, 69–74.
- 69 H. Tang, J. Tang, S. Ding, M. Radosz and Y. Shen, *J. Polym. Sci. Part A Polym. Chem.*, 2005, **43**, 1432–1443.
- 70 S. Ding, H. Tang, M. Radosz and Y. Shen, *J. Polym. Sci. Part A Polym. Chem.*, 2004, **42**, 5794–5801.
- 71 K. Vijayakrishna, S. K. Jewrajka, A. Ruiz, R. Marcilla, J. A. Pomposo, D. Mecerreyes, D. Taton and Y. Gnanou, *Macromolecules*, 2008, **41**, 6299–6308.
- 72 J. Yuan and M. Antonietti, in *Applications of Ionic Liquids in Polymer Science and Technology*,

- ed. D. Mecerreyes, Springer Berlin Heidelberg, Berlin, Heidelberg, 2015, pp. 47–67.
- 73 H. Mori, M. Yahagi and T. Endo, *Macromolecules*, 2009, **42**, 8082–8092.
- 74 P. Coupillaud and D. Taton, *Applications of Ionic Liquids in Polymer Science and Technology*, Springer Berlin Heidelberg, Berlin, Heidelberg, 2015.
- 75 X. Chen, J. Zhao, J. Zhang, L. Qiu, D. Xu, H. Zhang, X. Han, B. Sun, G. Fu, Y. Zhang and F. Yan, *J. Mater. Chem.*, 2012, **22**, 18018.
- 76 T. K. Carlisle, J. E. Bara, A. L. Lafrate, D. L. Gin and R. D. Noble, *J. Memb. Sci.*, 2010, **359**, 37–43.
- 77 A. M. Fernandes, M. Paulis, J. Yuan and D. Mecerreyes, *Part. Part. Syst. Charact.*, 2016, **33**, 734–739.
- 78 F. N. Ajjan, M. Ambrogi, G. A. Tiruye, D. Cordella, A. M. Fernandes, K. Grygiel, M. Isik, N. Patil, L. Porcarelli, G. Rocasalbas, G. Vendramiento, E. Zeglio, M. Antonietti, C. Detrembleur, O. Inganäs, C. Jérôme, R. Marcilla, D. Mecerreyes, M. Moreno, D. Taton, N. Solin and J. Yuan, *Polym. Int.*, 2017, **66**, 1119–1128.
- 79 Y. Li, C. Zhang, Y. Zhou, Y. Dong and W. Chen, *Eur. Polym. J.*, 2015, **69**, 441–448.
- 80 Y. Kohno, S. Saita, Y. Men, J. Yuan and H. Ohno, *Polym. Chem.*, 2015, **6**, 2163–2178.
- 81 S. Soll, M. Antonietti and J. Yuan, *ACS Macro Lett.*, 2012, **1**, 84–87.
- 82 Y. Men, M. Drechsler and J. Yuan, *Macromol. Rapid Commun.*, 2013, **34**, 1721–1727.
- 83 W. Cui, X. Lu, K. Cui, L. Niu, Y. Wei and Q. Lu, *Langmuir*, 2012, **28**, 9413–9420.
- 84 H. Mori, Y. Ebina, R. Kambara and K. Nakabayashi, *Polym. J.*, 2012, **44**, 550–560.
- 85 K. I. Seno, S. Kanaoka and S. Aoshima, *J. Polym. Sci. Part A Polym. Chem.*, 2008, **46**, 5724–5733.
- 86 K. Grygiel, W. Zhang, C. Detrembleur and J. Yuan, *RSC Adv.*, 2016, **6**, 57117–57121.
- 87 H. Yoshimitsu, A. Kanazawa, S. Kanaoka and S. Aoshima, *Macromolecules*, 2012, **45**, 9427–9434.
- 88 G. S. Owens and M. M. Abu-Omar, in *Ionic Liquids Industrial Applications for Green Chemistry*, ACS Symposium Series, 2002, pp. 321–333.
- 89 J. W. Lee, J. Y. Shin, Y. S. Chun, H. Bin Jang, C. E. Song and S. Lee, *Acc. Chem. Res.*, 2010, **43**, 985–994.
- 90 B. Wang, L. Qin, T. Mu, Z. Xue and G. Gao, *Chem. Rev.*, 2017, **117**, 7113–7131.
- 91 D. Zhao, M. Wu, Y. Kou and E. Min, *Catal. Today*, 2002, **74**, 157–189.
- 92 J. E. Bara, S. Lessmann, C. J. Gabriel, E. S. Hatakeyama, R. D. Noble and D. L. Gin, *Ind. Eng. Chem. Res.*, 2007, **46**, 5397–5404.
- 93 J. Estager, P. Nockemann, K. R. Seddon, M. Swadzba-Kwasny and S. Tyrrell, *Inorg. Chem.*, 2011, **50**, 5258–5271.

- 94 D. J. Keddie, *Chem. Soc. Rev.*, 2014, **43**, 496–505.
- 95 J. Steinkoenig, F. R. Bloesser, B. Huber, A. Welle, V. Trouillet, S. M. Weidner, L. Barner, P. W. Roesky, J. Yuan, A. S. Goldmann and C. Barner-Kowollik, *Polym. Chem.*, 2016, **7**, 451–461.
- 96 H. He, M. Zhong, B. Adzima, D. Luebke, H. Nulwala and K. Matyjaszewski, *J. Am. Chem. Soc.*, 2013, **135**, 4227–4230.
- 97 P. Maksym, M. Tarnacka, A. Dzieńia, K. Erfurt, A. Chrobok, A. Zięba, K. Wolnica, K. Kaminski and M. Paluch, *Polym. Chem.*, 2017, **8**, 5433–5443.
- 98 C. Pietsch, U. Mansfeld, C. Guerrero-Sanchez, S. Hoepfener, A. Vollrath, M. Wagner, R. Hoogenboom, S. Saubern, S. H. Thang, C. R. Becer, J. Chiefari and U. S. Schubert, *Macromolecules*, 2012, **45**, 9292–9302.
- 99 X. Liu, P. Ni, J. He and M. Zhang, *Macromolecules*, 2010, **43**, 4771–4781.
- 100 Z. Lu, X. Zhang, Z. Li, Z. Wu, J. Song and C. Li, *Polym. Chem.*, 2015, **6**, 772–779.
- 101 F. A. Plamper, M. Ruppel, A. Schmalz, O. Borisov, M. Ballauff and A. H. E. Müller, *Macromolecules*, 2007, **40**, 8361–8366.
- 102 V. D. Lechuga-Islas, G. Festag, M. Rosales-Guzmán, O. E. Vega-Becerra, R. Guerrero-Santos, U. S. Schubert and C. Guerrero-Sánchez, *Eur. Polym. J.*, 2020, **124**, 109457.
- 103 J. J. Haven, C. Guerrero-Sanchez, D. J. Keddie and G. Moad, *Macromol. Rapid Commun.*, 2014, **35**, 492–497.
- 104 J. J. Haven, C. Guerrero-Sanchez, D. J. Keddie, G. Moad, S. H. Thang and U. S. Schubert, *Polym. Chem.*, 2014, **5**, 5236–5246.
- 105 C. Guerrero-Sanchez, L. O'Brien, C. Brackley, D. J. Keddie, S. Saubern and J. Chiefari, *Polym. Chem.*, 2013, **4**, 1857–1862.
- 106 Y. Bakkour, V. Darcos, S. Li and J. Coudane, *Polym. Chem.*, 2012, **3**, 2006–2010.
- 107 J. Estager, J. D. Holbrey and M. Swadźba-Kwaśny, *Chem. Soc. Rev.*, 2014, **43**, 847–886.
- 108 R. Kore, P. Berton, S. P. Kelley, P. Aduri, S. S. Katti and R. D. Rogers, *ACS Catal.*, 2017, **7**, 7014–7028.
- 109 L. C. Brown, J. M. Hogg and M. Swadźba-Kwaśny, 2017, 185–224.
- 110 J. Estager, J. D. Holbrey and M. Swadźba-Kwaśny, *Chem. Soc. Rev.*, 2014, **43**, 847–886.
- 111 P. S. Campbell, C. C. Santini, D. Bouchu, B. Fenet, L. Rycerz, Y. Chauvin, M. Gaune-Escard, C. Bessada and A. L. Rollet, *Dalt. Trans.*, 2010, **39**, 1379–1388.
- 112 V. Lecocq, A. Graille, C. C. Santini, A. Baudouin, Y. Chauvin, J. M. Basset, L. Arzel, D. Bouchu and B. Fenet, *New J. Chem.*, 2005, **29**, 700–706.
- 113 J. G. Li, Y. F. Hu, S. F. Sun, S. Ling and J. Z. Zhang, *J. Phys. Chem. B*, 2012, **116**, 6461–6464.
- 114 M. B. Alves, V. O. Santos, V. C. D. Soares, P. A. Z. Suarez and J. C. Rubim, *J. Raman Spectrosc.*, 2008, **39**, 1388–1395.

- 115 H. Erdemi, A. Bozkurt and W. H. Meyer, *Synth. Met.*, 2004, **143**, 133–138.
- 116 A. C. Alba Rubio, M. R. Coleman, S. Kalidindi, A. Joshi, I. S. Omodolor, "Homogeneous and reusable superacid polymer catalyst useful for the synthesis of 5-hydroxymethylfurfural from glucose" Int. Patent **WO 2019/089448 A1**, 2019.
- 117 J. M. Hogg, L. C. Brown, K. Matuszek, P. Latos, A. Chrobok and M. Swadźba-Kwaśny, *Dalt. Trans.*, 2017, **46**, 11561–11574.
- 118 C. Ge, S. Liu, C. Liang, Y. Ling and H. Tang, *Polym. Chem.*, 2016, **7**, 5978–5987.
- 119 C. Liu, S. Wang, H. Zhou, C. Gao and W. Zhang, *J. Polym. Sci. Part A Polym. Chem.*, 2016, **54**, 945–954.
- 120 L. Zhao, L. Zhang, Z. Zheng, Y. Ling and H. Tang, *Macromol. Chem. Phys.*, 2019, **220**, 1–13.
- 121 B. Shkodra-Pula, C. Kretzer, P. M. Jordan, P. Klemm, A. Koeberle, D. Pretzel, E. Banoglu, S. Lorkowski, M. Wallert, S. Höppener, S. Stumpf, A. Vollrath, S. Schubert, O. Werz and U. S. Schubert, *J. Nanobiotechnology*, 2020, **18**, 1–14.
- 122 G. Bokias, D. Hourdet and I. Iliopoulos, *Macromolecules*, 2000, **33**, 2929–2935.
- 123 T. Manouras, E. Koufakis, S. H. Anastasiadis and M. Vamvakaki, *Soft Matter*, 2017, **13**, 3777–3782.
- 124 S. Amemori, K. Kokado and K. Sada, *J. Am. Chem. Soc.*, 2012, **134**, 8344–8347.
- 125 J. C. Peacock and B. L. D. Peacock, *J. Am. Pharm. Assoc.*, 1918, **7**, 689–697.
- 126 F. Neumaier, S. Alpdogan, J. Hescheler and T. Schneider, *Acta Physiol.*, 2018, **222**, e12988.
- 127 A. M. Al-Sabagh, F. Z. Yehia, A. M. M. F. Eissa, M. E. Moustafa, G. Eshaq, A. R. M. Rabie and A. E. Elmetwally, *Ind. Eng. Chem. Res.*, 2014, **53**, 18443–18451.
- 128 A. M. Al-Sabagh, F. Z. Yehia, A. M. F. Eissa, M. E. Moustafa, G. Eshaq, A. M. Rabie and A. E. Elmetwally, *Polym. Degrad. Stab.*, 2014, **110**, 364–377.
- 129 Z. Ju, W. Xiao, X. Lu, X. Liu, X. Yao, X. Zhang and S. Zhang, *RSC Adv.*, 2018, **8**, 8209–8219.
- 130 Q. Wang, X. Lu, X. Zhou, M. Zhu, H. He and X. Zhang, *J. Appl. Polym. Sci.*, 2013, **129**, 3574–3581.
- 131 H. Wang, R. Yan, Z. Li, X. Zhang and S. Zhang, *Catal. Commun.*, 2010, **11**, 763–767.
- 132 L. Wang, G. A. Nelson, J. Toland and J. D. Holbrey, 2020, **8**, 13362–13368.
- 133 A. Stoski, M. F. Viante, C. S. Nunes, E. C. Muniz, M. L. Felsner and C. A. P. Almeida, *Polym. Int.*, 2016, **65**, 1024–1030.
- 134 V. D. Lechuga-Islas, C. Guerrero-Sánchez and R. Guerrero-Santos, *Synthesis and characterization of ionic liquid-based polymeric catalyst for poly(ethylene terephthalate) glycolysis in an automated parallel platform*, 2020.
- 135 K. S. Lovejoy, C. A. Corley, E. K. Cope, M. C. Valentine, J. G. Leid, G. M. Purdy, J. S. Wilkes, A. T. Koppisch and R. E. Del Sesto, *Cryst. Growth Des.*, 2012, **12**, 5357–5364.

- 136 R. López-Fonseca, I. Duque-Ingunza, B. de Rivas, L. Flores-Giraldo and J. I. Gutiérrez-Ortiz, *Chem. Eng. J.*, 2011, **168**, 312–320.
- 137 M. Khoonkari, A. H. Haghighi, Y. Sefidbakht, K. Shekoochi and A. Ghaderian, *Int. J. Polym. Sci.*, 2015, **2015**, 1–11.
- 138 C. S. Nunes, P. R. Souza, A. R. Freitas, M. J. V. da Silva, F. A. Rosa and E. C. Muniz, *Catalysts*, 2017, **7**, 1–16.
- 139 R. Huang, Q. Zhang, H. Yao, X. Lu, Q. Zhou and D. Yan, *ACS Omega*, 2021, **6**, 12351–12360.
- 140 M. Li, J. Lu, X. Li, M. Ge and Y. Li, *Text. Res. J.*, 2020, **90**, 2058–2069.
- 141 J. T. Du, Q. Sun, X. F. Zeng, D. Wang, J. X. Wang and J. F. Chen, *Chem. Eng. Sci.*, 2020, **220**, 115642.
- 142 H. Abedsoltan, I. S. Omodolor, A. C. Alba-Rubio and M. R. Coleman, *Polymer (Guildf.)*, 2021, **222**, 123620.
- 143 E. Barnard, J. J. Rubio Arias and W. Thielemans, *Green Chem.*, 2021, **23**, 3765–3789.
- 144 S. L. Simon, *Thermochim. Acta*, 2001, **374**, 55–71.
- 145 N. Guigo and N. Sbirrazzuoli, 2018, pp. 399–429.
- 146 R. Urbani, F. Sussich, S. Prejac and A. Cesàro, *Thermochim. Acta*, 1997, **304–305**, 359–367.
- 147 M. Lappalainen and M. Karppinen, *J. Therm. Anal. Calorim.*, 2010, **102**, 171–180.

5.4. Appendix

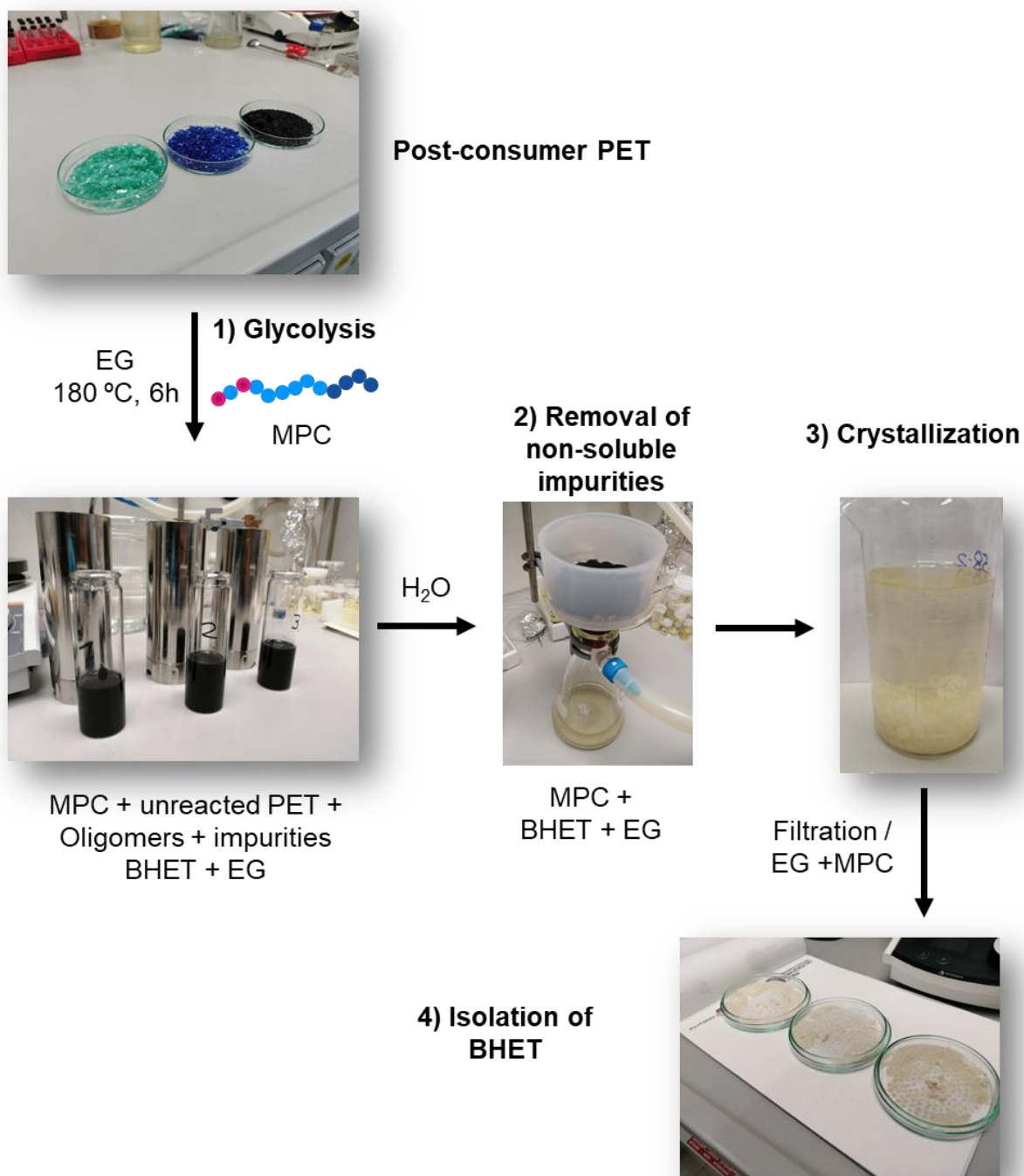


Figure SI 1 Experimental procedure of the glycolysis of post-consumer PET (black container), using a MPC, to obtain BHET.

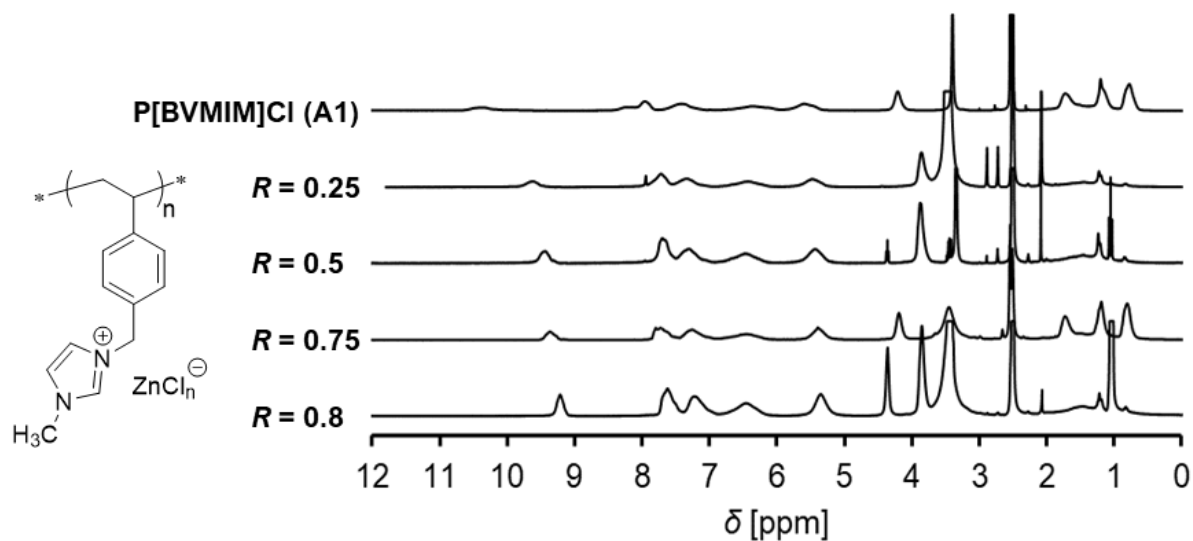


Figure SI 2 ^1H NMR spectra of P([BVMIM]Cl) and its anion exchanged chlorozincate derivatives.

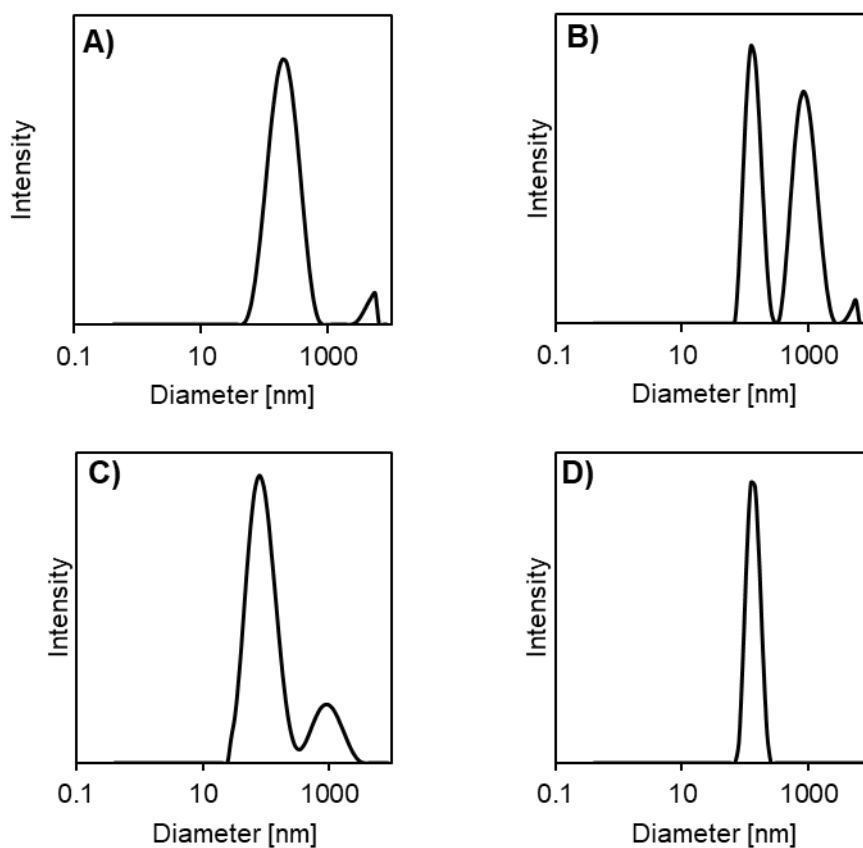


Figure SI 3 Plots of the d_H (nm) of solutions of P([BVMIM]ZnCl_n) (C2) in EG as a function of concentration: A) 1 mg mL⁻¹, B) 2 mg mL⁻¹, C) 5 mg mL⁻¹, and B) 10 mg mL⁻¹.

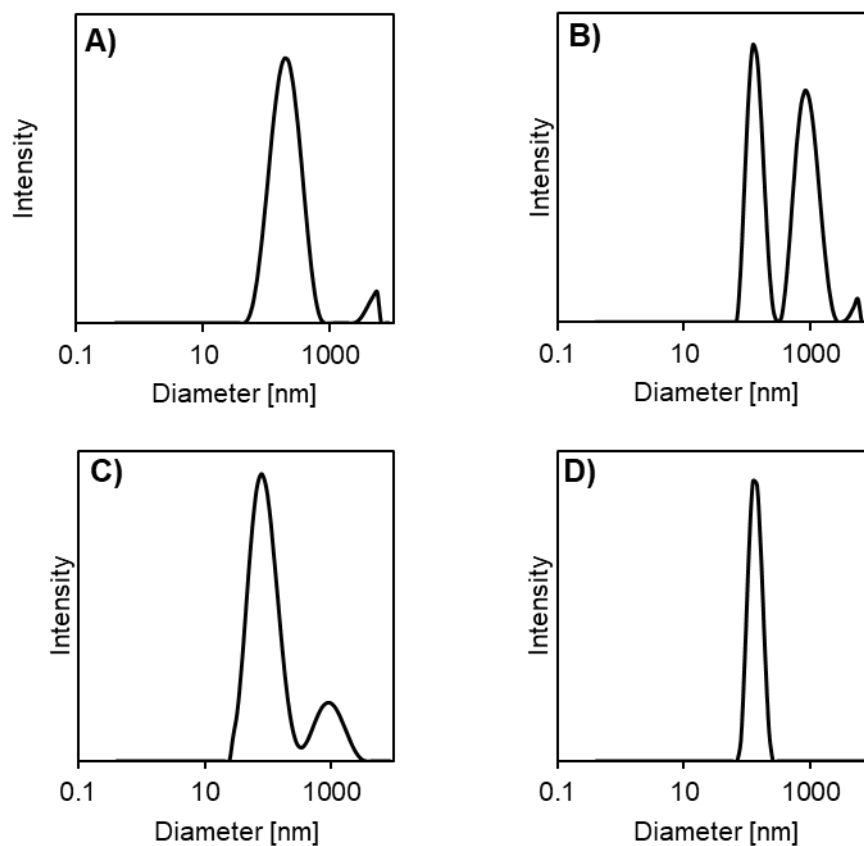


Figure SI 4 Plots of the d_H (nm) of solutions of P([BVMIM]ZnCl_n) (**M2**) in EG (5 mg mL⁻¹) as a function of the molar ratio of ZnCl₂: A) $R = 0.1$, B) $R = 0.25$, C) $R = 0.5$, and D) $R = 0.75$.

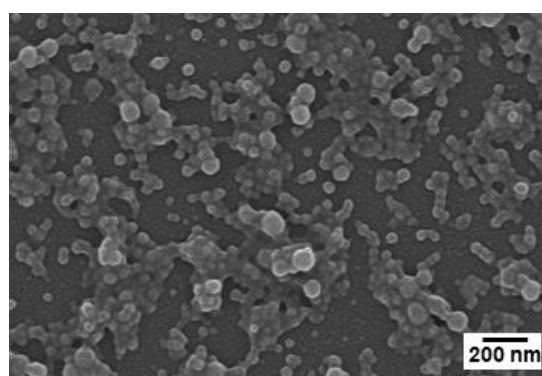


Figure SI 5 SEM image of polymer nanoparticles after casting a solution of P([BVMIM]ZnCl_n) (**M2**) in EG (5 mg mL⁻¹) at room temperature.

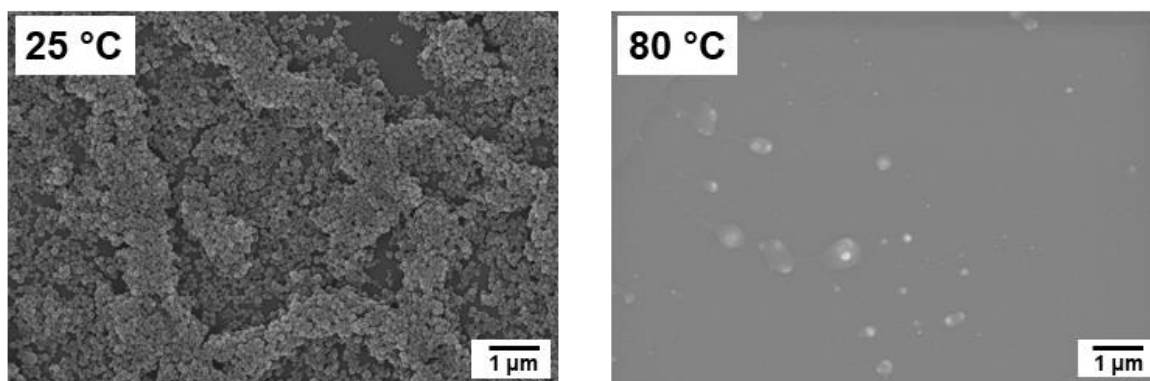


Figure SI 6 SEM comparison of polymer nanoparticles after casting a solution of P([BVMIM]ZnCl_n) (**M2**) in EG (10 mg mL⁻¹) at 25 °C and 80 °C.

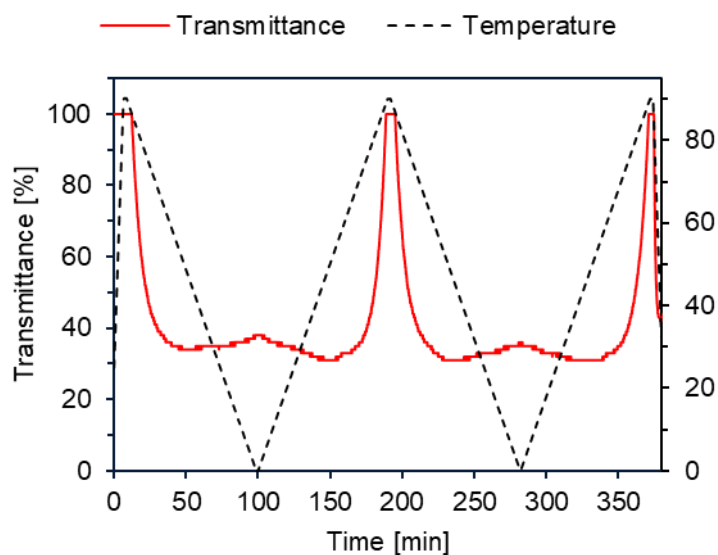


Figure SI 7 Temperature and transmittance curves of a solution of P([BVMIM]ZnCl_n) (**M2**) in 1,3-propanediol (10 mg mL⁻¹) as a function of time.

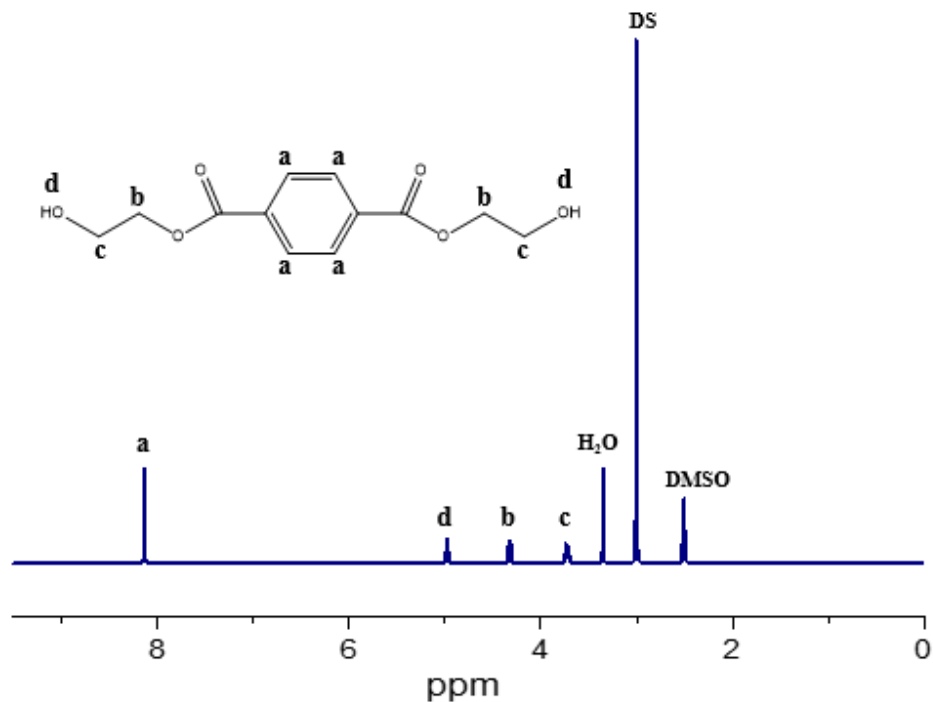


Figure SI 8 Representative ¹H NMR spectra (DMSO-*d*₆) of the glycolysis product (BHET) and the internal standard Dimethylsulfone (DS).

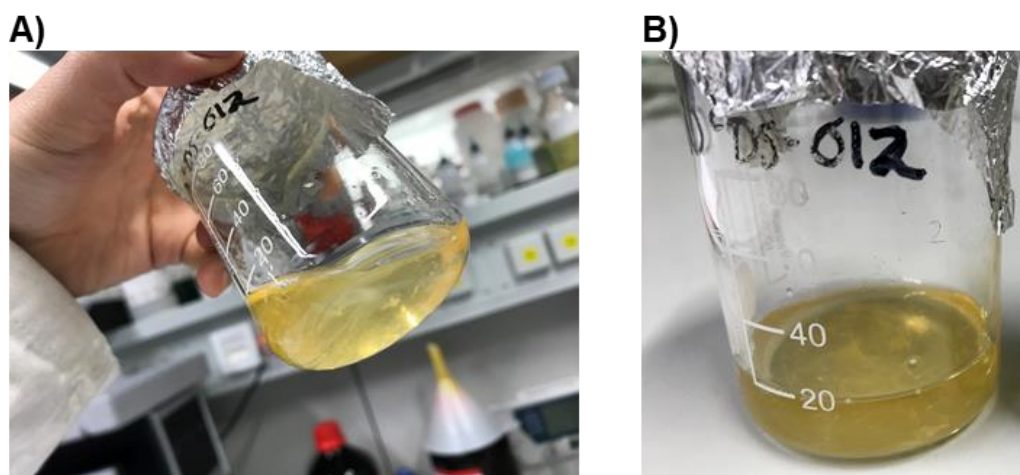


Figure SI 9 Representative images of the solution of MPC in EG obtained after the glycolysis of post-consumer PET and the subsequent isolation of BHET. After keeping the solution at 4°C for 24 h, a precipitate appeared in the solution (A). After manipulating the solution at room temperature, the precipitate began to dissolve (B).